SISSA
Scuola Internazionale Superiore di Studi Avanzati

Neuroscience Area – PhD course in

Functional and Structural Genomics

Glia-derived Extracellular Vesicles in motion at the neuron surface: involvement of the prion protein

Candidate:

Giulia D'Arrigo

Advisors:

Prof. Giuseppe Legname

Dr. Claudia Verderio

Academic Year 2018-19

TABLE OF CONTENTS

LIST OF ABBREVIATIONS

EVs - Extracellular Vesicles

PrP^{Sc} - Scrapie form of Prion Protein

miRNA - microRNA

CSF - Cerebrospinal Fluid

MVB - Multivesicular Body

ILV - Intraluminal Vesicle

ESCRT - Endosomal Sorting Complex Required for Transport

ATP - Adenosine-5'-triphosphate

ARF6 - ADP-ribosylation factor 6

SNARE - Soluble NSF Attachment protein REceptors

CNS - Central Nervous System

HSP70 - Heat Shock Protein 70

EAAT - Excitatory Amino-Acid Transporter

EAE - N-arachidonoylethanolamine

CB1 - Cannabinoid Receptor 1

PLP - Myelin Proteolipid Protein

CNP - 2’3’-cyclic-nucleotide-phosphodiesterase

MBP - Myelin Basic Protein

MOG - Myelin Oligodendrocyte Glycoprotein

IL-1β - Interleukin-1β

NLGN1- Neuroligin 1

Syt1- Synaptotagmin 1

BBB - Blood Brain Barrier

CJD - Creutzfeldt-Jacob disease

Aβ - β-amyloid

AD - Alzheimer’s Disease

PD - Parkinson’s disease

SOD - Superoxide Dismutase

TDP-43- Transactive Response Binding Protein-43

ALS - Amyotrophic Lateral Sclerosis

WT - Wild-Type

nSMase2 - Neutral Sphingomyelinase 2

EC - Entorhinal Cortex

PrP - Prion Protein

GSS - Gerstmann-Sträussler-Scheinker

FFI - Fatal Familial Insomnia

ER - Endoplasmic Reticulum

GPI - Glycophosphatidylinositol

NMR - Nuclear Magnetic Resonance

STI1- Stress-Inducible Protein 1

mGluRs - Metabotropic Glutamate Receptors

ROCK - Rho-Associated Protein Kinase

LTP - Long-Term Potentiation

Arp2/3 complex - Actin-related Protein 2/3 Complex

VASP - Vasodilator-stimulated Phosphoprotein

Eps8 - Epidermal Growth Factor Receptor Pathway Substrate 8

AIS - Axon Initial Segment

TRIM46 - Tripartite Motif-containing Protein 46

MTCL1- Microtubule Crosslinking Factor 1

γ-TuRC - γ-tubulin Ring Complex

PTMs - Post-translational Modifications

MAPs - Microtubule Associated-proteins

–TIPs - Minus-end-binding Proteins

+TIPs - Plus-end-binding Proteins

CAMSAP2 - Calmodulin Regulated Spectrin-associated Protein 2

EBs - End-binding Proteins

TRAK1 - Trafficking Kinesin-binding Protein 1

GluR1 - Glutamate Receptor 1

Kv4.2 - Voltage-gated Potassium Channels

AMPARs - α-amino-3-hydroxy-5-methyl-4-isoxazolepropionic acid receptors

LAMP-1 - Lysosomal-associated Membrane Protein 1

CAMs - Cell Adhesion Molecules

ABPs - Actin Binding Proteins

PS - Phosphatidyl-serine

CAR - Coxsackievirus and Adenovirus Receptor

Grb2 - Growth Factor Receptor-bound Protein 2

TNTs - Tunnelling Nanotubes

LIST OF MOVIES

Movie 1: EV dynamics on a growing axon.

The movie shows an OT delivered EV (white arrow) moving anterogradely while exploring filopodia on the way to the growth cone.

Movie 2: EV dynamics on the surface of a neuron cell body.

The movie shows an OT delivered EV (white arrow) moving within the somatic region of a neuron.

Movie 3: EV motion along connected processes.

The movie shows an OT delivered EV (white arrow) jumping from one process to another one.

Movie 4: Neuron-to-neuron EV motion.

The movie shows the transit of an OT delivered EV (white arrow) between neurites belonging to distinct neurons.

Movie 5: EV radial motion.

High frequency (20 Hz) time-lapse recording of an OT delivered EV showing radial motion.

Movie 6: EV motion induced by intracellular organelle transport.

The time-lapse recording of an OT delivered EV (white arrow) and an intracellular vesicle (black arrow) moving simultaneously along a neuron process.

Movie 7: EV motion induced by traffic of two intracellular vesicles.

The movie shows the shift of an OT delivered EV (white arrow) dragged by two intracellular vesicles (black and grey arrows) during their transport along the process.

Movie 8: Concomitant monitoring of intracellular lysosome trafficking and EV dynamics at the neuron surface.

The movie shows an OT delivered EV (white arrow) moving on a thin process where Lysotracker red-labelled vesicles are transported (black arrows). Yellow circle indicates the region of the neurite where first a lysosome (blue arrow) and then the EV (white arrow) linger.

Movie 9: Block of EV motion by Sodium Azide.

The movie shows an OT delivered EV (white arrow) which moves on a neuron process until Sodium Azide (+NaN_3) is added to the medium.

ABSTRACT

Extracellular Vesicles (EVs) shed from the plasma membrane of glia cells are key players in glia-neuron communication in healthy and diseased brain.

By exposing adhesion receptors, EVs can interact with specific cells and deliver complex "signals", including proteins, lipids and RNA between cells. Under pathological conditions EVs become vehicle for the transfer of pathogens. Indeed, EVs released in the brain have been described to contain misfolded proteins associated to neurodegenerative diseases such as scrapie prion protein (PrP^{Sc}), superoxide dismutase 1 (SOD1), α-synuclein, tau and amyloid-β (Aβ).

In the past years we highlighted the role of EVs in the transcellular signalling in the brain. EVs from glial cells modulate synaptic transmission, stimulating excitatory transmission and impairing the inhibitory one. Moreover, we demonstrated the transfer of the miR146a-5p mediated by EVs from glial cells to neurons. EV-neuron contact is critical for EV signalling to neurons, as preventing EV-neuron interaction by cloaking phosphatidylserine (PS) residues on the EV surface, inhibited EV-mediated effects.

Previous evidence in Alzheimer's Diseases (AD) cellular models showed that small EVs storing misfolded proteins can be internalized and transferred between neurons through axonal projections. However, if the diffusion of pathogenic proteins mediated by small EVs has been quite investigated, almost nothing is known about how large EVs can interact with neurons and reach preferential sites.

We combined optical manipulation to time-lapse imaging to trap and deliver glial EVs to cultured hippocampal neurons and monitor the interaction. We show that EVs efficiently adhered to the neuronal cell body, dendrites and axons. Surprisingly, after adhesion a large fraction of EVs moved on the surface of neurites in both retrograde and anterograde directions.

Interestingly, the EV velocity is in the same range of retrograde actin flow, which regulates membrane diffusion of receptors linked to actin. Accordingly, we found that EV movement is highly dependent on neuron energy metabolism. Moreover, inhibition of neuron actin filaments rearrangements with Cytochalasin D or Blebbistatin, but not depolymerization of microtubules with Nocodazole, reduced EVs in motion, revealing that neuronal actin cytoskeleton is implicated in EV-neuron dynamics.

Interestingly, the delivery of EVs derived from prion protein knock out ($PrP^{-/-}$) astrocytes on $PrP^{-/-}$ neurons and the use of PrP-coated synthetic beads point at neuronal PrP as the receptor for EV motion.

Unexpectedly, we found that EVs can contain actin filaments and ATP, suggesting an independent capacity to actively move at the neuron surface in an actin-mediated way, through intermittent contacts with the plasma membrane.

Our data support a dual mechanism exploited by astrocytic EVs to reach target sites on neurons.

First, EV displacement could be driven by the binding to a neuronal receptor linked to the actin cytoskeleton. Second, EVs could possess motile ability like that produced by actin in cells and move along a gradient of neuronal receptors. Moreover, for the first time, we show that astrocytic EVs exploit neuronal PrP to passively reach their target sites on neurons. Overall, our findings could have big implications for better use EVs as therapeutic tools as well as targets to prevent the spreading of pathogenic agents in the diseased brain.

INTRODUCTION

1 EXTRACELLULAR VESICLES (EVs)

Extracellular Vesicles are cell-derived circular membrane organelles. They are a heterogeneous family and result from the membrane shedding of most cell types. They can be detected in all biological fluids and universally recognized as important players in intercellular communication both in physiology and pathology [1].

Recent studies have shown that EVs can contain different molecules: proteins, lipids, nucleic acids including DNA, mRNA and miRNA, and carry membrane receptors through which they specifically interact with ligands on target cells [2]. EVs from diverse cell of origin communicate with the periphery influencing the behaviour of recipient cells in multiple ways, including transfer of bioactive cargoes and activation of signalling events at the cell surface [3]. They are also capable to modify the environment of the donor cells as they possess enzymatic activity that can change the molecular composition of extracellular fluid [4].

After shedding EVs can impact the fate of target cells in various ways: i) they can break and release their content directly in the extracellular space; ii) EVs can partially fuse with the plasma membrane of target cells ('kiss-and-run'); iii) they can completely fuse or being internalized through phagocytosis, micropinocytosis or clathrin-dependent endocytosis [5]. Nevertheless, EVs containing markers of the belonging cells have been found in bodily fluids including blood, lymph and cerebrospinal fluid (CSF), thus reaching distant targets widely far from their site of origin, acting as long-range messengers across organs [3, 6]. Moreover, EVs accumulate high levels of toxic proteins or biomarkers that are associated to the disease course. For example, EVs released from inflammatory cells also increase in pathological conditions and carry inflammatory cargoes. Thus, their isolation from peripheral body fluids may represents a useful diagnostic tool to detect early phases of inflammatory diseases as well as degenerative pathologies or cancer [7].

Furthermore, considering the EV key function as natural mediators in cell-cell communication and low immunogenicity, they are promising candidates as drug delivery in the treatment of numerous pathologies and in tissue regeneration [8].

In spite of numerous potentialities of EVs in diagnostic and therapy of brain diseases, in this work I tried to comprehend more closer the way by which glia-derived EVs move extracellularly and carry their cargoes far from the cell of origin to reach the recipient neuron. I found that glial EVs use neuronal processes as highways to move between connected neurons and to reach preferential contact sites on the somatodendritic region of target neuron.

1.1 EVs CLASSIFICATION

For long time extracellular vesicles have been for long time considered artefacts or debris released form degenerated or dead cells [5]. First evidence of EVs in literature goes back to the 1946 and 1967, when platelet-derived EVs were referred to as 'platelet dust' in normal plasma [9, 10]. EVs were also observed in matrix during bone calcification by Anderson in 1969 [11]. In the 1970-1980s, independent studies reported the presence of plasma membrane vesicles from rectal adenoma microvillus cells [12], virus-like particles in human cell cultures and bovine serum [13, 14] and in seminal plasma [15]. In the same years tumour derived procoagulant membrane fragments were observed for the first time [16, 17]. We must wait till 1983 to have a detailed ultrastructural study showing that a subpopulation of vesicles, that we now commonly call exosomes, were also released by multi-vesicular bodies (MVBs) fusing with the cell membrane during the maturation of reticulocytes [18-20]. In 1991, Stein and Luzio introduced the definition of exocytosis and describe the shedding of vesicles from the plasma membrane of stimulated neutrophil [21], opening to the ectosome nomenclature. Subsequentially, in 1996 Raposo and colleagues demonstrated that exosomes (this name was assigned in this work for the first time), isolated from Epstein-Barr virus transformed B lymphocytes, were antigen-presenting and able to induce T cell responses [22]. When finally in 2006-2007, EVs were discovered to contain RNA, including microRNA, they acquired a renewed interest in intercellular communication studies [23, 24]. Hereafter EVs have been isolated and studies in most cell types and body fluids, i.e. cerebrospinal fluid, blood, urine, faeces, saliva, seminal fluid, breast milk, amniotic fluid, synovial fluid, bronchoalveolar fluid, nasal secretion, ascites fluid and bile [7, 25].

Traditionally EVs can be classified into exosomes and ectosomes. However, we have to consider that in the latter class, EVs are often given other names, including shedding vesicles, microvesicles, exosome-like vesicles, nanoparticles, microparticles, and oncosomes [5]. This classification is based on the different site and membrane of origin of exosomes and ectosomes [5]. Exosomes are released into the extracellular space by the merger of a mature multivesicular body (MVB) containing intraluminal vesicles (ILVs) with the plasma membrane of the cell [26].

ILVs originate from the inward invagination of the membranes in early endosomes that become part of multivesicular bodies (MVBs) and undergo a maturation process characterized by a gradual change in the protein composition of ILVs. During this maturation process, the vesicles inside the MVBs can go through three different pathways: can be degraded by fusing with lysosomes, can constitute a temporary storage compartment or merge with the plasma membrane, releasing exosomes that maintain the same topological orientation as the cellular plasma membrane [27]. The most characterized mechanism of exosome release involved the endosomal sorting complex required for

transport (ESCRT) machinery. The ESCRT machinery comprehends four complexes (ESCRT-0, -I, -II, and -III) along with accessory proteins (Alix, VPS4, VTA-1). ESCRT-0 complex recruits ubiquitinated proteins, while ESCRT-I and -II mediate the budding of ILVs. The ESCRT-I subunit TSG101 recruits ESCRT-III complex which forms spirals that induce the inward budding and fission of vesicles in order to form MVBs [5, 27]. Two alternate pathways of exosome formation have been recently described. The first involves synthesis of ceramide as a mechanism to induce vesicle curvature and budding, while the second is tetraspanin-mediated (CD63, CD81, CD82, CD53 and CD37) pathway [28].

The budding of ectosomes occurs directly from the limiting plasma membrane and is a process that does not require exocytosis like for exosomes. Ectosomes shedding in immune cells (dendritic cells, macrophages, microglia) is induced within a few seconds after stimulation of the P2X7 receptor by adenosine-5'-triphosphate (ATP). Ectosome biogenesis utilizes components of the endosomal machinery too, including the Ras-related GTPase ADP-ribosylation factor 6 (ARF6), a small G protein of the Ras family, components of the ESCRT system, annexin-2, small GTPase protein (i.e. Rab11, Rab27 and Rab35) and SNARE (Soluble NSF Attachment protein REceptors) fusion machinery, and is likely triggered by rising of intracellular Ca^{2+} concentrations, which favours phospholipid exchange (i.e. ceramide) between the two leaflets and thus increases the membrane curvature [5, 26, 29].

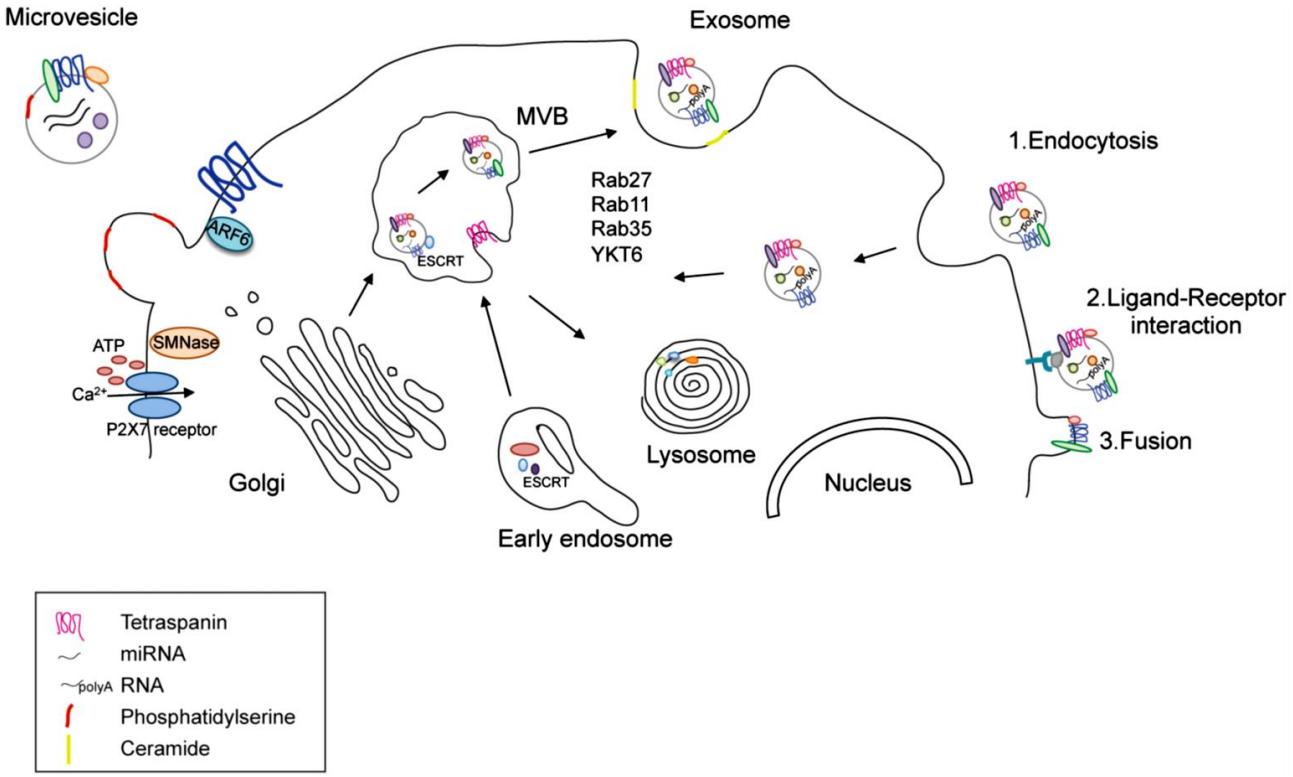

Fig.1: Ectosomes and exosomes release pathways. Ectosomes bud directly from the plasma membrane upon extracellular ATP stimulation of the P2X7 receptor that allows intracellular Ca^{2+} increase. Their membrane is enriched in

phosphatidyl-serine and tetraspanins. They contain cytoplasmic proteins, RNAs and DNAs. Exosomes originate from the exocytosis of MVBs. ESCRT coordinates the cargo loading and vesicle release. Rab GTPases and the SNARE protein coordinate vesicle fusion to the plasma membrane. The cargo content comprises proteins and RNAs like in ectosomes. Exosomes can enter in recipient cells by endocytosis, ligand-receptor interaction or fusion with the plasma membrane [30].

Because exosomes and ectosomes share different elements in the formation process and the scientific community has not yet defined specific markers that can identify with certainty their origin, it is more correct to refer to them as EVs when a specific biogenesis pathway cannot be assigned [31]. In this context, a list of minimal information for studies of extracellular vesicles (the MISEV2018) provides the researchers inside and outside the field of EVs with a guide towards a unique and better definition of EV subtypes. In the MISEV2018 list, EVs are classified based on: *"a) physical characteristics, such as size ("small EVs" (sEVs) and "medium/large EVs" (m/lEVs), with ranges defined, for instance, respectively, < 100nm or < 200nm [small], or > 200nm [large and/or medium]) or density (low, middle, high, with each range defined); b) biochemical composition (CD63+/CD81+- EVs, Annexin A5-stained EVs, etc.); or c) descriptions of conditions or cell of origin (podocyte EVs, hypoxic EVs, large oncosomes, apoptotic bodies). According to the MISEV2018 publication, if confirmation of EV identity cannot be achieved, the use of other terms such as extracellular particle (EP) might be more appropriate"* [31]. On that basis, in this work we will refer to astrocytes-derived medium/large EVs, alix- and flotillin-positive, as EVs.

1.2 EVs Deliver Complex Messages in the Central Nervous System

In the central nervous system (CNS), intercellular communication between glial cells and neurons is crucial for many biological functions: from brain development to neural circuit maturation and homeostasis maintenance. Glia cells not only drive inflammatory responses upon infections or diseases, but they also constantly provide neurotrophic support, and are implicated in circuit remodelling and synaptic pruning. Along with the classical direct cell-to-cell cross-talk and the paracrine action of secreted molecules, glia and neurons communicate by releasing and receiving EVs [32-35]. Emerging evidence indicates that EVs contribute to the regulation of neuronal firing, synaptic plasticity, and myelin formation in the brain [3].

EVs derived from astrocytes, for instance, have been shows to contain neuroprotective and neurite outgrowth promoting proteins such as HSP70 and synapsin I [36, 37]. Another study reported the presence of glutamate transporters (EAAT-1/2) in EVs released by astrocytes that is crucial for neural homeostasis [38]. Both neurons and astrocytes were reported to release Vascular Endothelial Growth

Factor (VEGF) and Fibroblast Growth Factor (FGF), two growth factors which promote vascularization of developing brain, in association to EVs [6].

Moreover, studies of our laboratory showed that EVs released by both microglia and astrocytes critically regulate synaptic transmission, by promoting neuronal production of ceramide and sphingosine. The enhancement of sphingolipid metabolism stimulates excitatory neurotransmission in vitro and in vivo, by favouring presynaptic release probability, supporting the ability of EVs to influence synaptic activity [39]. On the other hand, we provided evidence that microglia-derived EVs modulate presynaptic transmission of inhibitory neurons through the endocannabinoid system. Indeed, we reported that EVs secreted by microglia carry the endocannabinoid N-arachidonoylethanolamine (AEA) on their surface which stimulates type-1 cannabinoid receptors (CB1) expressed by GABAergic neurons and inhibit presynaptic transmission [40].

EVs derived from oligodendrocytes and internalized by neurons at axonal and somatodendritic sites can protect neurons from insults by inducing the transcription of genes involved in the neuronal antioxidant response, such as catalase and superoxide dismutase [41, 42]. Oligodendrocyte progenitor cells secrete EVs that carry myelin proteolipid protein (PLP), 2'3'-cyclic-nucleotide-phosphodiesterase (CNP), myelin basic protein (MBP), and myelin oligodendrocyte glycoprotein (MOG). These EVs may contribute to balance the production of myelin proteins and lipids and, therefore, can be part of the mechanism that controls myelin membrane biogenesis [43].

Not only glial EVs but also neuron-derived EVs are able to influence synaptic transmission. Indeed, it was shown that neuronal EVs can carry synaptotagmin 4 from the presynaptic terminals and transfer the protein to the postsynaptic cells, activating retrograde signaling and synaptic growth [44]. Sorting of specific RNAs into neuronal EVs also plays a role in plasticity-associated protein synthesis at synapses. An interesting study showed that depolarization of differentiated neuroblasts was correlated with a depletion of a set of miRNAs from the neurites, and with concomitant enrichment of the miRNAs in EVs [45]. Furthermore, in the Drosophila neuromuscular junction neuronal EVs were recently shown to package mRNAs in association with the activity-regulated cytoskeleton-associated protein Arc which has been described as a master regulator of synaptic plasticity and maturation [46].

Altogether, these observations indicate that EVs mediate the physiological cross-talk between glial cells and neurons in the brain. By the delivery of specific cargoes such as RNAs, lipids, enzymes, and membrane-bound signaling proteins, EVs alter target cell behaviour either at the cell surface or upon internalization and drive processes such as synaptic plasticity, maintenance of myelination, and neuronal and glial response to brain injury [3].

1.3 EVs IN THE PATHOGENIC BRAIN

In the last few decades, EVs in the CNS emerged not only as cell-cell mediators in physiological conditions, but as active participants in neuroinflammation, tumorigenic activity, and neurodegenerative disorders [34].

One of the first observation supporting the involvement of EVs in pathological brain conditions was that EVs released from reactive astrocytes and microglia are capable to spread proinflammatory signals as they contain the cytokine interleukin-1β (IL-1β), a key initiator of the acute inflammatory response, as well as the IL-1β processing enzyme caspase 1 and P2X7 receptors which drives the cytokine release. Indeed, in response to high levels of extracellular ATP, sites of tissue damage, vesicular P2X7 receptors are activated and drive IL-1β processing and release in the extracellular space [47, 48].

More recently, we found that EVs released by inflammatory microglia and astrocytes produce EVs i) contain and transfer IL-1β transcript among glial cells in vitro [7] and ii) are enriched in miR-146a-5p and other miRNAs that target synaptic proteins such as the postsynaptic adhesion protein Neuroligin 1 (NLGN1) and the synaptic vesicle protein Synaptotagmin 1 (Syt1) in the recipient neurons. Glia-to-neuron miRNA transfer leads to loss of excitatory synapses upon chronic exposure to EVs, unveiling a novel mechanism by which glia-derived EVs impact synaptic stability and strength under chronic neuroinflammation [49]. EVs have also been described to propagate neuroinflammation to the periphery. Indeed, in a mouse model of IL-1β-induced neuroinflammation, it has been shown that astrocyte-derived EVs enter the peripheral circulation and induce an acute cytokine response in the liver and promote leukocyte transmigration to the site of brain inflammation [50]. In addition to IL-1β, EVs produced by reactive astrocytes and microglia contain metalloproteinases and the cytokine TNF-alfa, which disrupts the blood brain barrier (BBB) and opens the brain to the infiltration by immune-cells by enhancing nitric oxide production and promoting the degradation of the extracellular matrix and cell junctions [51].

Farther, brain tumor derived-EVs can modulate the immune system promoting an immunosuppressed phenotype that favours cancer escape from immunosurveillance while EVs derived from cancer brain cells can cross the BBB and enter the circulation, participating to metastasis dissemination [52]. Interestingly, an elegant study recently showed that astrocytes interact with brain tumor cells via EV secretion of miRNAs that are able to inhibit the expression of the tumor suppressor gene PTEN in brain cancer cells, thus promoting brain tumor oncogenicity [53].

The typical trait of many neurodegenerative disorders is the accumulation of pathogenic proteins in aggregate form. The diffusion of these misfolded proteins seems to follow a prion-like manner, as they have the propensity to change the conformation of the physiological shaped protein and

propagate through different brain regions [3]. The pathogenic misfolded proteins reported to be released in association with EVs include prions in Creutzfeldt-Jacob disease (CJD) [54], β-amyloid (Aβ) peptide and tau in Alzheimer's Disease (AD) [55], α-synuclein in Parkinson's disease (PD) [56], superoxide dismutase (SOD) [57] and transactive response binding protein-43 (TDP-43) [58] in amyotrophic lateral sclerosis (ALS) and frontotemporal lobal degeneration. Since toxic proteins involved in neurodegenerative diseases have been found in EVs isolated from the CSF, it was proposed that EVs can participate in disseminating the pathogenic proteins to larger brain areas over time. However, a large body of evidence indicate that EVs may stimulate the clearance of the protein aggregates [29, 30, 59, 60]. For example, EVs released by microglia upon 5-HT receptors stimulation were shown to contain the insulin-degrading enzyme (IDE), which degrades Aβ, supporting a role for EVs in containing or preventing the pathology progression [34, 61].

A study conducted in our laboratory showed that EVs produced from microglia exposed to Aβ, to mimic in vitro the presence of Aβ plaques, carry toxic Aβ species, which affect the morphology and density of dendritic spines in hippocampal neuron in culture. Specifically Aβ-storing EVs, induce a decrease in total and mature spines, causing a loss of excitatory synapses [62]. Another work reported that astrocytes surrounding amyloid plaques were apoptotic and released EVs enriched in PAR-4, a ubiquitously expressed proapoptotic tumor suppressor protein, and ceramide, a key component in the regulation of apoptosis. Astrocyte apoptosis was not observed in neutral sphingomyelinase 2 (nSMase2) knock-out mice, where exosomes biogenesis is inhibited, supporting a role of glial EVs in cell damage associated to the neurodegenerative disease [63].

The contribution of glial EVs to AD was supported by data revealing that the production of microglial EVs is higher in the CSF of patients with AD and positively correlate with levels of p-tau, a biomarker of degeneration, and with hippocampal atrophy observed in MRI studies [64]. Similarly to Aβ-storing EVs, EV carry other misfolded proteins, i.e. prions, α-synuclein, mutant SOD1, or TDP-43 were shown to be toxic for wild-type (WT) recipient cells [54, 56, 58, 65] and to propagate cell damage among connected brain region.

For example, in the PS19 *transgenic* mouse model of AD (which develops tau aggregation by 3 months of age) propagation of tau aggregates from the entorhinal cortex to the dentate gyrus was inhibited by addition to the EC of GW4869, a brain penetrant inhibitor of exosome biogenesis [66]. In another AD model GW4869 was found to lower the amount of Aβ plaques [67], further supporting the capacity of EVs to transfer misfolded proteins throughout brain regions in the course of neurodegenerative diseases [30]. Consistent with this hypothesis, recent evidence showed that sEVs containing tau and Aβ can be internalized and transferred among neurons exploiting axonal projections [68]. However, how large EVs can move across synapse and reach distant cell targets

remains unknown. The analysis conducted in this thesis work aimed to investigate the mechanisms that might drive the transfer of astrocyte-derived EVs among neurons in vitro, with the future goal to define a novel strategy to limit the spreading of neurodegenerative diseases in the brain tissue.

1.4 *IN VITRO* AND *IN VIVO* IMAGING OF EVS

Extracellular vesicles have been highly investigated in many contexts exploiting different approaches [69]. Among these, imaging techniques offer the exclusive possibility to characterize spatiotemporal properties of the EV trafficking and interaction with target cells, and to visualize and label EV content. *In vitro* and *in vivo* EV imaging approaches provide different information. *In vitro* EV imaging gives an important contribution in understanding the mechanism of EV release and uptake, in identifying surface biomarkers [70] and investigating single EV-cell interaction [71]. *In vivo* imaging represents a useful method to study the biodistribution of EVs, to examine their invasive ability in pathophysiological conditions or characterize the pharmacokinetic properties of EVs as drug vehicles in theranostics [70].

Despite the fundamental insights provided by EV imaging, it should be taken into consideration that it may be very hard to detect EVs, especially small EVs (≤ 200 nm), because of their small size. While EVs larger than 200 nm in diameter can be detected using the light microscopy resolution, small EVs need to be labelled to amplify the signal and be identified [70].

By confocal live-imaging microscopy and the use of mCherry labelled EVs, Heusermann and colleagues showed that sEVs are very efficiently and quickly taken up by primary human fibroblasts and that most exosomes are internalized through endocytosis at the base of filopodia. To perform live-imaging experiments, Heusermann and colleagues generated sEVs from HEK293 (Human embryonic kidney 293) cells containing CD63 fused to GFP or mCherry. Interestingly, they observed that EVs uptake was preceded by the surfing of EVs on the surface of filopodia [72]. By labelling EVs with the self-quenching dye R18, we recently provided evidence that glial EVs can fuse with the plasma membranes of recipient neurons as highlighted by an increase in the EV fluorescence upon dilution with the plasma membrane of the target cells [49, 73].

Several microscopy studies combined to the use of labelled EVs showed that EVs accumulate in the endocytic or phagocytic compartments following uptake by the recipient cell, in an actin cytoskeleton, phosphatidylinositol 3-kinase activity, and dynamin-2 dependent way [74-76].

Beyond fluorescent microscopy, the best method to visualize EVs is represented by electron microscopy. Despite the sample is fixed or immobilized, transmission electron microscopy (TEM), scanning electron microscopy (SEM), atomic force microscopy (AFM) and cryo-electron microscopy (cryo-EM) provide detailed information about the inner and outer structure of EVs [70]. Compared

to traditional EM methods (TEM and SEM), cryo-EM allows a superior sample quality and morphology preservation [77] and is emerging as the most popular technique to characterized EVs [77-82]. Using this approach, EVs from human mast cell line (HMC-1) were classified in different categories according to their morphology and other peculiar features, e.g. distinguishing coated EVs with surface protrusions, from electron-dense EVs and from filamentous EVs, containing filaments in their lumen [79]. The latter vesicles population usually shows a tubular and elongated shape [78, 79].

Elegant strategies have also been recently developed to monitor EVs *in vivo*. Wiklander and his group characterized the biodistribution of EVs isolated from three different cell types and labelled with fluorescent lipophilic tracer DiR (1,1-dioctadecyl-3,3,3,3-tetramethylindotricarbocyanine iodide), after systemic delivery in mice. They found that the different origin of EVs, the dose and the route of administration influence the body distribution [83]. In addition to DiR, PKH67 and PKH26, lipophilic fluorophores which use aliphatic tails to anchor into the lipidic bilayer, have been widely used to label and study EVs *in vivo* [84]. However, these lipophilic dyes can aggregate and form micelle therefore generating false signals of EVs that last even after the real EVs are degraded.

Therefore, monitoring single EV in vivo, in the rodent brain, remains still challenging. To overcome these limitations, a recent study exploited zebrafish embryos, which are natural transparent, to study the interaction of circulating EVs expressing D63pHluorin with the surface of vascular endothelium, found that EVs are internalized by scavenger receptors in a dynamin-dependent manner. Interestingly, the uptake of EVs occurred via filopodia surfing by patrolling macrophages present in the lumen of blood vessels of the caudal vein plexus [85].

Another remarkable in vivo work carried out with computational tomography of C57BL/6 mice after intranasal administration of MSC-derived exosomes labelled with glucose-coated gold nanoparticles, showed a homogeneous distribution of EVs in control brain compare to that in the ischemic brain where they accumulate in the site of the injury [86].

Besides these fascinating results showing that EVs can diffuse in neighbouring tissues, up to now it is not clear if there is a specific mechanism that regulate migration of EVs within the brain parenchyma.

To study the interaction of EVs in their native shape with target cells and investigate their motion at single cell level, in our laboratory we have recently developed an in vitro technique that allows to image with high temporal and spatial resolution the EV-cell interface. This approach exploits optical manipulation: specifically, an infrared laser beam collimated into the optical path of a confocal microscope is used to trap single EVs added to a coverslip containing a cell monolayer and to deliver them to the surface of a specific target cells. In a previous work published by my lab colleagues, we

exploited optical tweezers to deliver microglial-derived EVs on the surface of glial cells, astrocytes and microglia in primary culture, and showed that they efficiently adhered to the cell surface [71]. Interestingly in some cases adhesion was not followed by fusion or rapid internalization but by EV motion on the surface of the glial cell, suggesting a novel mechanism which may underlie the migration of EVs described in *in vivo* studies [71].

2 PRION PROTEIN (PRP)

Cellular prion protein (PrP) is a GPI-anchored protein expressed on the cell surface of many tissues and organs, with a high expression in the central and peripheral nervous system [87]. PrP is well known for its role in prion diseases, transmissible spongiform neurodegenerative pathologies characterized by PrP misfolding and aggregation including Creutzfeldt-Jakob disease (CJD), Gerstmann-Sträussler-Scheinker (GSS) syndrome, Fatal Familial Insomnia (FFI), and kuru [88]. Research on the role of PrP in the CNS led to a significant number of studies that report the involvement of PrP in a wide spectrum of cell brain activity comprising development, cell adhesion, synaptic mechanisms and excitability, memory, circadian rhythm, neuroprotection oxidative stress and metal homeostasis [89].

PrP is encoded by the *PRNP* gene and is synthetized as a precursor protein of 253 amino acids. An N-terminal signal peptide then drives the protein to enter the endoplasmic reticulum (ER). Here, the precursor protein is subjected to the cleavage of a C-terminal signal peptide and addition of a glycophosphatidylinositol (GPI) anchor [90]. Removal of both N- and C-terminal signal sequences results in a mature protein of 208 amino acids. The N-terminal domain is intrinsically disordered but contains four conserved tandem repeats of a sequence of eight amino acids. A hydrophobic section divides the N- and C-terminal domains and might be involved in PrP dimerization [91, 92]. The PrP C-terminal domain has a globular structure and comprise three α-helices, two β-strands and interconnecting loops [93]. The majority of PrP is generally di-glycosylated. After passing through the ER, PrP moves to the Golgi apparatus where the N-linked glycans mature and the protein is sorted for trafficking to the cell surface. Once there, the GPI anchor attaches PrP to the extra-cytoplasmic face of the cell membrane, specifically in microdomains called lipid rafts [94]. Interestingly, PrP is found not only at the cell surface, but can be subjected to cycles of internalisation followed by trafficking back to the cell membrane via recycling endosomes, a process that serve to control the cell surface pool of PrP [95]. Furthermore, there are reports that PrP can be present in the nucleus [96-98] and in mitochondria [99, 100]. Nevertheless, the functional form is that present on the cell surface.

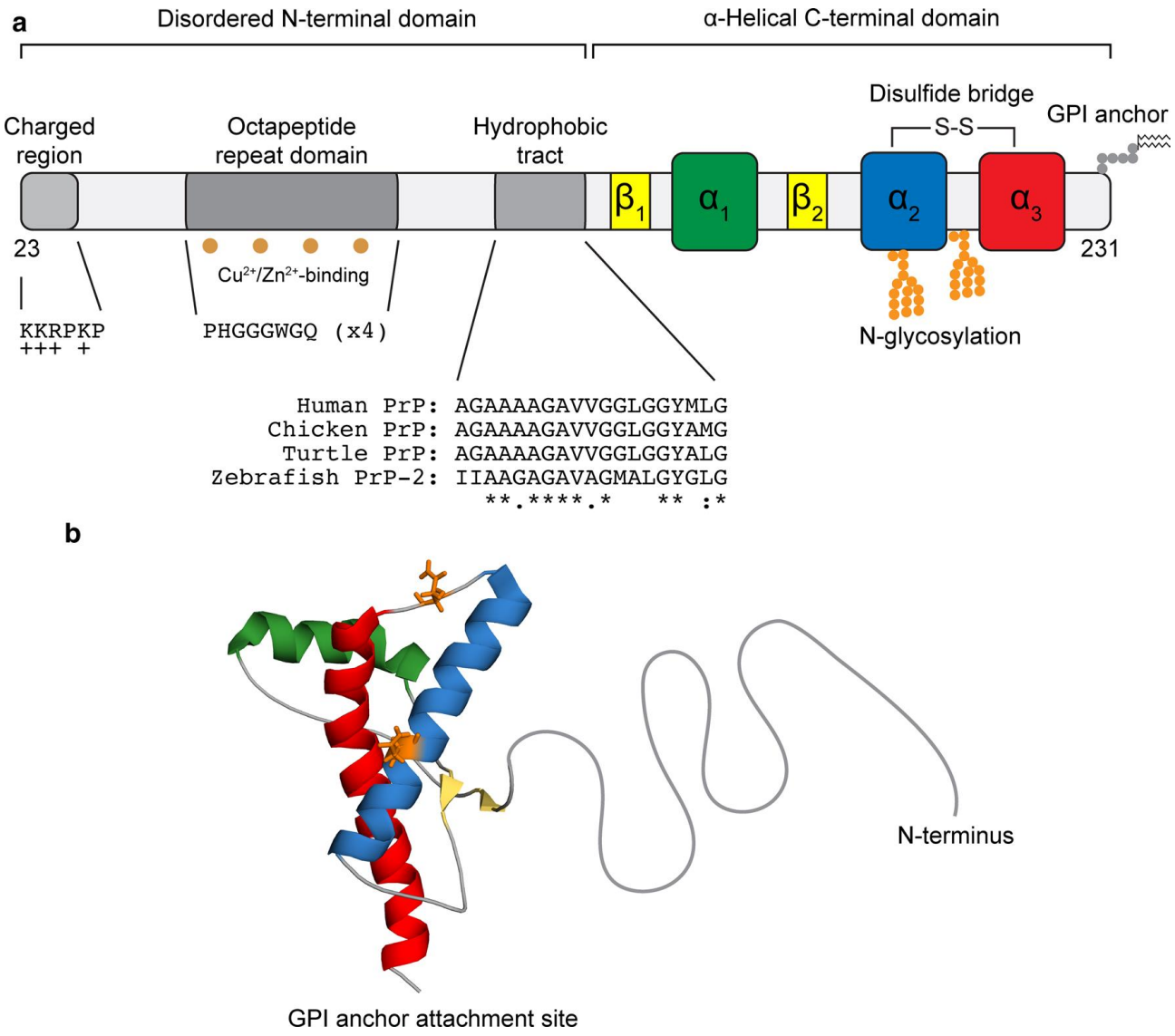

Fig.2: Cellular human PrP structure. a: PrP can be divided into two distinct domains: a N-terminal disordered domain and a C-terminal α-helical domain. N-terminal domain contains a positively charged region at the N-terminus that is important for the endocytosis of PrP, a series of four octapeptide repeats that allow PrP to bind divalent metal cations such as Cu^{2+} and Zn^{2+}, and a hydrophobic tract that is highly conserved. The C-terminal domain consists of three α-helices and two short β-strands. Up to two N-glycans can be added within the α-helical domain, a disulphide bridge links helices 2 and 3, and a GPI-anchor attaches PrP to the outer surface of the plasma membrane. **b:** Three-dimensional structure of recombinant human PrP (from PDB database) residues 121–230 at pH 7.0 determined by nuclear magnetic resonance (NMR) spectroscopy and rendered using PyMOL [101]. The location of the asparagine residues that become N-glycosylated is indicated in orange and the intrinsically disordered N-terminal domain, not present in the NMR structure, is shown as a theoretical representation [102].

2.1 PHYSIOLOGICAL ROLE OF PRP IN THE BRAIN

PrP expression in the brain appears to increase throughout development, reaching a peak in young age and reducing slightly toward the adulthood [103, 104]. In the CNS PrP is expressed not only in neurons but also in astrocytes [105, 106], oligodendrocytes [107, 108], and microglia [104].

Among PrP functions already cited in the previous paragraph, it has been reported that PrP is protective against **oxidative stress**. Indeed, PrP expression by primary neurons, astrocytes and cell lines has been associated with a lower level of damage upon exposure to different oxidative toxins [109, 110]. PrP may protect neurons by modulating the activity of the antioxidant enzymes that convert ROS into less toxic products [111-113] given that SOD and glutathione peroxidase activities are reduced in absence of PrP. Alternatively, PrP may translocate to the nucleus in response to DNA damage induced by oxidative stress and directly activate the base excision repair pathway [114]. Moreover, PrP may lead to a stress-protective release of calcium ions from the ER stores through activation of the tyrosine-protein kinase Fyn [115].

Other studies support the involvement of PrP in **cell differentiation**, by showing that PrP promotes neurite outgrowth via interaction with stress-inducible protein 1 (STI1) [116], NCAM1 [117], epidermal growth factor receptors [118], integrins [119], laminin [120], or metabotropic glutamate receptors (mGluRs) [121]. The downstream signalling responsible may involve inhibition of the Rho-associated protein kinase (ROCK) pathway [119]. The inhibition of this signalling pathway destabilises the actin cytoskeleton, thus promoting the development of filopodia (dynamic protrusions from the growing neurite cone that respond to the extracellular environment to drive migration of the developing process) [122]. A recent study published by Amin et al., showed that soluble PrP release extracellularly interacts with membrane-anchored PrP to promote neurite outgrowth and facilitate the growth cone guidance [123]. Interestingly, PrP may also have an evolutionarily-conserved role in regulating **cell adhesion.** Indeed, zebrafish PrP can regulate the connections between adherens junctions and the actin cytoskeleton, mainly by affecting the localisation of E-cadherin and β-catenin to these junctions [124, 125]. PrP, interacting with the zebrafish NCAM1 ortholog, could exert this function activating the signalling of the Src family of tyrosine-protein kinases [117, 125]. In a similar way, PrP expression has been shown to promote guided differentiation of neural precursors into neurons, astrocytes and oligodendrocytes [126, 127].

PrP is also involved in the modulation of **neuronal excitability**. Indeed, PrP inhibits the activity of NMDARs containing the GluN2D subunit, in prion diseases and neurodegenerative disorders, where NMDAR-mediated excitotoxicity contributes to neuronal death [128, 129], thus protecting neurons from excitotoxic death [130]. Moreover, PrP-expressing adenovirus construct injected into rat brains

were shown to reduce infarct volume and neuronal death after transient or permanent middle cerebral artery occlusion [131, 132].

Given that PrP can modulate neuronal excitability, it was expected that the lack of PrP expression may affect **synaptic plasticity**. Indeed, PrP-knockout mice were reported to be have disrupted hippocampal long-term potentiation (LTP), a form of synaptic plasticity involved in memory formation [133]. These mice also display abnormal behaviour in nest building and novel environment exploration tasks compared to wild type controls [134], while infusion of a peptide containing the putative PrP-binding site of stress-inducible protein 1(STI1) restores the deficits [135].

A role of PrP in **sleep and circadian rhythm** regulation has also been proposed. This can explain the disruption of sleep pattern that occurs in both sporadic and FFI prion diseases [136, 137]. PrP-knockout mice exhibit altered circadian rhythm, sleep fragmentation and increased slow wave activity that follows insomnia [138]. Since it is reported that calcium-dependent hyperpolarization is critical for sleep maintenance, and that sleep deterioration is associated with the impairment of calcium-dependent potassium channels, voltage gated calcium channels and NMDA receptors, sleep impairment might result from loss of PrP modulation of these channels in PrP-knockout mice and in prion diseases [139].

Further evidence supports a role for PrP in **iron homeostasis** and focused on PrP ability to bind and coordinate up to six Cu^{2+} ions at the cell membrane through the octapeptide repeat region [140-142]. PrP interactions with Cu^{2+} is involved in the regulation of NMDAR activity [143], astrocytic glutamate uptake [144], protection against oxidative stress [112, 145] and maintenance of Cu^{2+} homeostasis in the placenta [146] and play a role in the physiological uptake of iron by cells. *In vivo* studies showed that PrP-null mice display lower total levels of iron in the brain, spleen and liver compared to wild type controls [147, 148]. In the blood, the circulating iron is in the form of Fe^{3+} bound to transferrin [149]. However, Fe^{3+} must be reduced to Fe^{2+} by a ferrireductase to enable uptake by cells. PrP itself may have binds through its octapeptide repeat region to a ferrireductase in order to modulate its activity and may act to enhance iron uptake [150].

2.2 PRP RECEPTORS AND SIGNAL TRANSDUCTION

In the previous paragraph I described the different contexts in which PrP may be involved in physiological brain functions. To exert such activities PrP directly or indirectly interact with a series of molecules, some of them already cited above. Since PrP is a GPI-anchored protein lacking a cytosolic domain, it needs to interact with at least one co-receptor to mediate downstream signalling. Among potential co-receptors of PrP there are NCAM1 and mGluRs, which may be involved in PrP-dependent neurite outgrowth [117, 121]. Moreover, the extracellular matrix protein laminin may act

as a PrP ligand [120] to activate neuritogenic signalling downstream of mGluRs [121]. Equally, STI1, a heat shock protein released by astrocytes [106] may form a complex with nicotinic acetylcholine receptors and PrP and activate the acetylcholine receptors and consequently pro-survival and neuritogenic signalling [151].

PrP is a putative receptor also for cytoskeletal proteins, such as tubulin and vimentin [152, 153]. Alternatively, PrP could interact with cytoskeletal proteins indirectly. Desmoplakin, for example, could provide the link between PrP and tubulin or vimentin, since desmoplakin interacts with the microtubule-binding protein (MBP) [154] and with vimentin intermediate filaments [155].

Many studies showed the involvement of PrP in the neuropathology of AD. In particular, it has been observed that PrP is a high affinity receptor for oligomeric Aβ and can participate to the propagation of Aβ toxicity. However, other works reported that PrP is not responsible for cognitive impairment in AD despite it binds to Aβ oligomers [156-158].

Most of the proteins that appear to interact with PrP may merely be part of the same multiprotein complexes rather than being direct PrP binding partners. Alternatively, the relatively flexible structure of the PrP N-terminal domain may allow the protein to bind directly to multiple partners [159].

Evidence suggests that PrP expression affects the activities of the ERK1/2 [116, 121, 160] and PI3K-Akt signalling pathways [118, 161, 162], both involved in functions ascribed to PrP such as regulation of protein synthesis [161] and autophagy [163, 164]. Furthermore, PrP appears to modulate cAMP-PKA signalling, which stimulates myelin maintenance in the peripheral nervous system [165] and promotes cell survival [116].

PrP expression could also trigger signalling through Src family kinases, mediated by Fyn kinase [115, 166], leading to changes in cell adhesion properties [125] and at the same time potentially affecting glucose uptake [167]. Finally, PrP dependent regulation of several pathways, including RhoA-ROCK [119] and PKC [121] signalling, has reported to contribute to changes in cell morphology, such as neuritogenesis.

The flexible structure of PrP, the variety of binding partners and the strategic localization in lipid rafts suggest that PrP could serve as a dynamic platform on the cell surface with the capability to assemble multicomponent complexes and trigger different signaling pathways, according to the physiological state of the cell and the specific subtype [168].

3 NEURONS

In the central nervous system, neurons are the specialized cells that transport rapid and precise information to other neurons in different areas of the brain through electric and chemical signals. The ability to deliver fast messages is due to their special morphology and structure. Indeed, neurons are made up of three main compartments: the soma or cell body, containing the nucleus and from where depart two types of cell processes: dendrites that deliver incoming messages and the axon, the transmitting element for the transport of outcoming information [169].

During neuronal development axons and dendrites acquire molecular distinctions as soon as cytoskeletal and synaptic proteins are targeted to these compartments. The cytoskeleton, indeed, determines the shape of the cell and is responsible for the asymmetric distribution of organelles within the cytoplasm. It includes three filamentous structures: microtubules, microfilaments and neurofilaments [169].

3.1 NEURONAL CYTOSKELETON: STRUCTURE AND DYNAMICS

The ability of neurons to transmit their information to the neighbouring ones depends on the polarized organization of dendrites and axon defined by the cytoskeleton [170].

The neural cytoskeleton, comprising actin filaments (f-actin), microtubules and neurofilaments, provides structural support during neuronal development, maintains the cellular architecture and compartmentalization and permits cellular migration and intracellular trafficking [171-173]. To perform these functions, the cytoskeleton also makes use of cytoskeletal-associated regulatory proteins, which are extremely important during neuronal development and migration [172, 173]. Moreover, motor directional transport of cargoes is influenced by cytoskeletal characteristics (density, orientation of filaments and post-translational modifications), presence of cytoskeletal binding proteins and polarization of microtubule and f-actin [174].

Notably, neurological disorders can result from abnormalities in the machineries controlling the cytoskeletal cargo trafficking underlining the importance of the directional transport pathways in neurons [175, 176].

The most highly dynamic structures implicated in intracellular cargo transport are actin filaments (f-actin) and microtubule polymers which extend from the barber end (+ end) of actin and the plus (+) end of microtubules adding respectively ATP-bound G-actin monomers and GTP-bound α/β-tubulin heterodimers (Fig.3) [177, 178].

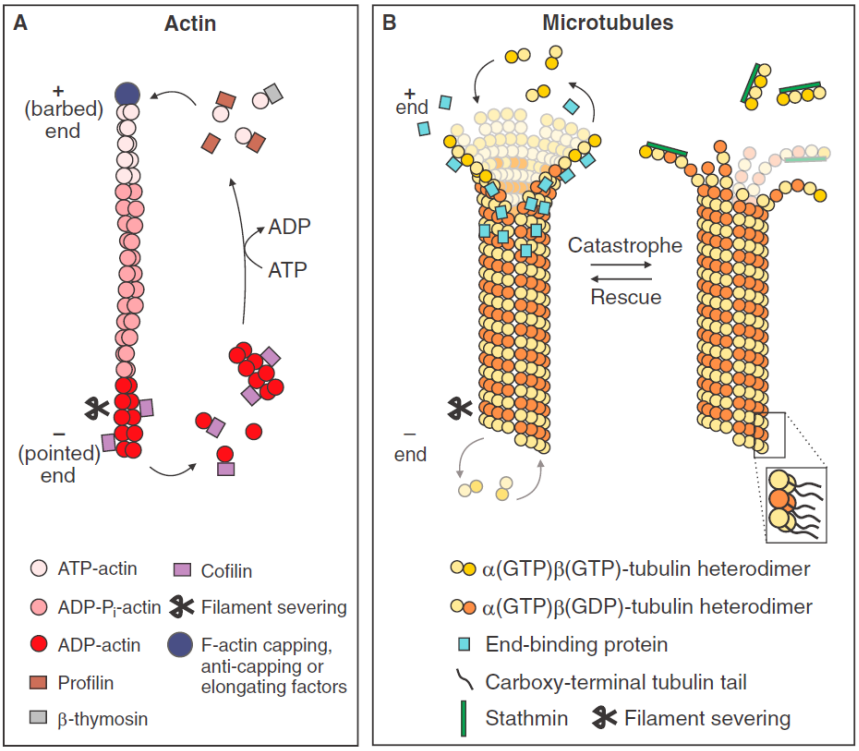

Fig.3: Actin and microtubules structure and dynamics. A: Schematic representation of actin polymerization and depolymerization. The addition of ATP-actin monomers occurs at the + end of the filament hydrolysing actin to ADP-actin. This process is mediated by profilin or barber-end-bound factors (such as formin). At the barber end also act proteins (such as b-thymosin) able to sequester G-actin and limit the polymerization rate. Depolymerizing factors (for example cofilin), indeed, can remove F-actin from the pointed end (- end) of the filament. Actin monomers that exchange their ADP for ATP can be newly bounded to the growing + end. **B:** Schematic representation of microtubules polymerization and depolymerization. Microtubule growth occurs faster at the + end by the addiction of α(GTP)/β(GTP)-tubulin heterodimers. The α(GTP)/β(GDP)-tubulin heterodimers bounded can be hydrolysed. Dynamics of polymerization of microtubules can be influenced by end-binding proteins and α/β-tubulin heterodimers availability. Sequestration of heterodimers by stathmin is an example through which microtubule catastrophe can occur [179].

Both actin and microtubule structures have been visualized and studied in fixed and stained samples by combining super resolution microscopy and live imaging, or through traditional- and cryo-electron microscopy [180, 181].

High concentration of f-actin has been found in the growth cone, the motile tip of the growing axon, along the axon like ring arrangements (located below the cell membrane with a periodicity of about 190 nm), in the axon initial segment organised in actin patches (that can be precursors of philopodia) and in dendritic spines (Fig.4) [180, 182-184].

In the neuronal **growth cone** actin polymerization occurs close to the plasma membrane. Four classes of protein regulate this process: formins, the Arp2/3 complex, tandem-monomer-binding nucleators and the Ena/VASP family [185]. Formins facilitate filament elongation, Arp2/3 complex is essential for the formation of filopodia and branching, tandem-monomer-binding nucleators induce branched

actin networks and neurite growth and the Ena/VASP family are required in filopodia formation and neurite initiation [185-188]. The Arp2/3 complex is involved in both axon and dendrite growth cone formation as it nucleates f-actin from a central region (C-domain) of the growth cone towards the cell periphery (P-domain) at a characteristic 70° angle, generating pushing forces against the plasma membrane, consistent with its prominent role in the maturation and enlargement of dendritic spines [189]. Actin polymerization is negatively regulated by capping proteins, such as epidermal growth factor receptor pathway substrate 8 (Eps8) and actin monomer-binding or 'sequestering' proteins, including profilin and b-thymosin [190, 191].

Nucleation of actin filaments at the edge of the growth cone generates a protrusive force upon the plasma membrane, while inversely regulator molecules which inhibit polymerization produce a '**retrograde flow**' [192]. Among them, there are actomyosins, whose contractile action either in the growth cone T-domain (between the P- and C-domains) or the spine neck generates actin retrograde flow and compete with actin protrusive forces [193]. Retrograde flow attenuates during the maturation of dendritic filopodia into stabilised spines and during the interaction of the growth cone with cell adhesion or 'clutch molecules', such as extracellular N-cadherin in primary rat hippocampal neurons [194].

In contrast to retrograde actin flow, during the axon maturation, the growth cone presents structures called **actin 'waves'** that periodically emerge from the base of the axon and diffuse up to the tip of the growth cone in an anterograde direction [195]. Actin waves are actin-based membrane deformation associated with outbursts of the growth cone that retracts at the tip when the wave leaves the soma and then grows forward when the wave reaches the growing cone (Ruthel and Banker, 1999). Actin waves have been reported in dendrites during neuron maturation and disappear when the process contacts other neurons [196, 197]. They exert a key role in neurite outgrowth and cell polarization and migration [198].

Actin waves have been also described to play a role in the transport of f-actin (in the CNS is about 0.4 mm per day) [199] and of actin-associated proteins such as shootin1, cortactin, cofilin, Arp2/3, ezrin, and Slingshot [196, 200, 201] and it has been demonstrated that actin-associated proteins are connected to the directional polymerization and depolymerization of actin filaments during wave migration [201].

This protein transport is 10 times slower than other motor protein-based transport (e.g. kinesin and dynein that is 2-4 mm per day) and can be linked to a slow motion compared to the fast transport that occurs along microtubules [198].

By sub-diffraction microscopy techniques, periodic cortical actin structure, called **actin rings**, were recognised in the actin cytoskeleton. These structures are present in dendrites, dendritic spines and

axons [202]. They are circumferential rings spaced at 190 nm and connected by tetramer of spectrin composed of βII-spectrin (also known as SPTBN1) and a still unknown a-spectrin subunit [184]. Actin rings also contain adducin, a capping protein that binds to and stabilizes the ends of short f-actin [203]. This structure play a role in neurite shaping, organization of proteins along the plasma membrane [184], stabilizing microtubules [204] and influencing spine neck elasticity during organelle transport [205].

Actin rings are also found in the axon initial segment (AIS) along with **actin patches**, little areas of a few µm enriched in branched f-actin [206] present also in dendrites which serve as outgrowth points for filopodia [207] or to sort vesicular transport by capturing myosin-bearing vesicles [208].

Finally, both axon and dendrites possess actin **hot spots**, highly dynamic structures where actin continuously polymerize and depolymerize, and longitudinal actin fibres also called '**actin trails**', long bundles of actin polymers (average length of 9 µm) that traverse the lengths of processes in both anterograde and retrograde directions [199, 202]. Actin trails emerge from hot spots regions and function as a nidus of polymerization from which the actin fibres elongate. This process of polymerization is very fast and is mediated by formins [209].

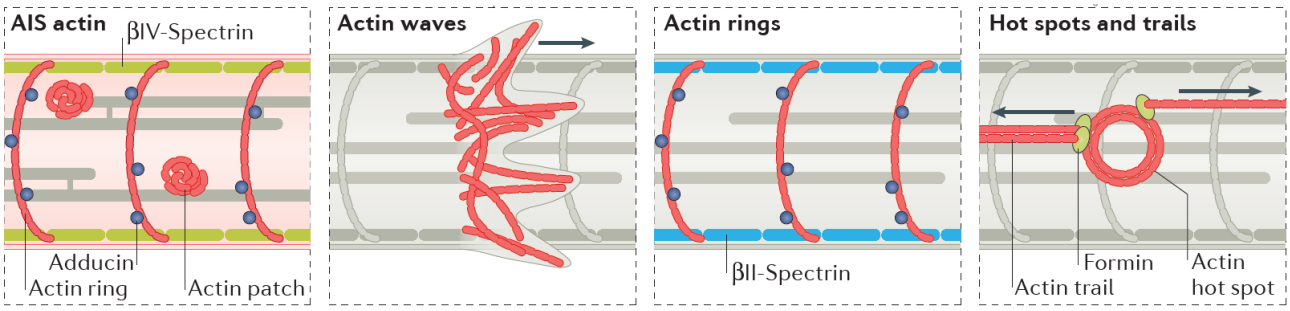

Fig.4: Actin organization in neurons. Actin in the AIS (first panel) organizes as 190 nm periodic rings and clusters patches (present also in dendrites). Actin waves (second panel) emerge from the base of the axon and run along the growth cone. In the distal axon and dendrites (second panel), actin rings are seen along with long actin polymers (last panel) that represent hot spots and actin trails whose nucleation is mediated by formins (in green). Spectrins, βIV in the AIS (first panel) and βII along the distal axon (third panel), connect actin rings and show the same 190 nm periodicity (modified from [199]).

Analysis of **microtubules** by cryo-electron microscopy revealed that they are differently oriented in axons and dendrites. While in axons microtubules are uniformly orientated with their + ends directed towards the tip, dendrites contain a mixture of distal plus-end and distal minus-end microtubules [210]. The polarity in axon develops from 80% to 100% of distal plus-end during maturation [211]. Compared to f-actin (diameter about 6 nm) microtubules are easier to visualize as they are 25 nm in diameter. Although they are densely packed in filaments reaching up to 100 filaments per μm^2 in

thinner axons [212], it is possible to discriminate between individual microtubules thanks to super resolution techniques [213].

At the AIS microtubules organize in tight bundles connected by electron-dense crosslinkers [214]. Among them, the tripartite motif-containing protein 46 (TRIM46) was shown to drive the establishment of uniformly oriented microtubules at the axon entrance [215]. Moreover, another microtubule associated protein, microtubule crosslinking factor 1 (MTCL1), was recently discovered to participate in maturation and maintenance of the AIS region in cerebellar Purkinje cells [216].

Microtubules can growth at a speed rate ranging from 1 to 100 μm per hour, however it is still debated how microtubules are supported in this fast elongation. Particularly, the question involves microtubule nucleation (new microtubules polymerization) and how they are eventually transported in the growing part of the process [199]. Microtubule nucleation is a kinetically unfavourable process that requires both a seed structure and accessory factors that increase nucleation activity [217]. It has been suggested that microtubules are nucleated at the centrosome situated in the cell body and cleaved by katanin and spastin in smaller fragments which are then transported and integrated into longer microtubules [218, 219]. In absence of the centrosome, the microtubule seed is commonly provided by a template of γ-tubulin and associated proteins in a γ-tubulin ring complex (γ-TuRC) [220, 221]. Microtubule fragments can also act as seeds. In this case nucleation occurs by the binding to the β-tubulin on the pre-existing fragment [217]. In addition, Golgi-nucleated microtubules have been described in dendrites of Drosophila melanogaster neurons [222, 223].

Transport of microtubules can be facilitated by motor proteins that, sliding along preassembled microtubules, drive the polymers from the soma into the dendrite [224, 225]. Moreover, during and after neuron maturation the dendrite motor proteins maintain and increase the minus-end distal population by selectively removing + end distal microtubules [226].

Polymerisation and depolymerization, also known as catastrophe event occur more rapidly at the microtubule plus end [227]. The stability of disordered C-terminal domains of α-/β-tubulin tails is determined by post-translational modifications (PTMs), including detyrosination, polyglutamylation and acetylation, which accumulate on more stable microtubules and alter the affinity of motor proteins and regulate the binding to microtubule associated-proteins (MAPs) [228].

MAPs interact with the main body of microtubule filaments and stabilise, bundle or sever microtubules. MAP1b, MAP2 and Tau, for example, stabilise microtubules and mediate microtubule bundling [171, 210, 229]. By contrast, as mentioned above, katanin and spastin are the main abundant severing proteins able to release microtubule fragments from filaments nucleated at the centrosome whose transport along axon and dendrites facilitates distal seeding of new microtubules centrosome-independent [230-232]. The transported fragments are protected from depolymerization at the minus-

end by minus-end-binding proteins (–TIPs) including the recently identified calmodulin regulated spectrin-associated protein 2 (CAMSAP2), that is capable to stabilize the minus ends of microtubule fragments [233]. Both –TIPs and plus-end binding proteins (+TIPs) possess a domain that mediates the interaction between microtubules and actin and regulate processes of catastrophe and polymerization in association with f-actin [179]. Interestingly, the prototypic +TIPs, the microtubule-associated end-binding proteins (EBs), provide a molecular link between the submembrane actin–spectrin complex in the AIS and microtubule fascicles [234] by binding the scaffold protein ankyrin-G [235, 236]. Ankyrin-G is bound to βIV-spectrin an actin binding protein [237]. Moreover, dynein has been proposed to link the microtubules to the actin network at the cell edge through the interaction with the cell surface receptor NCAM [238]. Dynein also generates forces between actin and microtubules in order to prevent the axonal retraction mediated by myosin II upon cortical actin in the axonal shaft [239].

Neurofilaments are the third class of cytoskeletal components in the CNS. They are heteropolymers composed of subunits of low, middle and high molecular weight and are organized in an extensive parallel network in which filaments are interconnected by cross bridges of 3-5 nm [240].

Despite neurofilaments are quite stable polymers, it has been observed that they can move with a velocity that resembles that of fast intermittent cargo transport leading to a ‘stop and go’ model where cargoes move fast but paused for a long time [241]. Neurofilaments are known to be transported as smaller polymers by conventional kinesins and dynein [242, 243] but the underneath mechanism is still unclear.

3.2 CARGO TRAFFICKING IN NEURONS

Intracellular transport of organelles in neurons occurs along microtubules and actin filaments. The intrinsic polarity of these structures and the motor protein determines the directionality of the cargo transported. Motor proteins include kinesins, that move towards the plus-end of microtubules, dynein, moving toward the minus-end of microtubules, and myosins, walking to the plus-end, also called barber end (except for myosin VI), of f-actin. While kinesins and myosins are about ten classes with different cargo-binding regions, there is only one dynein represented by a small set of related isoforms [244]. These motor proteins exploit non-motor tail domains or associated subunits to select and attach to cargoes [244-246]. On the cargo side, “receptor” proteins or cargo adaptor molecules can directly interact with the motor tail domains and regulate the motor protein function and localization in a temporal and spatial fashion [247]. Since most of the cargoes can be transported along microtubules in both directions, mechanistically this implies that every organelle has a dynein ‘receptor’ [244].

Intracellular cargo delivering by actin-based or microtubule-based motors require multiprotein complexes. Among them, many motor complexes include specific Rab GTPases that bind to the motor through an adaptor protein [244]. These adaptors, including melanophilin (Rab27a) [248], optineurin (Rab8) [249], bicaudal D (Rab6) [250], and RILP (Rab7) [251], usually recognize their related GTPase in its GTP-bound form and, binding concurrently to the activated motor and the Rab, act as Rab effectors [244]. For example, kinesin-I, the most versatile motor, binds to mitochondria via the complex Rho like GTPase Miro and the Milton1/TRAK1 adaptor that directly contacts the mitochondria [252].

The activity of some motors is regulated by their dimerization. Usually, two motor heads working in a coordinated fashion are required for motor processivity. Nevertheless, some motors exist as monomers and only dimerize when attached to the cargo. One clear example of this is myosin VI where the binding with the cargo converts the soluble monomer to a membrane-associated processive dimer [253], whose dimerization involves the interactions between the two myosin VI heavy chains [254]. Interestingly, different motors coexist on the same cargo and the knockdown of just plus or minus end-directed motor can cause a complete bock of the bidirectional motility [255].

Many organelles, such as mitochondria, exocytotic vesicles, and synaptic cargo are probably transported by kinesins that cooperate to make transport more robust [244]. Nevertheless, mitochondria transport could also be mediated by actin rings that serve as cargo-docking sites which monitor the mitochondria localization [256]. This is supported by a study showing that the transport of mitochondria is impacted when actin rings integrity is affected through knocking-out α-adducin or myosin V/VI [203, 257]. Thus, the transport of mitochondria and certain cargo, such as pigment granules or recycling endosomes, can be mediated by the contribution of both microtubule and actin-based motors [258, 259].

The actin motor myosin V, can support short motility on branched short actin cytoskeleton, but on the other hand can also drive transport in specific compartments with straight actin cables, such as filopodia and dendritic spines [260]. It has been reported that upon myosin-V knockdown the polarized distribution of glutamate receptor GluR1 and voltage-gated potassium channels Kv4.2 is disturbed. Consistently, disruption of actin using cytochalasin D also disrupts the polarized distribution of dendritic cargo [174]. Moreover, calcium can be an important regulator of motor complexes. Indeed, calcium influx arrests mitochondria movement driven by kynesin-1 through the recruitment of Rho-like GTPase Miro in neurons [261].

In 2002, it was reported that tubulin linear structures, probably short microtubules, were able to move rapidly in cultured rat neurons. However, this is not a common event as it can be observed every few minutes, and is a slower transport compared to that of vesicle transport. Remarkably, the microtubule

movement was pausing for about half of the time, a ‘stop and go’ dynamic very similar to that observed for neurofilament transport [241]. Moreover, the actors of this transport may involve dynein motors in both anterograde and retrograde directionality [262].
Slow axonal transport of actin was also shown in radiolabelling studies, whereas the rate of actin displacement is about 1.5 mm per day in motor neurons [263].

Lysosomes are membrane-bound degradative organelle working downstream the ESCRT pathway [264]. They play a strategic role in preserve cellular homeostasis degrading internalized membrane proteins [264]. Indeed, it has been reported that lysosomes can sense nutrient availability, regulate energy metabolism [265] and degrade α-amino-3-hydroxy-5-methyl-4-isoxazolepropionic acid receptors (AMPARs) in an activity-dependent manner [266, 267]. Lysosomes have been observed in all regions of the neuron, also in dendritic spines where they play an activity-dependent role in remodelling the spine density by local degradation [268]. LAMP-1 is a protein found in late endosomes and lysosomes exploited in immunocytochemistry to detect lysosomes. Most lysosomes have an acidic pH, and may therefore be stained with LysoTracker, a fluorescent dye for acidic organelles, which colocalizes with LAMP-1-GFP positive lysosomes in fluorescence experiments [268]. In addition, lysosomes have been shown to move bidirectionally in both dendrites and axons thanks to coupling to the plus end-directed kinesin (i.e. kinesin-I and kinesin-II) and the minus end-directed dynein microtubule motors through adaptors and regulatory molecules (e.g. the BORC–Arl8–SKIP complex) [269]. Interestingly, the average run length of moving lysosomes is shorter in dendrites than in axons [269]. Consistent with microtubule-dependent lysosome transport, trafficking of lysosomes is halted by Nocodazole, a drug that interferes with the polymerization of microtubules [268]. However, inhibition of f-actin dynamics by Cytochalasin D, that decrease the amount of F-actin by capping the fast-growing end of the filaments, increases periods of lysosome movement interruption while Latrunculin A, a toxin that binds to the G-actin and inhibits actin polymerization, increases lysosome motility [268, 270]. Collectively, these data suggest that lysosome motility occurs through its dynamic interactions with both the microtubules and the actin cytoskeleton, with F-actin being able to both drive lysosomes along neuronal processes and hold back them in specialized regions such as dendritic spines [268].

3.3 SURFACE RECEPTORS LINKED TO THE ACTIN CYTOSKELETON

The actin cytoskeleton is strictly associated to cell adhesion molecules (CAMs) on the plasma membrane which control neuronal cell migration, axon pathfinding, axon-dendrite contact formation and plasticity of dendritic spines [271]. CAMs are mechanically connected to the actin filaments undergoing polymerization/depolymerization by cytoplasmic linker proteins (clutch molecules) [272-274], whose absence causes abnormal cytoskeletal dynamics. CAMs associated with clutch molecules or actin binding proteins (ABPs) translate environmental signals in changes of actin cytoskeleton dynamics (polymerization and depolymerization) [198, 275]. Among them, NCAM1 has been widely studied because of its role in neuronal development [275, 276], particularly in dendrite arborization and morphology [277].

Moreover, integrins are surface receptors in direct contact with the actin cytoskeleton. Interacting with tyrosine kinases, especially with Arg in the nervous system, integrins can affect dendritic spine localization and dendrite arbor stability [278].

In addition, Reelin, an extracellular matrix glycoprotein that is able to bind lipoprotein receptors and activating both the GSK3b- and PI3K-Rho-GTPase-pathways, can influence the position of the Golgi apparatus in apical dendrites and maintain the molecular identity of dendritic spines in pyramidal neurons affecting both microtubules and F-actin [279-281].

The dynamic of F-actin coupled to clutch molecules produces traction forces on the cell adhesion molecules that converts actin polymerization and depolymerization into the force that pushes the leading edge of the membrane, promoting neurite outgrowth and cell migration [273, 274, 282]. ABPs co-migrate with the actin filament array through cycles of dissociation, directional diffusion, and association with the filaments. The transport velocity is approximately 100 times slower than that of motor protein-based transport. Surface molecules linked to ABPs may be shuttled and translocated by the directional actin diffusion. This process therefore represents a new type of intracellular transport system [198].

Mechanistically, if surface receptors linked to ABPs can be transported along neurites driven by actin dynamics, extracellular vesicles which adhere to surface receptors might be dragged along the outer membrane of neuronal processes following this intracellular transport system.

3.4 EV-NEURON INTERACTION HYPOTHESIS

A recent study showed that small EVs of neuronal origin are efficiently internalized by cultured neurons and once inside the neuron can be transferred to other connected neurons via active intracellular transport along axonal projections [68]. However, recent studies conducted in my laboratory and others showed that large EVs derived from microglia or astrocytes despite adhering to neurons with high efficiency, are very rarely internalized in hippocampal neurons [49, 283]. Specifically, we highlighted the contribution of phosphatidyl-serine (PS) residues present on EV surface to the EV-neuron contact [49] and showed that glial EVs deliver their cargo to neurons by transiently fusing with the plasma membrane [49], without being taken up in the neuron cytoplasm. In addition, other recent findings of our group and others indicate that EVs can move on the plasma membrane of receiving astrocytes, microglia [71] or fibroblasts [72]. In fibroblasts, EV movement occurs along filopodia, thin cell membrane protrusions, and drives EVs towards the site of endocytosis, thus favouring internalization. This was indicated by the reduced the rate of exosome uptake upon inhibition of formin-dependent actin polymerization in fibroblasts, which causes loss of filopodia. Importantly, strikingly similar extracellular motion along filopodia was previously described for viral particles, which surf along filopodia to reach the site of cell entry. Mechanistically the movement of viral particles is driven by virus binding to a surface receptor (CAR) coupled to a moving actin cytoskeleton [284]. Taken together these findings open the possibility that large glial EVs, which share with viruses many features and mechanism of cell interaction, especially those which cannot be taken up by neurons and exceed the neurite diameter, may move on the neuron surface by a similar mechanism.

We hypothesised that EVs can move on the neuronal surface following two possible mechanisms. First, EVs could bind to a surface receptor which move along the neuronal surface driven by actin dynamics, similarly to viral particles. These receptors can be coupled, directly or indirectly through clutch molecules, to the internal actin cytoskeleton by intermittent association and breaking of the transmembrane connections, creating a sort of sliding graft [285]. The second hypothesis assumes that EVs can have an intrinsic capacity to move on the surface of neurons along a gradient of adhesion molecules. This can be possible thanks to the presence of energy and of polymerized actin filaments inside the vesicle, which, through a de-polymerization and polymerization process, can mediate EV shape modification and permit the interaction with a surface receptor in proximity of the EV.

As a matter of fact, previous studies have shown that EVs obtained from the ejaculate can produce ATP, necessary for the polymerization of actin [286] and EVs have been also shown to lose their elongated structures, observed through electron microscopy morphological studies, which are energetically demanding to switch to a roundish shape which may facilitate the interaction of the EV

and the receptor. If extracellular vesicles produced by glia cells contain actin capable of polymerizing and depolymerizing and energy in the form of ATP, then these EVs could have independent capacity to move on long neuronal processes [78].

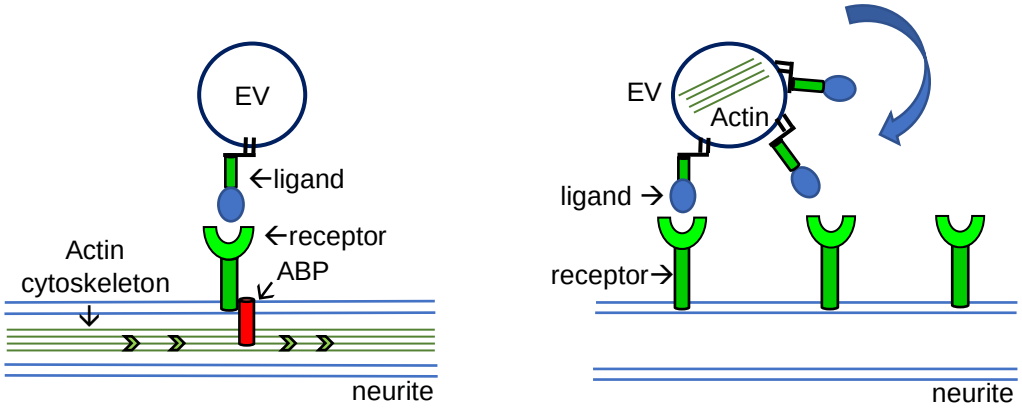

Fig.5: Cartoon representation of the two hypotheses of EV movement along neuron processes. On the left, EV binds to a surface receptor that moves along neuronal surface driven by actin flow. On the right, EV has an intrinsic capacity to move on the surface of neurons along gradient of adhesion molecules.

If EVs move at the neuron surface, understanding the factors that allow movement and their subsequent control could have big implications for better use of EVs as therapeutic tools as well as targets to prevent the spreading of pathogenic agents in the diseased brain.

AIM OF THE THESIS

Aim of my PhD work was to investigate the ability of glial EVs to interact with distinct neuron compartments and travel along connected neurons exploring the underlying mechanisms. For this purpose, I exploited optical manipulation to deliver single EVs to the cell body or neurites of primary hippocampal neurons and monitored the EV-neuron interaction and dynamics by time lapse imaging. To study the molecular mediators responsible for the EV movement I utilized pharmacological treatments that blocked cytoskeletal dynamics. The specific involvement of the prion protein was evaluated using EVs and neurons established from PrP knock-out mice.

RESULTS

4 RESULTS

Results of this thesis are modelled on the related manuscript:

Astrocytes-derived Extracellular Vesicles in motion at the neuron surface: involvement of the prion protein.
D'Arrigo G., Gabrielli M., Scaroni F., Swuec P., Amin L., Cojoc D., Legname G. and Verderio C. (Submitted in September 2019).

4.1 EVS PRODUCED FROM PRIMARY RAT ASTROCYTES HAVE DIFFERENT MORPHOLOGIES

Primary rat astrocytes were exposed to ATP for 30 min, to promote EV shedding, and large EVs were isolated by ultracentrifugation at 10,000x g after pre-clearing of cell supernatants from cells and debris at 300x g [47]. Our previous experiments indicate that EVs isolated upon short ATP stimulation are negative for apoptotic markers [7] and not contaminated with intracellular organelles [40]. Morphological analysis using high resolution cryo-electron microscopy (cryo-EM) [79, 82] revealed that most EVs were rounded in shape (83%, Fig.1A, C) and made by a single lipid bilayer (80%), although very heterogeneous in size (Fig.1A-B). Their size range was from 20 nm to 1300 nm (mean 217 ± 12 nm). A subpopulation of EVs were multi-lamellar, i.e. contained two or more vesicles in their lumen (20%, Fig.1A panel c), while a minor percentage of EVs had a tubular (3.6% Fig.1C and Fig.1A panel i) or irregular shape (1%, Fig.1C and Fig.1A panel g-i). Other peculiar features of some EVs were rough surface (2.6%, Fig.1A panel a), likely due to the presence of transmembrane proteins, electron dense content (24%, Fig.1A panel a-c) and presence of actin filaments in their lumen (2%, Fig.1A panel d-i), a typical feature of larger EVs, with a tubular/elongated shape. In tubular/elongated EVs actin filaments were oriented in parallel to one another and extended along the tubule (Fig.1A panel h-i and Fig.1D) while in rounded EVs were randomly distributed (Fig.1A panel d-f). Actin filaments in tubular EVs displayed canonical width of ~7 nm. Inter-filament distance was ~10 nm (Fig.1E) with inter-subunit distance of ~60 Å (Fig.1E). Cryo-EM confirmed that EVs were not contaminated with apoptotic bodies, intracellular organelles derived from damaged cells nor protein aggregates.

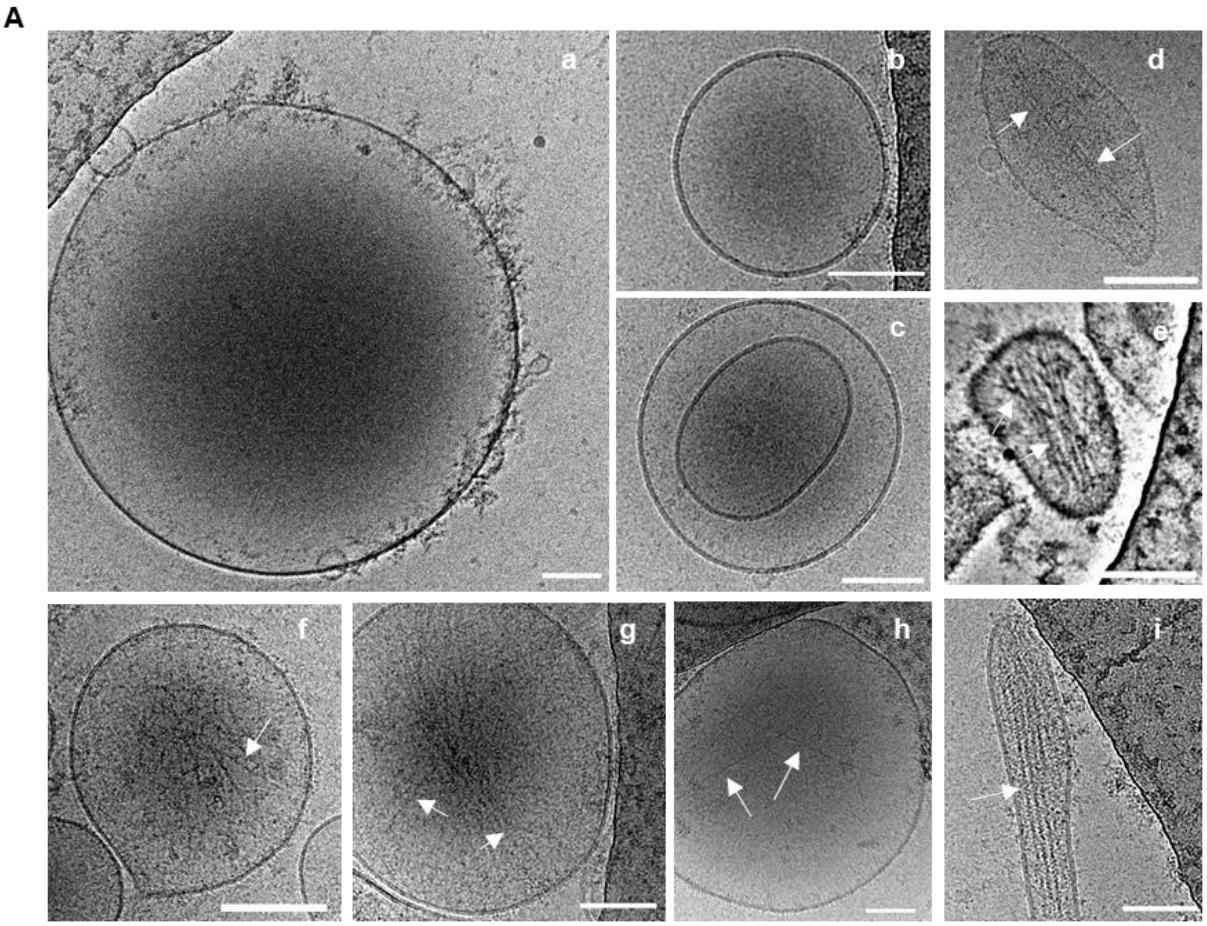
A
a
b
c
d
e
f
g
h
i

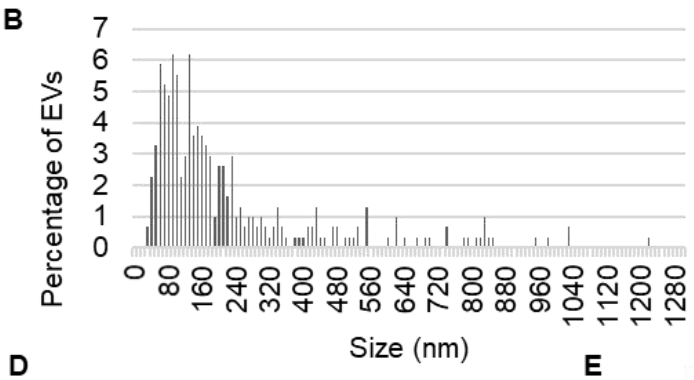
B
Percentage of EVs
0
1
2
3
4
5
6
7
0
80
160
240
320
400
480
560
640
720
800
880
960
1040
1120
1200
1280
Size (nm)

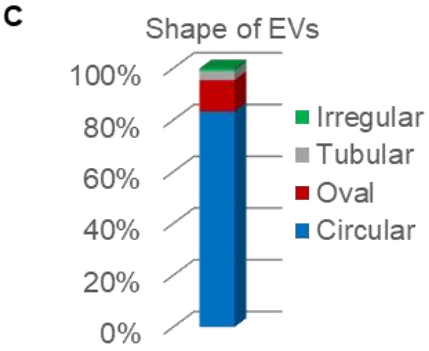
C
Shape of EVs
100%
80%
60%
40%
20%
0%
Irregular
Tubular
Oval
Circular

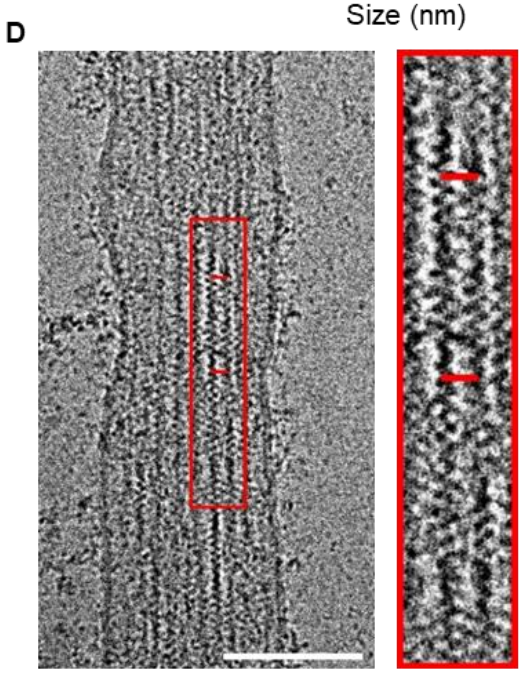
D

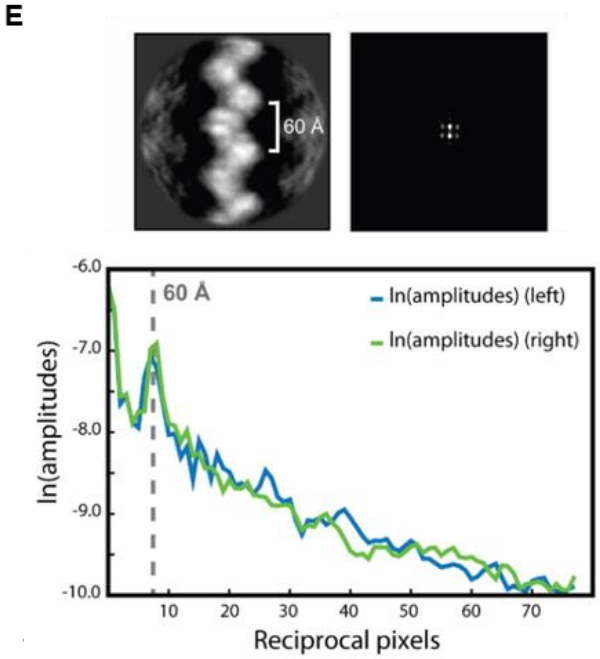
E
60 Å
-6.0
-7.0
-8.0
-9.0
-10.0
60 Å
ln(amplitudes) (left)
ln(amplitudes) (right)
ln(amplitudes)
10
20
30
40
50
60
70
Reciprocal pixels

Fig.1: Ultrastructure of EVs released from cultured astrocytes. A Representative cryo-EM micrograph of round EVs (a-f), made by the characteristic phospholipid bilayer, as well as of less abundant irregular or tubular EVs (g-i) in the 10,000x g pellet (low-pass filtered at 40 Å, except for the first micrograph). Note the presence of filaments (arrows) in elongated/tubular EVs (g-i) but also in a subpopulation of round EVs (d-f). Scale bars = 100 nm. **B** Size distribution of astrocyte-derived EVs in the 10,000x g pellet (bar size=10 nm; n=312). **C** Prevalence of astrocytic EVs with different shape and morphologies in the 10,000xg pellet. **D** Cryo-electron micrograph showing parallel actin filaments in the lumen of a tubular EV. Red rectangle shows the area zoomed on the right. **E** Reference-free 2D class average of intravesicular actin filaments (top right, box size 229 Å) is shown together with amplitudes in the frequency (Fourier) space (top left) and helical layer line profile.

4.2 SINGLE-PARTICLE TRACKING OF ASTROCYTIC EVS ON THE NEURON SURFACE

To elucidate whether EVs produced by astrocytes or microglia interact with neurons at preferential sites, we placed single EVs on different compartments of hippocampal neurons (cell body, dendrite and axon) by using optical manipulation [49] and followed EV-neuron interaction by live microscopy. EVs were added to neuronal medium, trapped by the infrared laser tweezers and positioned on the chosen compartment. The trapping laser was switched off and time-lapse images were collected at 2-20 Hz for 20 min to monitor EV-neuron dynamics (Fig.2A). We found that EVs efficiently adhered to both the cell body and neurites (Fig.2B-D, Movie S1 and Movie S2).

In few cases, after adhesion the EVs became undistinguishable from the cell surface suggesting fusion with the neuron membrane and it was impossible to follow them further.

Surprisingly, after adhesion a large fraction of astrocytic EVs (60 ± 3.29%, n=149/247) and a good percentage of microglial EVs (40 ± 8.48% n=21/52) displayed net movement from the contact site, surfing on the plasma membrane of neurons. Both astrocyte- and microglia-derived EVs moved more frequently on neuron processes compared to cell bodies (Fig.2E).

Phase contrast resolution does not allow to discriminate between intra- and extra- EV motion. Therefore, we first had to provide evidence that EVs were actually moving on the neuron surface. We found that recapturing of EVs by the laser tweezers transiently hampered EV motion (not shown) while not inhibited transport of intracellular organelles. This indicated that EVs were moving outside neurons. In addition, we observed few examples of EVs jumping from one process to another (Movie S3), even belonging to different neurons, allowing neuron-to-neuron EV transition (Movie S4). Given that to the best of our knowledge there is no communication between the cytoplasm of distinct neurites, this finding confirmed that EV were moving extracellularly. About 70% and 57% of EVs derived from astrocytes and microglia were in motion along neurites (astrocytic EVs n=135/212; microglial EVs n=19/36) (Fig.2B, E, Movie S1) and run sizable length (mean length = 143 ± 9.95 μm/20min), reaching a maximal distance of ~9 μm from the contact point (Fig.2F). A smaller percentage of glial EVs moved on the cell body (astrocytic EVs n= 14/35, Fig.2E; microglial EVs n=2/16) and the movement was confined to the somatic region (Fig.2C, Movie S2), although run length (mean length = 144 ± 41 μm/20min) and maximal distance from the contact point (~7 μm) were similar compared to neurites (Fig.2F). Because the aim of this work was to investigate whether EVs were able to travel along connected neurons, the following analysis were focus on EVs delivered on neuron processes, the compartment on which EVs showed a higher capacity to move.

Axons were distinguished from dendrites by their longer length and their smaller size in developing cultures (≤12 days in vitro) and by the absence of spines in mature cultures transfected with GFP (≥ 13 days in vitro) (Fig.3G).

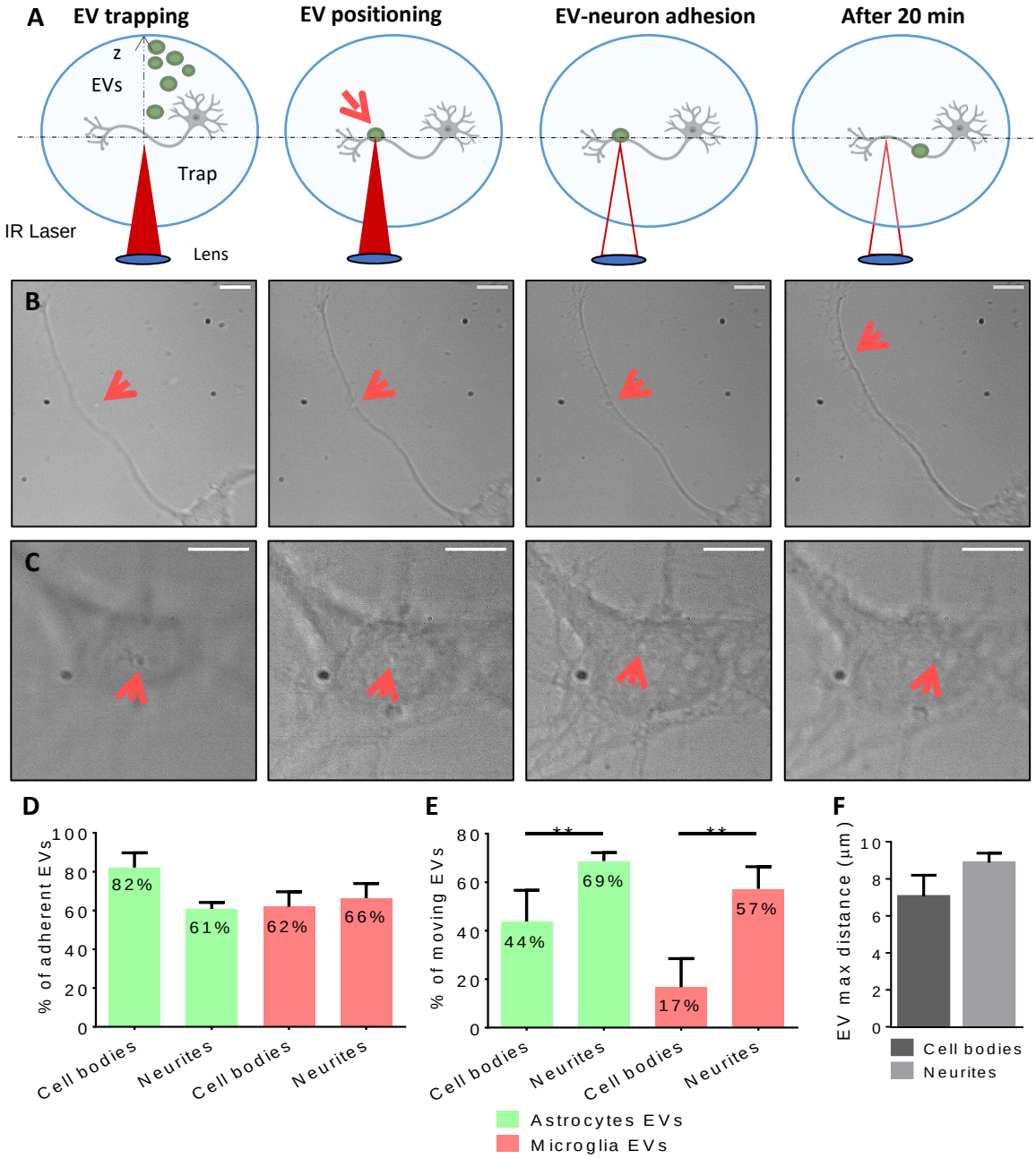

Fig.2: Features of EV motion on the neuron surface. A Schematic representation of single EV delivery to neurons by optical tweezers. EV is first trapped above the neurons by the IR laser tweezers (left), then the stage is moved in plane (XY) to reach the target neurons. Then, the trap is moved axially (Z) to set the EV in contact with the neuron (middle). The trapping laser is switched off (middle) and EV-neuron interaction is then monitored by time lapse imaging up to 20 min (right). **B-C** Sequence of phase contrast images showing examples of EVs driven to the growing axon (top) or the neuron cell body (bottom) following the procedure described in A (scale bar 10 µm). **D** Percentage of EVs that adhered to the neuron cell bodies and processes (astrocytic EVs: cell bodies n=47, processes n=396; microglial EVs: cell bodies n=30, processes n=59). **E** Percentage of EVs displaying motility on the cell bodies and neurites (astrocytic EVs: cell bodies n=35, processes n=212; microglial EVs: cell bodies n=16, processes n=36).

4.3 DIRECTIONAL MOVEMENT OF EVS ALONG NEURONAL PROCESSES

By a custom MATLAB code, we analyzed the dynamics of all EVs which adhered to neurites, including those that remained anchored to the contact site. Among the latter (~35% of total EVs) only few EVs were virtually immobile (EV displacement < EV diameter) while the remaining fraction showed random (Brownian) motion, restrained by a tether to the neuron membrane (Fig.3A). The mean radial displacement from the attachment point was 1.8 ± 1.1 µm. For simplicity, both virtually immobile EVs and EVs displaying only radial motion are referred to as "static EVs" hereafter (Fig.3C blue bars).

Most EVs (~65%) exhibited both radial and directional movement (mobile EVs, Fig.3C, red bars), with a prevalent directional component (Fig.3B). Directional movement was typically intermittent, characterized by interruptions between periods of motion ("stop and go" motion). "Stop" intervals are indicated by 0 values in the temporal plot of distances travelled by EVs in 200sec (Fig.3D). On average, EVs were in motion for nearly half the recording time (45 ± 2.2%). Radial motion was evident during "stop" intervals (Fig.3B arrow) or at high frequency (20Hz) acquisition (Movie S5). A typical feature of directional movement was back and forth motion, highlighted in the temporal plot of EV distance changes from the contact point, showing both positive and negative variations (Fig. 3E). As a consequence of back and forth movement, EVs repeatedly localized at the same sites on axons, dendrites or their protrusions (filopodia/dendritic spines). Movie S1 shows the typical trajectory of an EV that retraced several times the same regions of a growing axon while exploring filopodia on the way to the growth cone. Visualization of EV trajectories revealed that most EVs moved along axons and dendrites in a prevalent direction (run length > 2 x length in the opposite direction), either retrograde, towards the neuron cell body, or anterograde, away from the soma. However, a significant fraction of EVs (38%) were characterized by truly bidirectional movement, running similar length along neurites in both directions, as indicated by the plot of the maximal positive and negative distances from the contact point (Fig.3F). The speed of EVs along neurites ranged from 0.011 to 0.412 µm/sec (mean speed= 0.126 ± 0.008 µm/sec, n=135). EV velocity was similar on axons and dendrites in immature neurons, up 11 days in vitro (Fig.3H). With age, EV speed tended to decrease on dendrites while it did not change on axons with a significant difference between the two processes in neurons ≥12 days in vitro (Fig.3H).

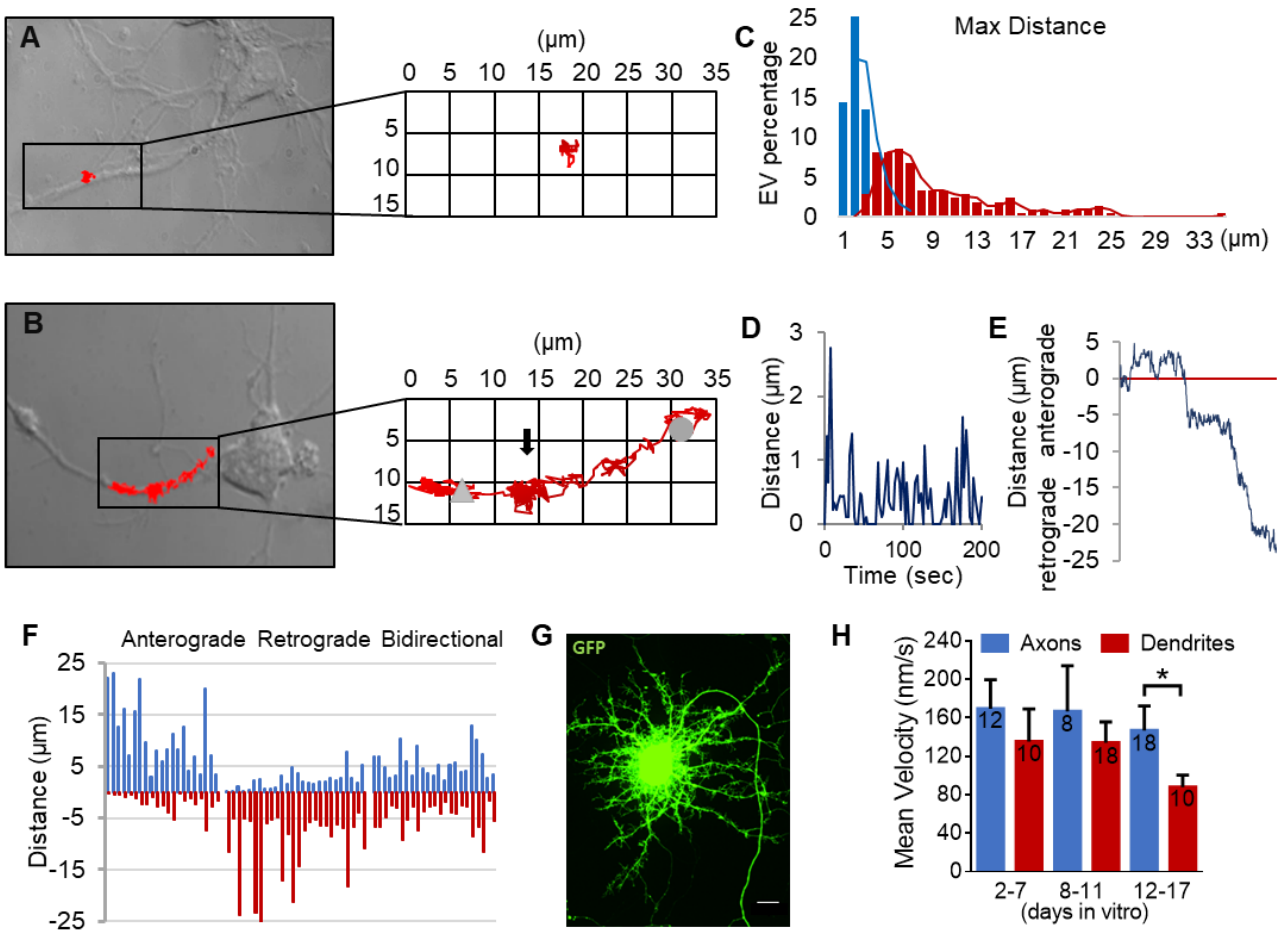

Fig.3: Dynamics of EV motion on the neuron surface. A-B The trajectory of EVs are represented in red, superposed on the phase contrast images of developing neurons and enlarged in the insets. The EV in G shows radial motion while the EV in H exhibits directional motion towards the cell body. Grey arrowhead indicates the starting point, grey circle the ending point. **C** Distribution of maximal distances from the contact point of EVs delivered to neurites (n=209). Static EVs are in blue, moving EVs are in red. **D** Distances traveled by the EV in H for 200 sec after adhesion and sampled every 2,5 sec, illustrating stop-and-go movement. **E** Temporal plot of the distance from the contact point of the EV in H during 20 min of recording sampling at 2 Hz, showing both anterograde and retrograde motion. **F** Distribution of maximal positive and negative distances from the contact point of moving EVs (n=76), showing anterograde (28%), retrograde (34%) or bidirectional (38%) motion. **G** Representative fluorescence image of a neuron transfected with GFP to delineate dendrite and axon morphology. Scale bar 10 µm. **H** Velocity of EVs (nm/sec) on dendrites and axons at different stages of neuronal development (12-17 DIV, one-tailed unpaired t test with Welch's correction, $p \leq 0.05$ axons vs dendrites). Number of EVs are indicated in the bars.

4.4 MOTION OF EVS DEPENDS ON INTACT ACTIN CYTOSKELETON IN NEURONS

Mechanistically, EV motion could be driven by binding to a neuronal receptor coupled to a moving cytoskeletal network (Fig.4A). This hypothesis was suggested by two independent observations. First we found that carboxylated microsynthetic particles covalently coupled with prion protein (PrP), a GPI anchor protein highly enriched in EVs [54, 287] (Fig.4A), were transported along neurites when delivered to neurons by OT (Fig.4B-C), mimicking the trafficking of astrocytic EVs outside neurons. This observation suggested that binding of PrP to a neuronal receptor is sufficient to drive passive movement of the synthetic particle on the neuron surface. Interestingly, a lower percentage of PrP-coated beads were transported along the surface of PrP knock out ($PrP^{-/-}$) neurites (Fig. 4B-C), suggesting that neuronal PrP may act as receptor for PrP coupled to the synthetic beads. Indeed, PrP is capable to undergo homophilic interaction with a PrP molecule in trans and can elicit contact formation [124].

Second, we found examples of EVs placed on very thin neuronal processes which were induced to move on the neuron surface by the transit of large intracellular vesicles, actively transported along the neuron processes (Fig.4D; Movie S6-7). These observations suggested that the large intraneuronal vesicles, which exceeded the diameter of the neurites, may drag the cytosolic portion of the EV receptor during their transport along the cytoskeleton, generating simultaneous intra- and extra-cellular vesicle motion (Fig.4A).

To assess whether energy-dependent cytoskeleton rearrangements could drive EV motion on the neuron surface we first intoxicated neurons with the metabolic inhibitor Rotenone (2µM) for 1 hour. Rotenone-treated neurons exhibited increased cytosolic calcium concentration, revealed by increased F340/F380 fluorescent ratio in cultures loaded with the calcium dye Fura-2 (Fig.4E), indicating an impairment of plasma membrane ATPase activity. In addition, Rotenone-treated neurons displayed reduced energy-dependent trafficking of LysoTracker labelled lysosomes inside the cells (Fig.4F), confirming depletion of energy reserves. Importantly, only 33% of EVs were in motion on intoxicated neurites, where lysosome transport was blocked, while ~80% of EVs drifted on the surface of control neurons (Fig.4G). In line with this evidence, acute application of the mitochondria inhibitor Sodium Azide (20 mM) [288] blocked the movement of a few EVs along neurites (Fig.4H movie S9). To corroborate these findings, we mildly fixed neurons with cold methanol (at 4 degrees Celsius) and placed single EVs on the surface of dead neurons. Only 8% of EVs exhibited a net displacement from the contact point at the surface of dead cells (Fig.4I). Altogether these findings showed that EV motion largely depends on neuron energy metabolism.

To assess the involvement of the cytoskeleton in extracellular EV motion we next blocked actin filaments, a component of the cytoskeleton involved in various types of cellular motility [289], by exposing neurons to 1 µM cytochalasin D (CytoD) for 60 min, a drug that binds to the fast growing end of actin, or to 100 µM Blebbistatin for 30 min, an inhibitor of motor dependent restructuring of actin network [290]. CytoD-dependent depolymerization of actin filament was indicated by increased ratio of globular (G-) versus filamentous (F-) actin, as revealed by western blot analysis (Fig.4J). Importantly, by positioning EVs on CytoD-treated neurites, where lysosome movement was blocked, we found no changes in EV adhesion (48% Ctrl n=57; 47% CytoD n=79) but a decrease of extracellular EV motion (Fig.4K). Inhibition of actin filaments rearrangements by Blebbistatin caused a significant reduction of extracellular EV motion (Fig.4L), confirming the involvement of the actin cytoskeleton. By contrast, depolymerization of the microtubule cytoskeleton by Nocodazole (10-30 µM for 60 min), did not alter extracellular EV motion (Fig.4M), ruling out a major role of microtubules in EV dynamics at the cell surface.

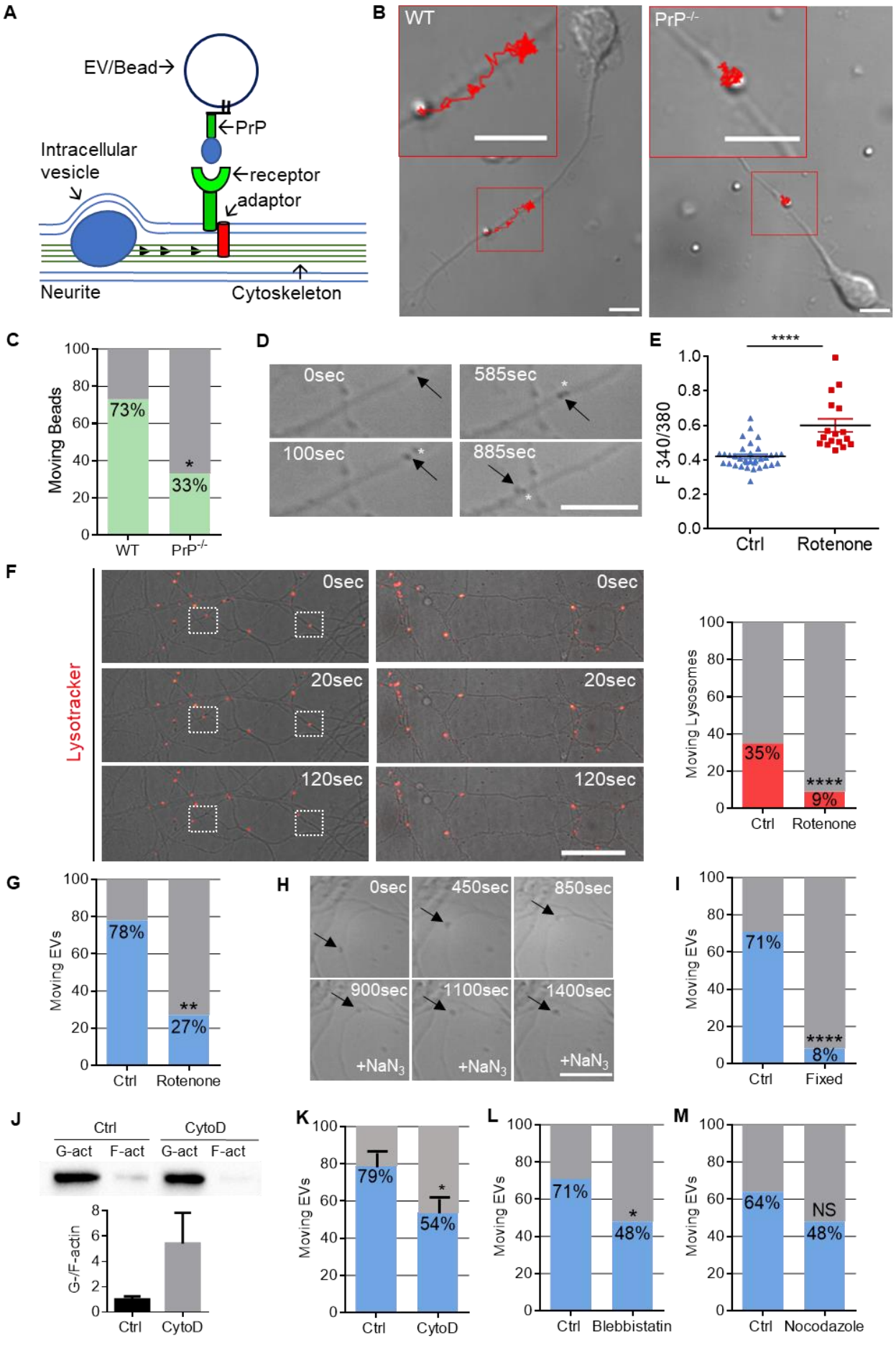
A
EV/Bead
PrP
Intracellular vesicle
receptor
adaptor
Neurite
Cytoskeleton
B
WT
PrP-/-
C
Moving Beads
73%
33%
*
WT
PrP-/-
D
0sec
585sec
100sec
885sec
E
****
F 340/380
Ctrl
Rotenone
F
Lysotracker
0sec
20sec
120sec
Moving Lysosomes
35%
****
9%
Ctrl
Rotenone
G
Moving EVs
78%
**
27%
Ctrl
Rotenone
H
0sec
450sec
850sec
900sec
1100sec
1400sec
+NaN3
I
Moving EVs
71%
****
8%
Ctrl
Fixed
J
Ctrl
CytoD
G-act
F-act
G-/F-actin
Ctrl
CytoD
K
Moving EVs
79%
*
54%
Ctrl
CytoD
L
Moving EVs
71%
*
48%
Ctrl
Blebbistatin
M
Moving EVs
64%
NS
48%
Ctrl
Nocodazole

Fig. 4: Actin cytoskeleton dynamics drive extracellular EV motion. A The scheme shows possible coupling of EV to the moving cytoskeleton of neuron via binding to a neuronal receptor. It also shows that transport of large intracellular vesicles along the cytoskeleton may alter EV motion by dragging the cytosolic portion of EV receptor or adaptor protein. **B** Phase contrast images showing the transport of PrP-coated synthetic particles on the surface of wild type (left) but not $PrP^{-/-}$ (right) growing axons (scale bar 5 µm). The trajectories of the PrP-coated beads are represented in red, superposed on the neuron images and shown at high magnifications in the insets. **C** Percentage of moving beads on the growing axons of wild type (WT) and $PrP^{-/-}$ neurons (WT n=16; $PrP^{-/-}$ n=6; one-sided chi-square test, $p \leq 0.05$). **D** Sequence of phase contrast images showing simultaneous motion of extracellular (black arrow) and intracellular (white star) vesicles along a thin process (from movie S7). **E** Control and Rotenone-treated neurons were loaded with the ratiometric calcium dye FURA-2 prior to single cell calcium imaging. The values are mean 340/380 fluorescent ratios, a measure of cytosolic calcium concentrations. Dead neurons (340/380 Ratio values >1) were excluded from the analysis (Ctrl n=49; Rotenone n=34; Mann-Whitney test, $p \leq 0.0001$). **F** Control and Rotenone-treated neurons were loaded with lysotracker and the trafficking of lysotracker-positive organelles was analyzed by confocal video recording. ROIs indicate moving lysosomes in the overlay of phase contrast with fluorescence images. The percentage of moving lysosomes in control and Rotenone-treated neurons is shown on the right (Ctrl n=445; Rotenone n=284; chi-square test, $p \leq 0.0001$). **G** Percentage of EVs moving along the surface of neurites in control and Rotenone-treated neurons. Only EVs delivered to neurites of Rotenone-treated neurons, where lysosome trafficking was blocked, were included in the analysis (Ctrl n=14; Rotenone n=26; chi-square test, $p \leq 0.01$). **H** Sequence of phase contrast images showing block of EV motion (black arrow) upon treatment with 20mM Sodium Azide (+NaN3). **I** Percentage of moving EVs on live and fixed neurons (live neuron n=14; fixed neuron n=12; chi-square test, $p \leq 0.0001$). **J** Immunoblot of hippocampal neurons extracts showing actin depolymerization upon CytoD treatment (top). Bottom histogram shows the ratio between G-actin and F-actin in control and CytoD-treated neurons. **K-M** Percentage of moving EVs on the surface of CytoD-treated neurons (J; Ctrl n=21; CytoD n=33; one-sided T test $p \leq 0.05$; chi-square test, $p > 0.05$), Blebbistatin-treated neurons (K; Ctrl n=23; Blebbistatin n=27; one-sided chi-square test, $p \leq 0.05$) or Nocodazolo-treated neurons (L: Ctrl n=25; Nocodazole n=21; one-sided T test and chi-square test, $p > 0.05$).

4.5 INVOLVEMENT OF THE PRION PROTEIN IN EV MOTION

Drift of astrocytic EVs on the neuron surface strikingly resembles movement of adenoviral particles on target cells, which enhances infection by transporting viruses to sites competent for endocytosis [291-293]. Indeed, a parallel between virus and EVs extracellular motion has been recently established by a study showing that EV surfing along filopodia facilitates cell entry in analogy to virus infection [72]. Binding of viral particles to plasma membrane coxsackievirus adenovirus receptor (CAR), a GPI anchor-protein, was shown to give rise to extracellular virus motion, by coupling the viruses with the actin cytoskeleton of target cells [284]. Among surface neuronal receptors which may elicit motion of glial EVs, our experiments with PrP-coated synthetic particles (Fig.4B-C) pointed to the GPI anchor-protein PrP, as putative linker between EV and the moving actin cytoskeleton. The protein is expressed in astrocytes, in addition to neurons, and highly enriched in EVs thereof, as indicated by Western blot analysis (Fig.5A).

To explore the involvement of PrP in trafficking of astrocytic EVs along the neuron surface we silenced PrP in both neurons and donor astrocytes using specific smart pool siRNAs (Dharmacon). Western blot analysis showed that PrP was downregulated by 80% and 40% in neurons and astrocytes respectively, compared to vehicle-treated cultures (Fig.5A). By positioning EVs produced by PrP-silenced astrocytes along processes of PrP silenced neurons we found an increase in the percentage of static EVs (Fig.5B), suggesting the involvement of vesicular and/or neuronal PrP in the extracellular motion. Similar results were obtained with control EVs delivered to PrP silenced neurons (Fig.5B). To corroborate these findings, we isolated EVs from PrP knock out [275] astrocytes ($PrP^{-/-}$-EVs) and placed $PrP^{-/-}$-EVs on neurites of PrP knock out neurons ($PrP^{-/-}$neurons) (Fig.5C-D). Lack of PrP in both EVs and neurons did not influence EV-neuron adhesion (67% of adhesion of $PrP^{-/-}$-EVs on $PrP^{-/-}$ neurons compared to 76% in wild type conditions), excluding that homophilic PrP interaction is necessary for EV-neuron contact, but it caused a significant decrease in the percentage of moving EVs (Fig.5E), confirming the involvement of neuronal and/or vesicular PrP in extracellular EV motion.

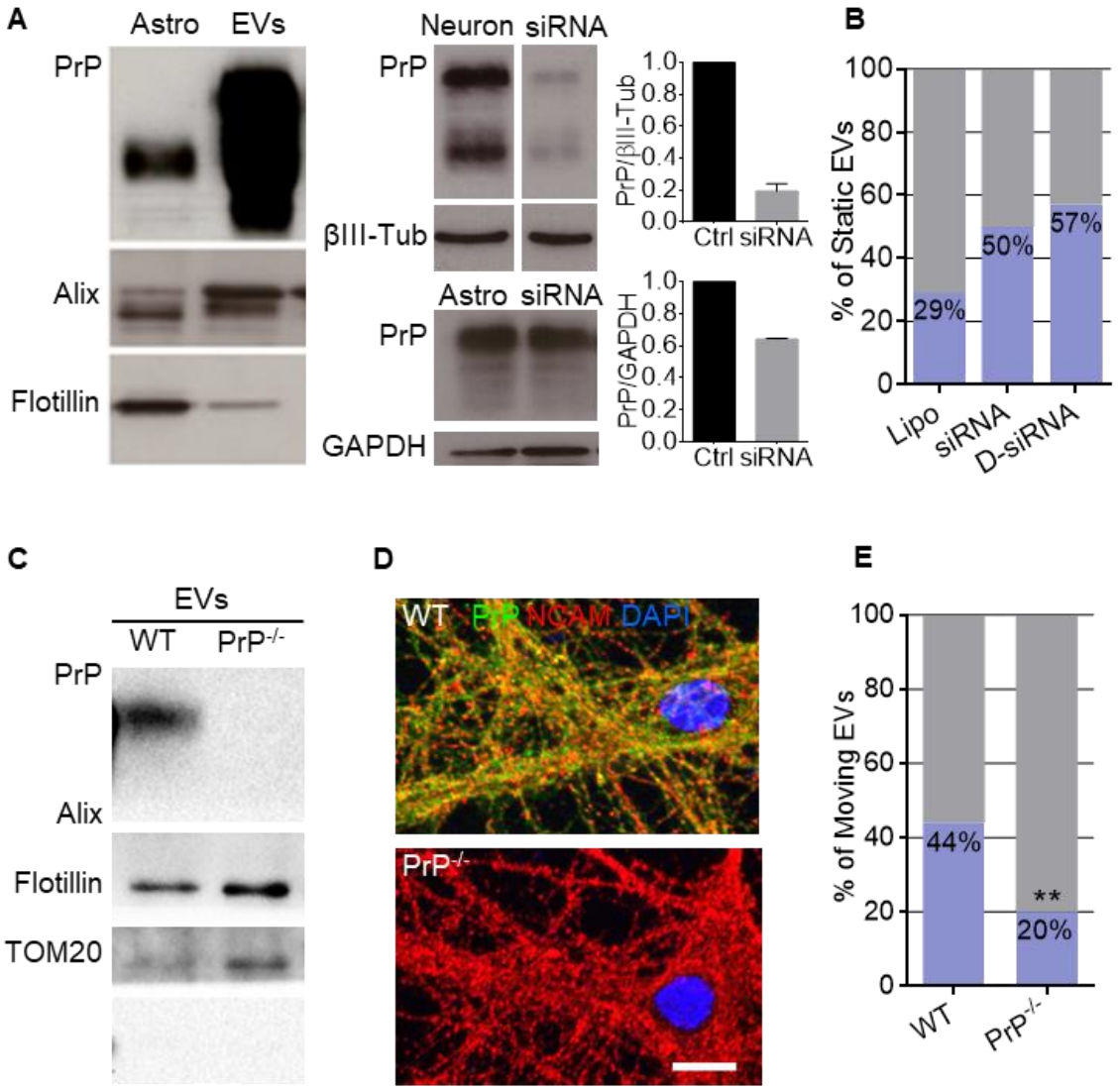

Fig. 5: Role of PrP in extracellular EV motion. A Immunoblot of astrocytes and astrocyte-derived EVs for PrP and the EV markers alix and flotillin1 (left). PrP expression (middle) and quantification relative to reference proteins (right) in control and siRNA-treated neurons and astrocytes. **B** Percentage of static EVs from control astrocytes on the surface of lipofectamine-treated neurons (lipo, n=7) or PrP-silenced neurons (siRNA, n=12) and from PrP-silenced astrocytes on the surface of PrP-silenced neurons (double siRNA, D-siRNA, n=14). **C** Immunoblot for PrP, EV markers and the mitochondrial marker TOM20 of EVs from wild type (WT) and $PrP^{-/-}$ astrocytes. **D** Representative confocal images of wild type (WT) and $PrP^{-/-}$ neurons stained for PrP (green), NCAM (red) and the nuclear marker DAPI (blue) (scale bar 10 µm). **E** Percentage of moving EVs from $PrP^{-/-}$ astrocytes on $PrP^{-/-}$ neurons (WT n=71; KO n=71; unpaired t test, $p \leq 0.01$).

4.6 A FRACTION OF EVS ACTIVELY MOVES ON THE NEURON SURFACE

Being equipped with actin filaments, as indicated by cryo-EM (this study, [78, 79]) as well as actin binding proteins [294], a fraction of astrocyte-derived EVs may possess independent motile capability, similar to that produced by actin in cells [78]. Support to this hypothesis (Fig.6A) was provided by time lapse video recordings of single EV dynamics at the neuron surface, which showed examples of EVs jumping from one neurite to one another, as described above (Movie S3 and S4). To the best of our knowledge there is no direct communication between the cytoplasm of adjacent neurites in differentiated neurons. Therefore, the saltatory motion could only rely on the capability of EVs to change their shape [78] and to interact with surface EV receptors on adjacent neurites.

Following this hypothesis, active EV movement should be sensitive to block of actin dynamics inside EVs. Western blot analysis for F- and G- actin confirmed the presence of actin filaments in astrocyte-derived EVs (Fig.6B). Importantly, both F- and G- actin fractions isolated from EVs were negative for markers of intracellular organelles, thus excluding contamination with cytosolic actin. EV treatment with CytoD for 60 min caused an increase in the ratio between G- and F-actin in EVs (Fig.6B), indicating F-actin depolymerization, and lowered the percentage of EVs in motion at the neuron surface (Fig.6C). This suggests that actin rearrangements inside EVs may produce motion in at least a fraction of EVs.

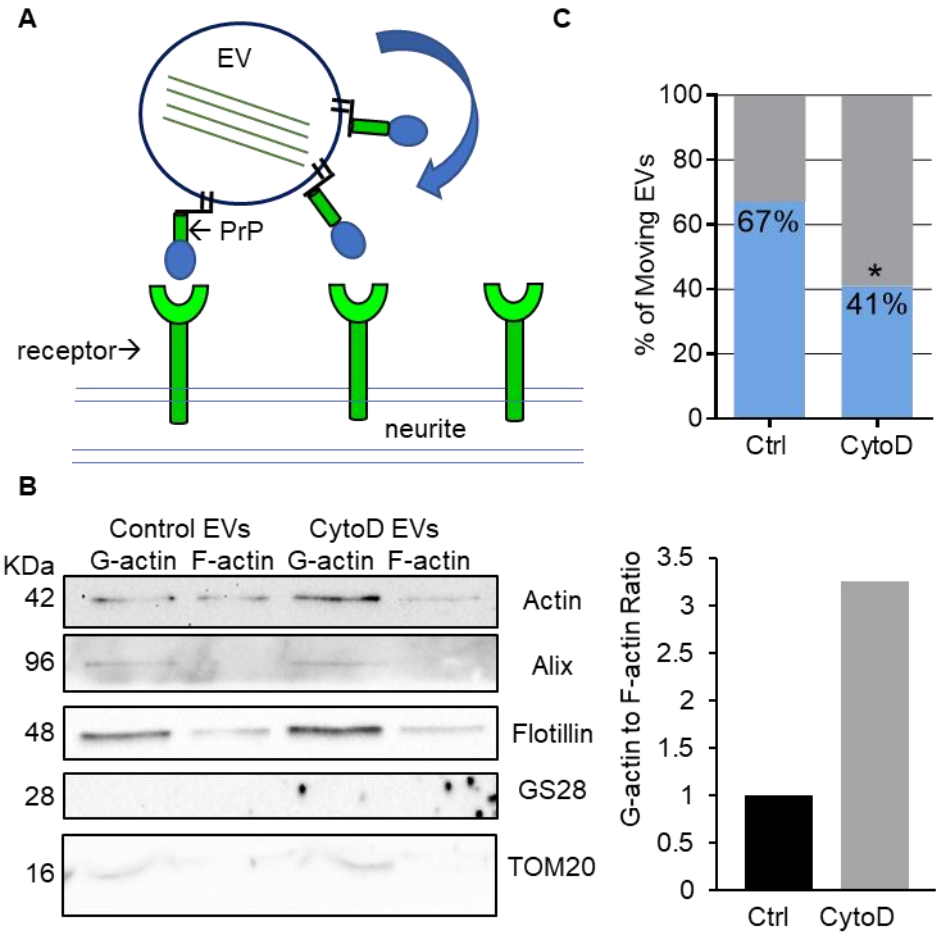

Figure 6: Active motion of astrocytes-derived EVs. A Schematic representation of active motion of EVs, through intermitted contact with neuronal surface receptors. **B** Representative western blot (left) and summary data (right) of F-actin and G-actin in EVs from control and CytoD-treated astrocytes. F- and G- actin fractions are positive for the EV markers alix and flotillin1 and negative for the Golgi and mitochondrial markers GS28 and TOM20. **C** Percentage of moving EVs from control and CytoD-treated EVs on the neuron surface (Ctrl n=18; CytoD n=32; one-sided chi-square test, $p \leq 0.05$).

4.7 EVs CONTAIN ATP AS ENERGY SOURCE

To modify their shape and to actively move on the neuron surface EVs should possess an energy source that supports actin cytoskeleton rearrangements.

To assess whether astrocyte-derived EVs contain ATP, the main cellular energy source, we used a bioassay previously established to measure ATP [295]. Oligodendroglial cells, which respond to low ATP concentration (in the nM-µM range) with rapid intracellular Ca^{2+} elevations [296], were used as ATP sensor cells. Addition of EVs to Fura-2-loaded oligodendrocytes evoked calcium transients in ~30% of the cells (n=84) (Fig.7A). Calcium responses were completely abrogated by treatment of EVs with the ATP degrading enzyme apyrase (3 units/100 µl) (Fig.7A), indicating that ATP was the compound evoking Ca^{2+} transients. Much lower calcium responses were evoked by broken EVs, depleted of their cytosolic cargo by hypo-osmotic shock [40] (Fig.7B), revealing that ATP was coming from the EV lumen. The presence of ATP inside astrocyte-derived EVs was confirmed by EV labeling with 1 µM quinacrine, a fluorescence dye which stains intracellular ATP stores [295] (Fig.7C). Most EVs were quinacrine positive, indicating that they store ATP (Fig. 7C).

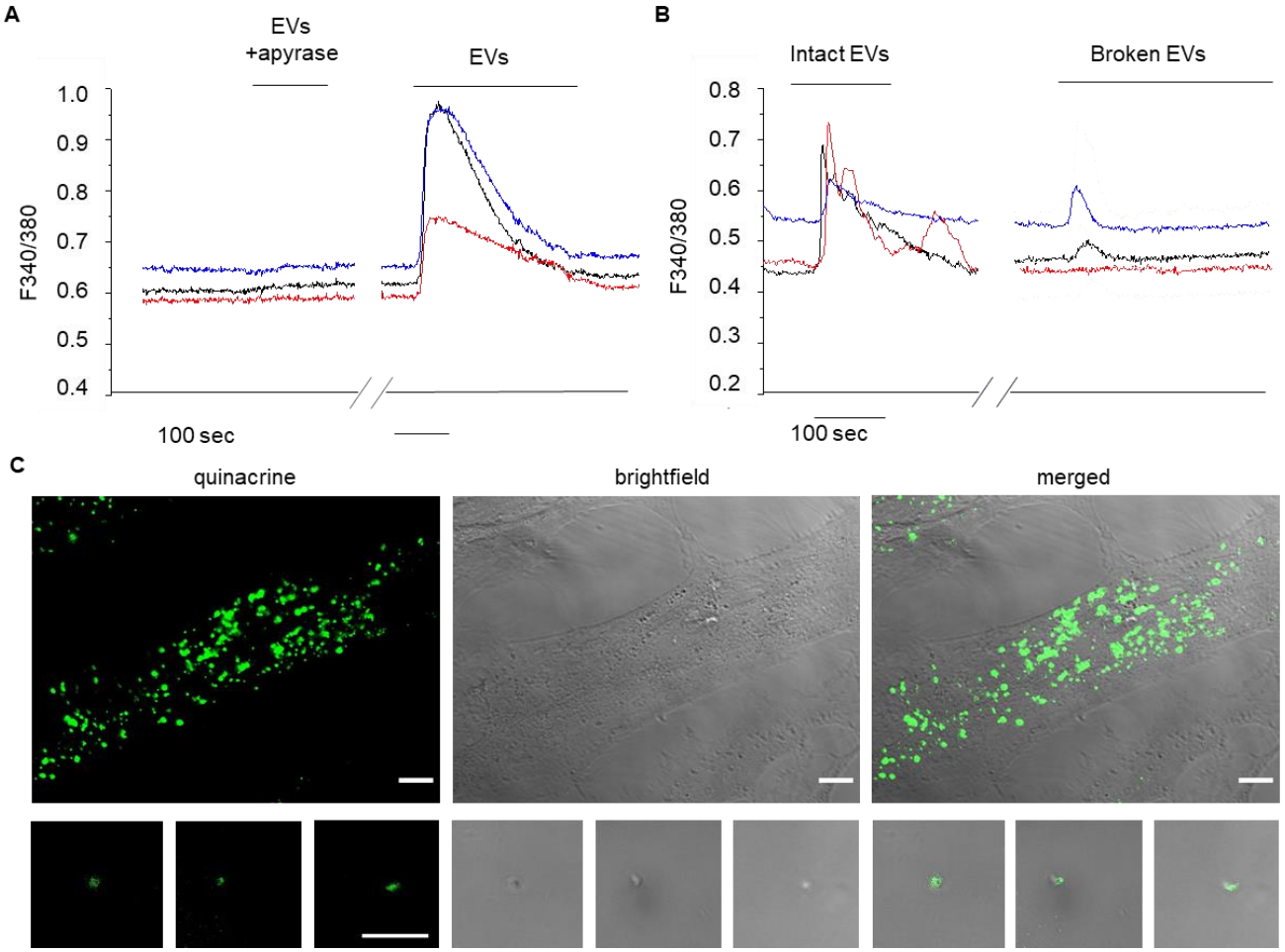

Fig.7: ATP store in astrocytes-derived EVs. A Temporal analysis of calcium changes in fura-2 loaded oligodendrocytes induced by EVs in the presence and in the absence of apyrase. Each trace is from a distinct oligodendroglial cell**. B** Representative calcium responses evoked in oligodendrocytes by intact and broken EVs, depleted of luminal cargo. **C** Representative fluorescent images of quinacrine (green) positive astrocytes (top) and EVs (bottom) merged with bright field images (Scale bar: 10μm).

DISCUSSION

5 DISCUSSION

Glia-derived EVs signal to neurons via multiple mechanisms, including transfer of RNA and protein cargoes and activation of signalling events at the neuron surface, influencing synaptic activity at both pre- and post-synaptic sites [39, 40, 49, 297]. However, how glial EVs interact with distinct neuron compartments has never been analyzed systematically and whether EVs interact with neurons at preferential sites to influence synaptic transmission is unknown.

By using OT combined to time-lapse imaging we here show that both microglial and astrocytic EVs adhere to any neuronal compartment (cell body, dendrites, axon) but, after adhesion, most EVs move from the contact site scanning the neuron surface to reach preferential interaction sites in the somatodendritic compartment.

5.1 FEATURES OF GLIAL EV MOTION ON THE NEURON SURFACE

EVs exhibited both radial and directional motion. Directional movement, the main component of EV motion, is intermittent and characterized by interruptions between periods of movement ("stop and go" motion). On average, EVs were in motion for nearly half the recording time.

We found that on the cell body, the amount of EVs moving extracellularly, derived either from microglia or astrocytes, is significantly lower compared to the moving fraction of EVs delivered on neuron processes. Accordingly, despite the velocity and the distance travelled on cell body and neurites are similar, EVs never exit the cell body to explore the surrounding processes, suggesting that the soma may be the final destination point of EVs. In rare cases EVs disappeared from the field likely fusing with the plasma membrane of neurons.

Along dendrites and axons EV motion occurs in both retrograde and anterograde direction reaching the soma of the neuron to which the neurite belongs to or the soma of a connected cell. Interestingly, EV motion may occur in the opposite direction of intracellular vesicles trafficking inside neurites (movie S8).

Monitoring of EV motion revealed that sometimes EVs stop along their path, especially when exploring dendritic spine protrusions on mature dendrites, resulting in lower EV speed on dendrites compared to axons in fully differentiated cultures. Further work would be necessary to define whether the preferential contact points along mature dendrites have a synaptic localization and represent the destination sites of EVs where the transfer of cargoes may occur.

Importantly, in developing cultures EVs are able to move from neuron-to-neuron along axons and EV speed on axons remains elevated during neuronal differentiation. This suggests that astrocytic EVs may use axonal projection as routes to spread their cargoes between synaptically-coupled neurons. Because the cargoes of astrocyte-derived EVs include misfolded proteins, such as tau and β-amyloid (Aβ) [298, 299], extracellular EV motion along projecting axons may underlie the propagation of Aβ/tau aggregates, which occurs through an anatomically defined pattern of connections, from the entorhinal cortex up to the hippocampal region and the neocortex in the brain of Alzheimer's disease (AD) patients [300]. Although previous evidence in AD cellular models shows that small EVs storing misfolded proteins can be internalized and transferred between neurons through axonal projections [68, 301], intra- and extra-cellular EV trafficking may be complementary, not mutually exclusive. Indeed, extracellular motion may represent a specific route to spread misfolded proteins for large-EVs, which exceed the axon diameter, and cannot be transported intracellularly without impairing vesicle trafficking.

5.2 SIMILARITIES BETWEEN EV AND VIRUS MOTION

A prominent finding of our study is that extracellular EV motion is strikingly similar to virus motion on the surface of infected cells. Both EVs (this study) and viruses [284] are passively transported at the target cell surface by rearrangements of actin (not microtubule) cytoskeleton. Indeed, in analogy to viral particle motion we here show that EV movement is sensitive to neuron treatment with Cytochalasin D, Blebbistatin and Sodium Azide but not Nocodazole despite being strongly inhibited in neurons treated with the metabolic inhibitor Rotenone.

As mentioned above EV movement is intermittent ('stop and go' motion), characterized by intervals during which the EV transiently stops on the neuron surface. We cannot unequivocally ascribe this behaviour to a precise molecular mechanism. However, the intermittent motion and the velocity of movement strikingly resemble that of f-actin transport [199] and of actin-associated proteins driven by actin waves.

'Stop and go' transport has been also described for microtubules and neurofilaments, through a poorly defined mechanism involving kinesin and dynein [199]. However, the EV speed is significantly slower compared to the velocity of dynein- and kinesin-mediated cargo transport (about 2-10 mm per day). In addition, EV movement is not significantly affected by microtubule depolymerization with nocodazole, ruling out a contribution of microtubules in EVs motion at the neuron surface.

Moreover, we show that both EV and virus motion are likely elicited by binding to a GPI anchor receptor, PrP on the neuron surface (this study) and CAR receptor on the surface of infected cells

[284]. Like CAR receptor, PrP does not contact directly the actin cytoskeleton. However, PrP interacts with a number of actin-binding intracellular partners, including the synaptic vesicle protein synapsin, and the adaptor protein critical for actin-based cell motility Growth factor receptor-bound protein 2 (Grb2) [302], which may couple EVs to the actin cytoskeleton. Alternatively, PrP may indirectly interact with actin via NCAM, which binds to both PrP and cytoplasmic proteins that interact with actin filaments, such as Ankyrin B and ezrin [303, 304]. Accordingly, NCAM was reported to colocalize with PrP at the neuron surface [123, 305].

EVs share with viruses many features, including physical and chemical characteristics and mechanisms of biogenesis and cellular uptake [306]. We here show that extracellular motion at target cell surface is an additional characteristic which EVs and viruses have in common, further strengthening similarities between viruses and EVs.

While providing first evidence for PrP involvement in extracellular EV transport, our study leaves more questions open. Among them, addressing whether homophilic interaction between neuronal and vesicular PrP is necessary for extracellular EV motion and which is the reciprocal contribution of neuronal versus vesicular PrP in the process will help to define whether PrP may represent a new target to limit diffusion of EV-associated toxic amyloid proteins in patients affected by neurodegenerative diseases.

5.3 A FRACTION OF EVS ACTIVELY MOVE AT THE NEURON SURFACE

The main accomplishment of our study is the demonstration that a fraction of EVs contains actin and has an independent capacity to move at the neuron surface, highlighting the active role of EVs in intercellular communication.

According to previous evidence we found by cryo-EM that EVs containing actin filaments are a small fraction of EVs (2%), characterized by a quite large diameter (> 200 nm) and often elongated or tubular in shape [78]. Given that by optical manipulation we can deliver to neurons only large EVs (> 200 nm, which are detectable in bright field), we can assume that a higher percentage of EVs carrying actin filaments were delivered to neurons. This would explain why by treating EVs with Cytochalasin D to block actin dynamics in the EV lumen, we found a block of EV motion in about 30% of EVs.

The independent capacity of EVs to move on the neuron surface, without the need of a neuronal dragging force, is corroborated by the observation that EVs are able to move on energy depleted or fixed neurons and can jump from one process to another, a transition that cannot be driven by

rearrangements of the intracellular cytoskeleton. Finally, we suggest that the energy source to support the actin cytoskeleton rearrangements inside the EVs, may be represented by ATP, which we detected in the lumen of the EVs and in the medium in which EVs were resuspended.

Importantly, tubular EVs which contain actin filaments strikingly resemble actin-rich membrane protrusions, such as philopodia and isolated tunnelling nanotubes (TNTs), recently characterized plasma membrane structures which assemble together to form connections between cells [307]. Similar to philopodia and isolated TNT, tubular EVs carry actin filaments oriented in parallel one to another, as evidenced by cryo-EM, suggesting that EVs could derived from either budding or fission from isolated TNT/philopodia [307]. Future characterization of the membrane and cytoskeleton-associated protein involved in EV budding at the plasma membrane and philopodia/TNT formation may help to clarify this intriguing hypothesis.

MATERIALS AND METHODS

6 MATERIAL AND METHODS

6.1 PRIMARY CULTURES AND TREATMENT

All the experimental procedures to establish primary cultures followed the guidelines defined by the European legislation (Directive 2010/63/EU), and the Italian Legislation (LD no. 26/2014). Astrocytic cultures were established from rat Sprague–Dawley pups (P2) (Charles River, Lecco, Italy), wild type FVB or FVB/ *Prnp*$^{0/0}$ pups (of either sex) [308]. Briefly, after dissection, hippocampi and cortices were dissociated by treatment with trypsin (0.25%, Gibco, Thermo Fisher, Leicestershire, UK) and DNase-I (Sigma-Aldrich, St. Louis, MO, USA) for 15 min at 37°C, followed by fragmentation with a pipette. Dissociated cells were plated on poly-L-lysine-coated (Sigma Aldrich, St. Louis, MO, USA) T75 flasks in minimal essential medium (MEM, Invitrogen, Life Technologies, Carlsbad, CA, USA) supplemented with 20% fetal bovine serum (FBS) (Gibco, Life Technologies, Carlsbad, CA, USA) and glucose (5.5 g/L, Sigma Aldrich, St. Louis, MO, USA). To obtain a pure astrocyte monolayer, microglial cells were harvested from 10–14-day-old cultures by orbital shaking for 30 min at 200 rpm. Hippocampal neurons were established from the hippocampi of 18-day-old fetal Sprague Dawley rats (E18) of either sex (Charles River, Lecco, Italy), wild-type (wt) FVB and FVB/*Prnp*$^{0/0}$ mice mouse embryos of either sex. Briefly, dissociated cells were plated onto poly-L-lysine treated coverslips and maintained in Neurobasal with 2% B27 supplement (Invitrogen, Carlsbad, CA, USA), antibiotics, glutamine and glutamate (Sigma Aldrich, St. Louis, MO, USA). Neurons were used at 2–17 DIV. To distinguish axon from dendrites neurons were transfected at DIV15 with a GFP expressing vector using Lipofectamine 2000 (0.75 μg of plasmid). At this developmental stage the efficiency of transfection is quite low (~5%) and allows distinction of axons from dendrites (Fig.2M). To block cytoskeleton dynamics, neurons were treated with 2 μM Rotenone (Sigma Aldrich, St. Louis, MO, USA) or 1 μM Cytochalasin D (Sigma Aldrich, St. Louis, MO) for 1 hour, 100 μM Blebbistatin (Sigma Aldrich, St. Louis, MO, USA) or 10-30 μM Nocodazolo (Sigma Aldrich, St. Louis, MO, USA) for 30 min. Sodium Azide (NaN_3, Sigma Aldrich, St. Louis, MO, USA) was added at a final 20 mM concentration to acute treatments. To verify inhibition of active lysosome transport in Rotenone-treated cultures, neurons were loaded with 100 nM LysoTracker DND-99 (Life Technologies, Carlsbad, CA, USA) for 30 min, washed and imaged by time lapse confocal microscopy. To downregulate PrP in astrocytes or neurons, cells were transfected with PrP-specific Accell smart pool siRNAs (1:500, Dharmacon, Carlo Erba Reagents Srl, Cornaredo, Italy) using Lipofectamine 2000 (Life Technologies, Carlsbad, CA, USA) for 48 h. Cells were then lysated and PrP-protein levels evaluated by western blotting analysis.

6.2 EVs ISOLATION TREATMENT AND LABELLING

Astrocytes were exposed to 1 mM ATP (Sigma-Aldrich, St. Louis, MO, USA) for 30 min in Krebs-Ringer's HEPES solution (KRH) (125 mM NaCl, 5 mM KCl, 1.2 mM MgSO4, 1.2 mM KH2PO, 2 mM CaCl2, 6 mM D-glucose, 25 mM HEPES/NaOH, pH 7.4). Conditioned KRH was collected and pre-cleared from cells and debris by centrifugation at 300× g for 10 min (twice). Large EVs were then pelleted from the supernatant by centrifugation at 10,000× g for 30 min and used immediately after isolation. In a set of experiments, isolated EVs were incubated with 3 µM Cytochalasin D for 1 hour at room temperature before being delivered by optical tweezers. To stain ATP store, EVs were incubated with 1 µM Quinacrine (Sigma Aldrich, St. Louis, MO, USA) for 30 min, washed with KRH and re-pelleted. The pellet was suspended in 150 µl of KRH and spotted on a glass coverslip for confocal microscopy.

6.3 F-ACTIN AND G-ACTIN ISOLATION FROM NEURONS AND EVs

F-actin/G-actin ratio was assessed as previously described [309]. Briefly, cultured neurons or freshly isolated EVs were resuspended in cold lysis buffer [10 mM K2HPO4, 100 mM NaF, 50 mM KCl, 2 mM MgCl2, 1 mM EGTA, 0.2 mM DTT, 0.5% Triton X-100, 1 mM sucrose (pH 7.0)] and centrifuged at 15,000x g for 30 min. The G-actin supernatant was transferred to a fresh tube, and the F-actin pellet was resuspended in lysis buffer plus an equal volume of a second buffer [1.5 mM guanidine hydrochloride, 1 mM sodium acetate, 1 mM CaCl2, 1 mM ATP, 20 mM tris-HCl (pH 7.5)] and then incubated on ice for 1 hour to convert F-actin into soluble G-actin. Samples were centrifuged at 15,000g for 30 min, and the supernatant (containing the F-actin, which was converted to G-actin) was transferred to a fresh tube. F-actin and G-actin samples were loaded with equal volumes and analyzed by Western blotting.

6.4 WESTERN BLOTTING

Astrocytes were lysed with a buffer containing 290 mM sucrose, 1% sodium dodecyl sulfate (SDS), 62.5 mM Tris-HCl pH 6.8 and proteases inhibitor (1:500). Neurons were lysed with a buffer containing 1% SDS, 2 mM EDTA pH 7.4, 10 mM Tris-HCl pH 7.4 and proteases inhibitor (1:500). EVs were lysed with a modified version of the Laemmli buffer (15% SDS, 575 mM sucrose, 325 mM Tris-HCl pH 6.8, 0.5% β-mercaptoethanol, 0.01% bromo-phenol blue) that was also added to lysated astrocytes and neurons to a final 1× concentration. Proteins were then separated by gel electrophoresis, blotted on nitrocellulose membrane filters and probed using mouse anti-PrP (1:1000; W226 (Dr Lothar Stitz, Institute of Immunology, Tuebingen, Germany), rabbit anti-Alix (1:500;

Covalab, Villeurbanne, France), mouse anti-Flotillin (1:1000, BD Biosciences, CA, USA), rabbit anti-Tom-20 (1:500; Santa Cruz Biotechnology, CA, USA), mouse anti-GS28 (1:1000; BD Biosciences, Franklin Lakes, NJ, USA), mouse anti-Actin (1:500; Sigma, St. Louis, MO, USA) antibodies, mouse anti-βIII-tubulin (1:4000; Promega, Madison, WI, USA) or Rabbit anti-GAPDH (1:2000; Synaptic Systems, Gottingen, Germany). Photographic development was by chemiluminescence (ECL, Euroclone or FEMTO, Thermo Scientific, MA, USA) according to the manufacturer's instructions. Western blot bands were quantified by ImageJ software.

6.5 BEAD FUNCTIONALIZATION

1 µm silica beads coated with COOH groups (Kisker-biotech, Steinfurt, Germany, cat PSi-1.5COOH) were functionalized using PolyLink Protein Coupling Kit (Bangs Laboratories Inc., Fishers, IN, USA, cat PL01N) following the manufacturer's protocol. Briefly, about 1.4 × 105 beads were incubated with 1 µg of recombinant PrP or C-terminal of PrP in the presence of 20 mg/mL EDAC for 1 h at room temperature (RT). Functionalized beads were then washed and stored in storage buffer at 4°C. Protein coupling was tested by Immunohistochemistry assay in which coated microspheres were incubated for 1 hour with primary anti-PrP antibodies (W226) followed by a 30-min incubation with secondary antibodies conjugated to Alexa Fluor 488 (Invitrogen, Life Technologies, Carlsbad, CA). Finally, beads were analyzed using fluorescence microscopy.

6.6 CRYO-EM OF EVS AND ACTIN ANALYSIS

Cryo-EM allows imaging of samples without the addition of any heavy metals or fixatives, which might cause artefacts, with the drawback of yielding a lower contrast. The sample is frozen so rapidly that the water vitrifies forming no ordered crystals, and the native structure of the sample is preserved. Freshly prepared EVs resuspended in saline were vitrified by applying a 3.5-µl droplet onto a holey carbon grids (Copper 300-mesh Quantifoil R2/1) glow discharged for 45 seconds at 40 mA using a GloQube system (Quorum Technologies, East Sussex, UK). After 60 seconds incubation, the grid was plunge-frozen in liquid ethane using a Vitrobot Mk IV (Thermo Fischer Scientific, Waltham, MA, USA) operating at 4°C and 100% RH. Images of the vitrified specimen were acquired using a Talos Arctica transmission electron microscope (Thermo Fisher Scientific, Waltham, MA, USA) operating at 200 kV and equipped with a Falcon 3EC direct electron detector (Thermo Fischer Scientific, Waltham, MA, USA). Images were acquired with an exposure time of 1 s and a total accumulated dose of 80 electrons per A2 at a nominal magnification of 45,000×, corresponding to a pixel size of 2.29 Å/pixel at the specimen level, with applied defocus values between 2 and 4 µm. Images acquired with Volta phase-plate were recorded at defocus values between 0.5 and 1 µm.

Contrast transfer function (CTF) estimation was performed using CTFFIND4 [310]. All EVs contained within the image were measured using ImageJ software. EVs were classified in single round EVs, oval EVs, tubular EVs, irregular EVs or double/multilamellar EVs. Oval EVs and tubular EVs were measured along their long axis.

Actin filament picking, segments extraction and analyses were performed using RELION-3 software [311]. Filaments were manually picked using RELION's helix picker and a total of 1,381 segments were extracted using a box size of 100 pixel and inter-box distance of ~10% [310],[311].

6.7 OPTICAL TWEEZERS

An IR laser beam (1064 nm, CW) for trapping was collimated into the optical path of an inverted microscope (Axiovert 200 M, Zeiss, Oberkochen, Germany) through the right port of the microscope. The trapping beam was directed to the microscope lens (Zeiss 63X objective, oil immersion, NA 1.4) by the corresponding port mirror (100%) and the tube lens. Optical trapping and manipulation of EVs was performed following the approach previously described [71]. Immediately before recording, neurons were washed to remove EVs constitutively released by neurons, and EVs produced by ~2500 K astrocytes pre-loaded with Calcein (FilmTracer™ Calcein Green Biofilm Stain, Life Technologies, Carlsbad, CA, USA; 26 μM for 1 hour) were added to neurons plated on glass coverslips and maintained in 400 μl of neuronal medium in a 5% CO_2 and temperature controlled recording chamber at 37°C. As soon as a Calcein-positive EV appeared in the recording field, it was trapped and positioned on a selected neuron by moving the cell stage horizontally and the microscope lens axially. A set of experiments were carried out with EVs released by astrocytes not stained with Calcein. After about 30 sec from contact, the laser was switched off to prove EV–neuron interaction. During the experiments neurons were live imaged using a digital camera (High Sensitivity USB 3.0 CMOS Camera 1280 × 1024 Global Shutter Monochrome Sensor, Thorlabs, Newton, NJ, USA) at a frame rate of 2 Hz.

6.8 TRACKING OF SINGLE EV

EV position was determined for each video frame (2 frames every 5 seconds) using a custom MATLAB code (it.mathworks.com). To characterize the EV displacement on the neuron process, 2 distances were calculated: the maximum distance the EV reached from the initial position (in both directions), and the length of the path travelled by the EV in 20 minutes. Mean velocity and distances were extracted from EV coordinates using a custom R code that exploits the Pythagorean theorem to reconstruct the EV path point-to-point (www.r-project.org). As the code works well only for straight

path, the distance from the starting point was calculated using ImageJ software (www.imagej.nih.gov/ij/), when the EV trajectory was not linear, tracing the path manually. We classified as "static EVs" i) the EVs with net displacement < of the EV diameter and ii) EVs showing only random (Brownian) motion.

6.9 FURA-2 VIDEOMICROSCOPY

14 DIV hippocampal neurons were loaded with 2 μM Fura-2 (Invitrogen, Carlsbad, CA, USA) pentacetoxy methylester for 45 min at 37 °C, washed and transferred to the recording chamber of an inverted microscope (Axiovert 100; Zeiss, Oberkochen, Germany) equipped with a calcium imaging unit Polychrome V (TILL Photonics GmbH, Planegg, Germany). Images were collected with a CCD Imago-QE camera (TILL Photonics GmbH, Planegg, Germany) and analyzed with TILLvisION 4.5.66 software (TILL Photonics GmbH, Planegg, Germany). After excitation at 340 and 380 nm wavelengths, the emitted light was acquired at 505 nm at 1 Hz. Calcium concentration was expressed as F340/F380 fluorescence ratio. The ratio values in selected region of interest corresponding to neuronal cell bodies were calculated from sequences of images to obtain temporal analysis.

6.10 ATP MEASUREMENTS IN EVS

The biological assay for ATP detection was performed following a modification of the method previously described[295], using fura-2 loaded oligodendrocytes as ATP sensor cells. Glial EVs, derived from $5X10^6$ cells, were resuspended in KRH and split into two aliquots before testing on oligodendrocytes. Only one aliquot was pretreated with Apyrase (30 units/ml, Sigma, St. Louis, MO, USA) for 15 min to verify that the calcium responses evoked by the EVs in oligodendrocytes were due to EVs-associated ATP. The other aliquot was used as a positive control. The increases in calcium were quantified by measuring the peak of the response. To deplete EVs from their luminal content, EVs were broken or not by hypo-osmotic stress (via suspension in 7.3 mM Phosphate Buffer at 4°C for 30 min) and re-pelleted at 10000g for 1h before being resuspended in KRH and tested on oligodendrocytes.

6.11 DATA ANALYSIS

All data are expressed as means ± SEM. Data were first tested for normal distribution with GraphPad Prism 6 software, then the appropriate statistical test has been used (see figure legends). The accepted level of significance was $p \leq 0.05$, indicated by one asterisk; those at $p \leq 0.01$ are indicated by double asterisks, while the ones at $p \leq 0.001$ are indicated by triple asterisk.

7 REFERENCES

1. Cocucci, E., G. Racchetti, and J. Meldolesi, *Shedding microvesicles: artefacts no more.* Trends Cell Biol, 2009. **19**(2): p. 43-51.
2. Camussi, G., et al., *Exosomes/microvesicles as a mechanism of cell-to-cell communication.* Kidney Int, 2010. **78**(9): p. 838-48.
3. Holm, M.M., J. Kaiser, and M.E. Schwab, *Extracellular Vesicles: Multimodal Envoys in Neural Maintenance and Repair.* Trends Neurosci, 2018. **41**(6): p. 360-372.
4. Iraci, N., et al., *Extracellular vesicles are independent metabolic units with asparaginase activity.* Nat Chem Biol, 2017. **13**(9): p. 951-955.
5. Cocucci, E. and J. Meldolesi, *Ectosomes and exosomes: shedding the confusion between extracellular vesicles.* Trends Cell Biol, 2015. **25**(6): p. 364-72.
6. Schiera, G., C.M. Di Liegro, and I. Di Liegro, *Extracellular Membrane Vesicles as Vehicles for Brain Cell-to-Cell Interactions in Physiological as well as Pathological Conditions.* Biomed Res Int, 2015. **2015**: p. 152926.
7. Verderio, C., et al., *Myeloid microvesicles are a marker and therapeutic target for neuroinflammation.* Ann Neurol, 2012. **72**(4): p. 610-24.
8. Campanella, C., et al., *On the Choice of the Extracellular Vesicles for Therapeutic Purposes.* Int J Mol Sci, 2019. **20**(2).
9. Chargaff, E. and R. West, *The biological significance of the thromboplastic protein of blood.* J Biol Chem, 1946. **166**(1): p. 189-97.
10. Wolf, P., *The nature and significance of platelet products in human plasma.* Br J Haematol, 1967. **13**(3): p. 269-88.
11. Anderson, H.C., *Vesicles associated with calcification in the matrix of epiphyseal cartilage.* J Cell Biol, 1969. **41**(1): p. 59-72.
12. De Broe M, W.R., Roels F, *Letter: membrane fragments with koinozymic properties released from villous adenoma of the rectum.* Lancet, 1975. **2**: p. 1214-5.
13. Benz, E.W., Jr. and H.L. Moses, *Small, virus-like particles detected in bovine sera by electron microscopy.* J Natl Cancer Inst, 1974. **52**(6): p. 1931-4.
14. Dalton, A.J., *Microvesicles and vesicles of multivesicular bodies versus "virus-like" particles.* J Natl Cancer Inst, 1975. **54**(5): p. 1137-48.
15. Ronquist, G., et al., *An Mg2+ and Ca2+-stimulated adenosine triphosphatase in human prostatic fluid--part II.* Andrologia, 1978. **10**(6): p. 427-33.
16. Taylor, D.D., H.D. Homesley, and G.J. Doellgast, *Binding of specific peroxidase-labeled antibody to placental-type phosphatase on tumor-derived membrane fragments.* Cancer Res, 1980. **40**(11): p. 4064-9.
17. Dvorak, H.F., et al., *Tumor shedding and coagulation.* Science, 1981. **212**(4497): p. 923-4.
18. Harding, C., J. Heuser, and P. Stahl, *Receptor-mediated endocytosis of transferrin and recycling of the transferrin receptor in rat reticulocytes.* J Cell Biol, 1983. **97**(2): p. 329-39.
19. Pan, B.T., et al., *Electron microscopic evidence for externalization of the transferrin receptor in vesicular form in sheep reticulocytes.* J Cell Biol, 1985. **101**(3): p. 942-8.
20. Johnstone, R.M., et al., *Vesicle formation during reticulocyte maturation. Association of plasma membrane activities with released vesicles (exosomes).* J Biol Chem, 1987. **262**(19): p. 9412-20.

21. Stein, J.M.a.L., J.P., *Exocytosis caused by sublytic autologous complement attack on human neutophils. The sorting of endogenous plasma membrane proteins and lipids into shed vesicles.* Biochem. J., 1991. **274**: p. 381–386.
22. Raposo, G., et al., *B lymphocytes secrete antigen-presenting vesicles.* J Exp Med, 1996. **183**(3): p. 1161-72.
23. Ratajczak, J., et al., *Embryonic stem cell-derived microvesicles reprogram hematopoietic progenitors: evidence for horizontal transfer of mRNA and protein delivery.* Leukemia, 2006. **20**(5): p. 847-56.
24. Valadi, H., et al., *Exosome-mediated transfer of mRNAs and microRNAs is a novel mechanism of genetic exchange between cells.* Nat Cell Biol, 2007. **9**(6): p. 654-9.
25. Yanez-Mo, M., et al., *Biological properties of extracellular vesicles and their physiological functions.* J Extracell Vesicles, 2015. **4**: p. 27066.
26. Tricarico, C., J. Clancy, and C. D'Souza-Schorey, *Biology and biogenesis of shed microvesicles.* Small GTPases, 2017. **8**(4): p. 220-232.
27. Caruso Bavisotto, C., et al., *Extracellular Vesicle-Mediated Cell(-)Cell Communication in the Nervous System: Focus on Neurological Diseases.* Int J Mol Sci, 2019. **20**(2).
28. Maas, S.L.N., X.O. Breakefield, and A.M. Weaver, *Extracellular Vesicles: Unique Intercellular Delivery Vehicles.* Trends Cell Biol, 2017. **27**(3): p. 172-188.
29. Raposo, G. and W. Stoorvogel, *Extracellular vesicles: exosomes, microvesicles, and friends.* J Cell Biol, 2013. **200**(4): p. 373-83.
30. Basso, M. and V. Bonetto, *Extracellular Vesicles and a Novel Form of Communication in the Brain.* Front Neurosci, 2016. **10**: p. 127.
31. Thery, C., et al., *Minimal information for studies of extracellular vesicles 2018 (MISEV2018): a position statement of the International Society for Extracellular Vesicles and update of the MISEV2014 guidelines.* J Extracell Vesicles, 2018. **7**(1): p. 1535750.
32. Lai, C.P. and X.O. Breakefield, *Role of exosomes/microvesicles in the nervous system and use in emerging therapies.* Front Physiol, 2012. **3**: p. 228.
33. Rajendran, L., et al., *Emerging roles of extracellular vesicles in the nervous system.* J Neurosci, 2014. **34**(46): p. 15482-9.
34. Budnik, V., C. Ruiz-Canada, and F. Wendler, *Extracellular vesicles round off communication in the nervous system.* Nat Rev Neurosci, 2016. **17**(3): p. 160-72.
35. Kramer-Albers, E.M. and A.F. Hill, *Extracellular vesicles: interneural shuttles of complex messages.* Curr Opin Neurobiol, 2016. **39**: p. 101-7.
36. Taylor, A.R., et al., *Regulation of heat shock protein 70 release in astrocytes: role of signaling kinases.* Dev Neurobiol, 2007. **67**(13): p. 1815-29.
37. Wang, S., et al., *Synapsin I is an oligomannose-carrying glycoprotein, acts as an oligomannose-binding lectin, and promotes neurite outgrowth and neuronal survival when released via glia-derived exosomes.* J Neurosci, 2011. **31**(20): p. 7275-90.
38. Gosselin, R.D., P. Meylan, and I. Decosterd, *Extracellular microvesicles from astrocytes contain functional glutamate transporters: regulation by protein kinase C and cell activation.* Front Cell Neurosci, 2013. **7**: p. 251.
39. Antonucci, F., et al., *Microvesicles released from microglia stimulate synaptic activity via enhanced sphingolipid metabolism.* EMBO J, 2012. **31**(5): p. 1231-40.
40. Gabrielli, M., et al., *Active endocannabinoids are secreted on extracellular membrane vesicles.* EMBO Rep, 2015. **16**(2): p. 213-20.

41. Fruhbeis, C., et al., *Neurotransmitter-triggered transfer of exosomes mediates oligodendrocyte-neuron communication.* PLoS Biol, 2013. **11**(7): p. e1001604.
42. Frohlich, D., et al., *Multifaceted effects of oligodendroglial exosomes on neurons: impact on neuronal firing rate, signal transduction and gene regulation.* Philos Trans R Soc Lond B Biol Sci, 2014. **369**(1652).
43. Kramer-Albers, E.M., et al., *Oligodendrocytes secrete exosomes containing major myelin and stress-protective proteins: Trophic support for axons?* Proteomics Clin Appl, 2007. **1**(11): p. 1446-61.
44. Korkut, C., et al., *Regulation of postsynaptic retrograde signaling by presynaptic exosome release.* Neuron, 2013. **77**(6): p. 1039-46.
45. Goldie, B.J., et al., *Activity-associated miRNA are packaged in Map1b-enriched exosomes released from depolarized neurons.* Nucleic Acids Res, 2014. **42**(14): p. 9195-208.
46. Ashley, J., et al., *Retrovirus-like Gag Protein Arc1 Binds RNA and Traffics across Synaptic Boutons.* Cell, 2018. **172**(1-2): p. 262-274 e11.
47. Bianco, F., et al., *Acid sphingomyelinase activity triggers microparticle release from glial cells.* EMBO J, 2009. **28**(8): p. 1043-54.
48. Bianco, F., et al., *Astrocyte-derived ATP induces vesicle shedding and IL-1 beta release from microglia.* J Immunol, 2005. **174**(11): p. 7268-77.
49. Prada, I., et al., *Glia-to-neuron transfer of miRNAs via extracellular vesicles: a new mechanism underlying inflammation-induced synaptic alterations.* Acta Neuropathol, 2018. **135**(4): p. 529-550.
50. Dickens, A.M., et al., *Astrocyte-shed extracellular vesicles regulate the peripheral leukocyte response to inflammatory brain lesions.* Sci Signal, 2017. **10**(473).
51. Saenz-Cuesta, M., I. Osorio-Querejeta, and D. Otaegui, *Extracellular Vesicles in Multiple Sclerosis: What are They Telling Us?* Front Cell Neurosci, 2014. **8**: p. 100.
52. Schiera, G., C.M. Di Liegro, and I. Di Liegro, *Molecular Determinants of Malignant Brain Cancers: From Intracellular Alterations to Invasion Mediated by Extracellular Vesicles.* Int J Mol Sci, 2017. **18**(12).
53. Zhang, L., et al., *Microenvironment-induced PTEN loss by exosomal microRNA primes brain metastasis outgrowth.* Nature, 2015. **527**(7576): p. 100-104.
54. Fevrier, B., et al., *Cells release prions in association with exosomes.* Proc Natl Acad Sci U S A, 2004. **101**(26): p. 9683-8.
55. Rajendran, L., et al., *Alzheimer's disease beta-amyloid peptides are released in association with exosomes.* Proc Natl Acad Sci U S A, 2006. **103**(30): p. 11172-7.
56. Emmanouilidou, E., et al., *Cell-produced alpha-synuclein is secreted in a calcium-dependent manner by exosomes and impacts neuronal survival.* J Neurosci, 2010. **30**(20): p. 6838-51.
57. Gomes, C., et al., *Evidence for secretion of Cu,Zn superoxide dismutase via exosomes from a cell model of amyotrophic lateral sclerosis.* Neurosci Lett, 2007. **428**(1): p. 43-6.
58. Ding, X., et al., *Exposure to ALS-FTD-CSF generates TDP-43 aggregates in glioblastoma cells through exosomes and TNTs-like structure.* Oncotarget, 2015. **6**(27): p. 24178-91.
59. Saman, S., et al., *Exosome-associated tau is secreted in tauopathy models and is selectively phosphorylated in cerebrospinal fluid in early Alzheimer disease.* J Biol Chem, 2012. **287**(6): p. 3842-9.
60. Vella, L.J., et al., *Enrichment of prion protein in exosomes derived from ovine cerebral spinal fluid.* Vet Immunol Immunopathol, 2008. **124**(3-4): p. 385-93.

61. Cirrito, J.R., et al., *Serotonin signaling is associated with lower amyloid-beta levels and plaques in transgenic mice and humans.* Proc Natl Acad Sci U S A, 2011. **108**(36): p. 14968-73.
62. Joshi, P., et al., *Microglia convert aggregated amyloid-beta into neurotoxic forms through the shedding of microvesicles.* Cell Death Differ, 2014. **21**(4): p. 582-93.
63. Wang, G., et al., *Astrocytes secrete exosomes enriched with proapoptotic ceramide and prostate apoptosis response 4 (PAR-4): potential mechanism of apoptosis induction in Alzheimer disease (AD).* J Biol Chem, 2012. **287**(25): p. 21384-95.
64. Agosta, F., et al., *Myeloid microvesicles in cerebrospinal fluid are associated with myelin damage and neuronal loss in mild cognitive impairment and Alzheimer disease.* Ann Neurol, 2014. **76**(6): p. 813-25.
65. Basso, M., et al., *Mutant copper-zinc superoxide dismutase (SOD1) induces protein secretion pathway alterations and exosome release in astrocytes: implications for disease spreading and motor neuron pathology in amyotrophic lateral sclerosis.* J Biol Chem, 2013. **288**(22): p. 15699-711.
66. Asai, H., et al., *Depletion of microglia and inhibition of exosome synthesis halt tau propagation.* Nat Neurosci, 2015. **18**(11): p. 1584-93.
67. Dinkins, M.B., et al., *Exosome reduction in vivo is associated with lower amyloid plaque load in the 5XFAD mouse model of Alzheimer's disease.* Neurobiol Aging, 2014. **35**(8): p. 1792-800.
68. Wang, Y., et al., *The release and trans-synaptic transmission of Tau via exosomes.* Mol Neurodegener, 2017. **12**(1): p. 5.
69. Doyle, L.M. and M.Z. Wang, *Overview of Extracellular Vesicles, Their Origin, Composition, Purpose, and Methods for Exosome Isolation and Analysis.* Cells, 2019. **8**(7).
70. Chuo, S.T., J.C. Chien, and C.P. Lai, *Imaging extracellular vesicles: current and emerging methods.* J Biomed Sci, 2018. **25**(1): p. 91.
71. Prada, I., et al., *A new approach to follow a single extracellular vesicle-cell interaction using optical tweezers.* Biotechniques, 2016. **60**(1): p. 35-41.
72. Heusermann, W., et al., *Exosomes surf on filopodia to enter cells at endocytic hot spots, traffic within endosomes, and are targeted to the ER.* J Cell Biol, 2016. **213**(2): p. 173-84.
73. Montecalvo, A., et al., *Mechanism of transfer of functional microRNAs between mouse dendritic cells via exosomes.* Blood, 2012. **119**(3): p. 756-66.
74. Barres, C., et al., *Galectin-5 is bound onto the surface of rat reticulocyte exosomes and modulates vesicle uptake by macrophages.* Blood, 2010. **115**(3): p. 696-705.
75. Morelli, A.E., *The immune regulatory effect of apoptotic cells and exosomes on dendritic cells: its impact on transplantation.* Am J Transplant, 2006. **6**(2): p. 254-61.
76. Tian, T., et al., *Visualizing of the cellular uptake and intracellular trafficking of exosomes by live-cell microscopy.* J Cell Biochem, 2010. **111**(2): p. 488-96.
77. Choi, H., Mun JY., *Structural Analysis of Exosomes Using Different Types of Electron Microscopy.* Applied Microscopy, 2017.
78. Cvjetkovic A., C.R., Lässer C., Zabeo D., Widlund P., Nyström T., Höög JL., Lötvall J., *Extracellular Vesicles in Motion.* Matters, 2017.
79. Zabeo, D., et al., *Exosomes purified from a single cell type have diverse morphology.* J Extracell Vesicles, 2017. **6**(1): p. 1329476.

80. Brisson, A.R., et al., *Extracellular vesicles from activated platelets: a semiquantitative cryo-electron microscopy and immuno-gold labeling study.* Platelets, 2017. **28**(3): p. 263-271.
81. Koifman, N., et al., *A direct-imaging cryo-EM study of shedding extracellular vesicles from leukemic monocytes.* J Struct Biol, 2017. **198**(3): p. 177-185.
82. Yuana, Y., et al., *Cryo-electron microscopy of extracellular vesicles in fresh plasma.* J Extracell Vesicles, 2013. **2**.
83. Wiklander, O.P., et al., *Extracellular vesicle in vivo biodistribution is determined by cell source, route of administration and targeting.* J Extracell Vesicles, 2015. **4**: p. 26316.
84. Askenasy, N. and D.L. Farkas, *Optical imaging of PKH-labeled hematopoietic cells in recipient bone marrow in vivo.* Stem Cells, 2002. **20**(6): p. 501-13.
85. Verweij, F.J., et al., *Extracellular Vesicles: Catching the Light in Zebrafish.* Trends Cell Biol, 2019.
86. Betzer, O., et al., *In Vivo Neuroimaging of Exosomes Using Gold Nanoparticles.* ACS Nano, 2017. **11**(11): p. 10883-10893.
87. Bendheim, P.E., et al., *Nearly ubiquitous tissue distribution of the scrapie agent precursor protein.* Neurology, 1992. **42**(1): p. 149-56.
88. Prusiner, S.B., *Novel proteinaceous infectious particles cause scrapie.* Science, 1982. **216**(4542): p. 136-44.
89. Wulf, M.A., A. Senatore, and A. Aguzzi, *The biological function of the cellular prion protein: an update.* BMC Biol, 2017. **15**(1): p. 34.
90. Castle, A.R. and A.C. Gill, *Physiological Functions of the Cellular Prion Protein.* Front Mol Biosci, 2017. **4**: p. 19.
91. Rambold, A.S., et al., *Stress-protective signalling of prion protein is corrupted by scrapie prions.* EMBO J, 2008. **27**(14): p. 1974-84.
92. Beland, M. and X. Roucou, *Homodimerization as a molecular switch between low and high efficiency PrP C cell surface delivery and neuroprotective activity.* Prion, 2013. **7**(2): p. 170-4.
93. Haire, L.F., et al., *The crystal structure of the globular domain of sheep prion protein.* J Mol Biol, 2004. **336**(5): p. 1175-83.
94. Vey, M., et al., *Subcellular colocalization of the cellular and scrapie prion proteins in caveolae-like membranous domains.* Proc Natl Acad Sci U S A, 1996. **93**(25): p. 14945-9.
95. Sunyach, C., et al., *The mechanism of internalization of glycosylphosphatidylinositol-anchored prion protein.* EMBO J, 2003. **22**(14): p. 3591-601.
96. Gu, Y., et al., *Identification of cryptic nuclear localization signals in the prion protein.* Neurobiol Dis, 2003. **12**(2): p. 133-49.
97. Morel, E., et al., *The cellular prion protein PrP(c) is involved in the proliferation of epithelial cells and in the distribution of junction-associated proteins.* PLoS One, 2008. **3**(8): p. e3000.
98. Besnier, L.S., et al., *The cellular prion protein PrPc is a partner of the Wnt pathway in intestinal epithelial cells.* Mol Biol Cell, 2015. **26**(18): p. 3313-28.
99. Hachiya, N.S., et al., *Mitochondrial localization of cellular prion protein (PrPC) invokes neuronal apoptosis in aged transgenic mice overexpressing PrPC.* Neurosci Lett, 2005. **374**(2): p. 98-103.
100. Faris, R., et al., *Cellular prion protein is present in mitochondria of healthy mice.* Sci Rep, 2017. **7**: p. 41556.

101. Calzolai, L. and R. Zahn, *Influence of pH on NMR structure and stability of the human prion protein globular domain.* J Biol Chem, 2003. **278**(37): p. 35592-6.
102. Watts, J.C., M.E.C. Bourkas, and H. Arshad, *The function of the cellular prion protein in health and disease.* Acta Neuropathol, 2018. **135**(2): p. 159-178.
103. Sales, N., et al., *Developmental expression of the cellular prion protein in elongating axons.* Eur J Neurosci, 2002. **15**(7): p. 1163-77.
104. Adle-Biassette, H., et al., *Immunohistochemical expression of prion protein (PrPC) in the human forebrain during development.* J Neuropathol Exp Neurol, 2006. **65**(7): p. 698-706.
105. Hartmann, C.A., V.R. Martins, and F.R. Lima, *High levels of cellular prion protein improve astrocyte development.* FEBS Lett, 2013. **587**(2): p. 238-44.
106. Lima, F.R., et al., *Cellular prion protein expression in astrocytes modulates neuronal survival and differentiation.* J Neurochem, 2007. **103**(6): p. 2164-76.
107. Moser, M., et al., *Developmental expression of the prion protein gene in glial cells.* Neuron, 1995. **14**(3): p. 509-17.
108. Bribian, A., et al., *Role of the cellular prion protein in oligodendrocyte precursor cell proliferation and differentiation in the developing and adult mouse CNS.* PLoS One, 2012. **7**(4): p. e33872.
109. Anantharam, V., et al., *Opposing roles of prion protein in oxidative stress- and ER stress-induced apoptotic signaling.* Free Radic Biol Med, 2008. **45**(11): p. 1530-41.
110. Bertuchi, F.R., et al., *PrPC displays an essential protective role from oxidative stress in an astrocyte cell line derived from PrPC knockout mice.* Biochem Biophys Res Commun, 2012. **418**(1): p. 27-32.
111. Brown, D.R., et al., *Prion protein-deficient cells show altered response to oxidative stress due to decreased SOD-1 activity.* Exp Neurol, 1997. **146**(1): p. 104-12.
112. Rachidi, W., et al., *Expression of prion protein increases cellular copper binding and antioxidant enzyme activities but not copper delivery.* J Biol Chem, 2003. **278**(11): p. 9064-72.
113. Paterson, A.W., J.C. Curtis, and N.K. Macleod, *Complex I specific increase in superoxide formation and respiration rate by PrP-null mouse brain mitochondria.* J Neurochem, 2008. **105**(1): p. 177-91.
114. Bravard, A., et al., *The prion protein is critical for DNA repair and cell survival after genotoxic stress.* Nucleic Acids Res, 2015. **43**(2): p. 904-16.
115. Krebs, B., et al., *Cellular prion protein modulates the intracellular calcium response to hydrogen peroxide.* J Neurochem, 2007. **100**(2): p. 358-67.
116. Lopes, M.H., et al., *Interaction of cellular prion and stress-inducible protein 1 promotes neuritogenesis and neuroprotection by distinct signaling pathways.* J Neurosci, 2005. **25**(49): p. 11330-9.
117. Santuccione, A., et al., *Prion protein recruits its neuronal receptor NCAM to lipid rafts to activate p59fyn and to enhance neurite outgrowth.* J Cell Biol, 2005. **169**(2): p. 341-54.
118. Llorens, F., et al., *PrP(C) regulates epidermal growth factor receptor function and cell shape dynamics in Neuro2a cells.* J Neurochem, 2013. **127**(1): p. 124-38.
119. Loubet, D., et al., *Neuritogenesis: the prion protein controls beta1 integrin signaling activity.* FASEB J, 2012. **26**(2): p. 678-90.
120. Graner, E., et al., *Cellular prion protein binds laminin and mediates neuritogenesis.* Brain Res Mol Brain Res, 2000. **76**(1): p. 85-92.

121. Beraldo, F.H., et al., *Metabotropic glutamate receptors transduce signals for neurite outgrowth after binding of the prion protein to laminin gamma1 chain.* FASEB J, 2011. **25**(1): p. 265-79.
122. O'Connor, T.P., J.S. Duerr, and D. Bentley, *Pioneer growth cone steering decisions mediated by single filopodial contacts in situ.* J Neurosci, 1990. **10**(12): p. 3935-46.
123. Amin, L., et al., *Characterization of prion protein function by focal neurite stimulation.* J Cell Sci, 2016. **129**(20): p. 3878-3891.
124. Malaga-Trillo, E., et al., *Regulation of embryonic cell adhesion by the prion protein.* PLoS Biol, 2009. **7**(3): p. e55.
125. Sempou, E., et al., *Activation of zebrafish Src family kinases by the prion protein is an amyloid-beta-sensitive signal that prevents the endocytosis and degradation of E-cadherin/beta-catenin complexes in vivo.* Mol Neurodegener, 2016. **11**: p. 18.
126. Steele, A.D., et al., *Prion protein (PrPc) positively regulates neural precursor proliferation during developmental and adult mammalian neurogenesis.* Proc Natl Acad Sci U S A, 2006. **103**(9): p. 3416-21.
127. Lee, Y.J. and I.V. Baskakov, *The cellular form of the prion protein guides the differentiation of human embryonic stem cells into neuron-, oligodendrocyte-, and astrocyte-committed lineages.* Prion, 2014. **8**(3): p. 266-75.
128. Muller, W.E., et al., *Cytoprotective effect of NMDA receptor antagonists on prion protein (PrionSc)-induced toxicity in rat cortical cell cultures.* Eur J Pharmacol, 1993. **246**(3): p. 261-7.
129. Gorman, A.M., *Neuronal cell death in neurodegenerative diseases: recurring themes around protein handling.* J Cell Mol Med, 2008. **12**(6A): p. 2263-80.
130. Khosravani, H., et al., *Prion protein attenuates excitotoxicity by inhibiting NMDA receptors.* J Gen Physiol, 2008. **131**(6): p. i5.
131. Lai, T.W., S. Zhang, and Y.T. Wang, *Excitotoxicity and stroke: identifying novel targets for neuroprotection.* Prog Neurobiol, 2014. **115**: p. 157-88.
132. Shyu, W.C., et al., *Hypoglycemia enhances the expression of prion protein and heat-shock protein 70 in a mouse neuroblastoma cell line.* J Neurosci Res, 2005. **80**(6): p. 887-94.
133. Collinge, J., et al., *Prion protein is necessary for normal synaptic function.* Nature, 1994. **370**(6487): p. 295-7.
134. Schmitz, M., et al., *Loss of prion protein leads to age-dependent behavioral abnormalities and changes in cytoskeletal protein expression.* Mol Neurobiol, 2014. **50**(3): p. 923-36.
135. Rial, D., et al., *Cellular prion protein modulates age-related behavioral and neurochemical alterations in mice.* Neuroscience, 2009. **164**(3): p. 896-907.
136. Lugaresi, E., et al., *Fatal familial insomnia and dysautonomia with selective degeneration of thalamic nuclei.* N Engl J Med, 1986. **315**(16): p. 997-1003.
137. Mastrianni, J.A., et al., *Prion protein conformation in a patient with sporadic fatal insomnia.* N Engl J Med, 1999. **340**(21): p. 1630-8.
138. Tobler, I., et al., *Altered circadian activity rhythms and sleep in mice devoid of prion protein.* Nature, 1996. **380**(6575): p. 639-42.
139. Tatsuki, F., et al., *Involvement of Ca(2+)-Dependent Hyperpolarization in Sleep Duration in Mammals.* Neuron, 2016. **90**(1): p. 70-85.
140. Brown, D.R., et al., *The cellular prion protein binds copper in vivo.* Nature, 1997. **390**(6661): p. 684-7.

141. Hornshaw, M.P., J.R. McDermott, and J.M. Candy, *Copper binding to the N-terminal tandem repeat regions of mammalian and avian prion protein.* Biochem Biophys Res Commun, 1995. **207**(2): p. 621-9.
142. Hornshaw, M.P., et al., *Copper binding to the N-terminal tandem repeat region of mammalian and avian prion protein: structural studies using synthetic peptides.* Biochem Biophys Res Commun, 1995. **214**(3): p. 993-9.
143. Gasperini, L., et al., *Prion protein and copper cooperatively protect neurons by modulating NMDA receptor through S-nitrosylation.* Antioxid Redox Signal, 2015. **22**(9): p. 772-84.
144. Brown, D.R. and C.M. Mohn, *Astrocytic glutamate uptake and prion protein expression.* Glia, 1999. **25**(3): p. 282-92.
145. Watt, N.T., et al., *Cellular prion protein protects against reactive-oxygen-species-induced DNA damage.* Free Radic Biol Med, 2007. **43**(6): p. 959-67.
146. Alfaidy, N., et al., *Prion protein expression and functional importance in developmental angiogenesis: role in oxidative stress and copper homeostasis.* Antioxid Redox Signal, 2013. **18**(4): p. 400-11.
147. Singh, A., et al., *Prion protein (PrP) knock-out mice show altered iron metabolism: a functional role for PrP in iron uptake and transport.* PLoS One, 2009. **4**(7): p. e6115.
148. Haldar, S., et al., *Prion protein promotes kidney iron uptake via its ferrireductase activity.* J Biol Chem, 2015. **290**(9): p. 5512-22.
149. Hare, D., et al., *A delicate balance: Iron metabolism and diseases of the brain.* Front Aging Neurosci, 2013. **5**: p. 34.
150. Tripathi, A.K., et al., *Prion protein functions as a ferrireductase partner for ZIP14 and DMT1.* Free Radic Biol Med, 2015. **84**: p. 322-330.
151. Beraldo, F.H., et al., *Role of alpha7 nicotinic acetylcholine receptor in calcium signaling induced by prion protein interaction with stress-inducible protein 1.* J Biol Chem, 2010. **285**(47): p. 36542-50.
152. Nieznanski, K., et al., *Direct interaction between prion protein and tubulin.* Biochem Biophys Res Commun, 2005. **334**(2): p. 403-11.
153. Zafar, S., et al., *Proteomics approach to identify the interacting partners of cellular prion protein and characterization of Rab7a interaction in neuronal cells.* J Proteome Res, 2011. **10**(7): p. 3123-35.
154. Patel, D.M., et al., *Disease mutations in desmoplakin inhibit Cx43 membrane targeting mediated by desmoplakin-EB1 interactions.* J Cell Biol, 2014. **206**(6): p. 779-97.
155. Stappenbeck, T.S. and K.J. Green, *The desmoplakin carboxyl terminus coaligns with and specifically disrupts intermediate filament networks when expressed in cultured cells.* J Cell Biol, 1992. **116**(5): p. 1197-209.
156. Balducci, C., et al., *Synthetic amyloid-beta oligomers impair long-term memory independently of cellular prion protein.* Proc Natl Acad Sci U S A, 2010. **107**(5): p. 2295-300.
157. Larson, M., et al., *The complex PrP(c)-Fyn couples human oligomeric Abeta with pathological tau changes in Alzheimer's disease.* J Neurosci, 2012. **32**(47): p. 16857-71a.
158. Zhang, Y., et al., *Cellular Prion Protein as a Receptor of Toxic Amyloid-beta42 Oligomers Is Important for Alzheimer's Disease.* Front Cell Neurosci, 2019. **13**: p. 339.
159. Bakkebo, M.K., et al., *The Cellular Prion Protein: A Player in Immunological Quiescence.* Front Immunol, 2015. **6**: p. 450.

160. Caetano, F.A., et al., *Endocytosis of prion protein is required for ERK1/2 signaling induced by stress-inducible protein 1.* J Neurosci, 2008. **28**(26): p. 6691-702.
161. Roffe, M., et al., *Prion protein interaction with stress-inducible protein 1 enhances neuronal protein synthesis via mTOR.* Proc Natl Acad Sci U S A, 2010. **107**(29): p. 13147-52.
162. Vassallo, N., et al., *Activation of phosphatidylinositol 3-kinase by cellular prion protein and its role in cell survival.* Biochem Biophys Res Commun, 2005. **332**(1): p. 75-82.
163. Nah, J., et al., *BECN1/Beclin 1 is recruited into lipid rafts by prion to activate autophagy in response to amyloid beta 42.* Autophagy, 2013. **9**(12): p. 2009-21.
164. Shin, H.Y., et al., *Deficiency of prion protein induces impaired autophagic flux in neurons.* Front Aging Neurosci, 2014. **6**: p. 207.
165. Kuffer, A., et al., *The prion protein is an agonistic ligand of the G protein-coupled receptor Adgrg6.* Nature, 2016. **536**(7617): p. 464-8.
166. Chen, R.J., et al., *Alzheimer's amyloid-beta oligomers rescue cellular prion protein induced tau reduction via the Fyn pathway.* ACS Chem Neurosci, 2013. **4**(9): p. 1287-96.
167. Li, Q.Q., et al., *Cellular prion protein promotes glucose uptake through the Fyn-HIF-2alpha-Glut1 pathway to support colorectal cancer cell survival.* Cancer Sci, 2011. **102**(2): p. 400-6.
168. Didonna, A., *Prion protein and its role in signal transduction.* Cell Mol Biol Lett, 2013. **18**(2): p. 209-30.
169. Kandel, E., *Principles of Neural Science*. 2013.
170. Craig, A.M. and G. Banker, *Neuronal polarity.* Annu Rev Neurosci, 1994. **17**: p. 267-310.
171. Dent, E.W., S.L. Gupton, and F.B. Gertler, *The growth cone cytoskeleton in axon outgrowth and guidance.* Cold Spring Harb Perspect Biol, 2011. **3**(3).
172. Laser-Azogui, A., et al., *Neurofilament assembly and function during neuronal development.* Curr Opin Cell Biol, 2015. **32**: p. 92-101.
173. Moon, H.M. and A. Wynshaw-Boris, *Cytoskeleton in action: lissencephaly, a neuronal migration disorder.* Wiley Interdiscip Rev Dev Biol, 2013. **2**(2): p. 229-45.
174. Kapitein, L.C. and C.C. Hoogenraad, *Which way to go? Cytoskeletal organization and polarized transport in neurons.* Mol Cell Neurosci, 2011. **46**(1): p. 9-20.
175. Chevalier-Larsen, E. and E.L. Holzbaur, *Axonal transport and neurodegenerative disease.* Biochim Biophys Acta, 2006. **1762**(11-12): p. 1094-108.
176. Gunawardena, S. and L.S. Goldstein, *Cargo-carrying motor vehicles on the neuronal highway: transport pathways and neurodegenerative disease.* J Neurobiol, 2004. **58**(2): p. 258-71.
177. Mallavarapu, A. and T. Mitchison, *Regulated actin cytoskeleton assembly at filopodium tips controls their extension and retraction.* J Cell Biol, 1999. **146**(5): p. 1097-106.
178. Stiess, M. and F. Bradke, *Neuronal polarization: the cytoskeleton leads the way.* Dev Neurobiol, 2011. **71**(6): p. 430-44.
179. Coles, C.H. and F. Bradke, *Coordinating neuronal actin-microtubule dynamics.* Curr Biol, 2015. **25**(15): p. R677-91.
180. Letourneau, P.C., *Differences in the organization of actin in the growth cones compared with the neurites of cultured neurons from chick embryos.* J Cell Biol, 1983. **97**(4): p. 963-73.
181. Alushin, G.M., et al., *High-resolution microtubule structures reveal the structural transitions in alphabeta-tubulin upon GTP hydrolysis.* Cell, 2014. **157**(5): p. 1117-29.
182. Matus, A., et al., *High actin concentrations in brain dendritic spines and postsynaptic densities.* Proc Natl Acad Sci U S A, 1982. **79**(23): p. 7590-4.

183. Waites, C.L., et al., *Piccolo regulates the dynamic assembly of presynaptic F-actin.* J Neurosci, 2011. **31**(40): p. 14250-63.
184. Xu, K., G. Zhong, and X. Zhuang, *Actin, spectrin, and associated proteins form a periodic cytoskeletal structure in axons.* Science, 2013. **339**(6118): p. 452-6.
185. Campellone, K.G. and M.D. Welch, *A nucleator arms race: cellular control of actin assembly.* Nat Rev Mol Cell Biol, 2010. **11**(4): p. 237-51.
186. Chesarone, M.A., A.G. DuPage, and B.L. Goode, *Unleashing formins to remodel the actin and microtubule cytoskeletons.* Nat Rev Mol Cell Biol, 2010. **11**(1): p. 62-74.
187. Korobova, F. and T. Svitkina, *Arp2/3 complex is important for filopodia formation, growth cone motility, and neuritogenesis in neuronal cells.* Mol Biol Cell, 2008. **19**(4): p. 1561-74.
188. Dent, E.W., et al., *Filopodia are required for cortical neurite initiation.* Nat Cell Biol, 2007. **9**(12): p. 1347-59.
189. Pollard, T.D., *Regulation of actin filament assembly by Arp2/3 complex and formins.* Annu Rev Biophys Biomol Struct, 2007. **36**: p. 451-77.
190. Menna, E., et al., *Eps8 regulates axonal filopodia in hippocampal neurons in response to brain-derived neurotrophic factor (BDNF).* PLoS Biol, 2009. **7**(6): p. e1000138.
191. Flynn, K.C., *The cytoskeleton and neurite initiation.* Bioarchitecture, 2013. **3**(4): p. 86-109.
192. Craig, E.M., et al., *Membrane tension, myosin force, and actin turnover maintain actin treadmill in the nerve growth cone.* Biophys J, 2012. **102**(7): p. 1503-13.
193. Lin, C.H., et al., *Myosin drives retrograde F-actin flow in neuronal growth cones.* Neuron, 1996. **16**(4): p. 769-82.
194. Bard, L., et al., *A molecular clutch between the actin flow and N-cadherin adhesions drives growth cone migration.* J Neurosci, 2008. **28**(23): p. 5879-90.
195. Tomba, C., et al., *Geometrical Determinants of Neuronal Actin Waves.* Front Cell Neurosci, 2017. **11**: p. 86.
196. Flynn, K.C., et al., *Growth cone-like waves transport actin and promote axonogenesis and neurite branching.* Dev Neurobiol, 2009. **69**(12): p. 761-79.
197. Roy, S., *Waves, rings, and trails: The scenic landscape of axonal actin.* J Cell Biol, 2016. **212**(2): p. 131-4.
198. Inagaki, N. and H. Katsuno, *Actin Waves: Origin of Cell Polarization and Migration?* Trends Cell Biol, 2017. **27**(7): p. 515-526.
199. Leterrier, C., P. Dubey, and S. Roy, *The nano-architecture of the axonal cytoskeleton.* Nat Rev Neurosci, 2017. **18**(12): p. 713-726.
200. Toriyama, M., et al., *Shootin1: A protein involved in the organization of an asymmetric signal for neuronal polarization.* J Cell Biol, 2006. **175**(1): p. 147-57.
201. Katsuno, H., et al., *Actin Migration Driven by Directional Assembly and Disassembly of Membrane-Anchored Actin Filaments.* Cell Rep, 2015. **12**(4): p. 648-60.
202. D'Este, E., et al., *STED nanoscopy reveals the ubiquity of subcortical cytoskeleton periodicity in living neurons.* Cell Rep, 2015. **10**(8): p. 1246-51.
203. Leite, S.C., et al., *The Actin-Binding Protein alpha-Adducin Is Required for Maintaining Axon Diameter.* Cell Rep, 2016. **15**(3): p. 490-498.
204. Qu, Y., et al., *Periodic actin structures in neuronal axons are required to maintain microtubules.* Mol Biol Cell, 2017. **28**(2): p. 296-308.
205. Bar, J., et al., *Periodic F-actin structures shape the neck of dendritic spines.* Sci Rep, 2016. **6**: p. 37136.

206. Willig, K.I., et al., *Nanoscopy of filamentous actin in cortical dendrites of a living mouse.* Biophys J, 2014. **106**(1): p. L01-3.
207. Korobova, F. and T. Svitkina, *Molecular architecture of synaptic actin cytoskeleton in hippocampal neurons reveals a mechanism of dendritic spine morphogenesis.* Mol Biol Cell, 2010. **21**(1): p. 165-76.
208. Nirschl, J.J., A.E. Ghiretti, and E.L.F. Holzbaur, *The impact of cytoskeletal organization on the local regulation of neuronal transport.* Nat Rev Neurosci, 2017. **18**(10): p. 585-597.
209. Ganguly, A., et al., *A dynamic formin-dependent deep F-actin network in axons.* J Cell Biol, 2015. **210**(3): p. 401-17.
210. Conde, C. and A. Caceres, *Microtubule assembly, organization and dynamics in axons and dendrites.* Nat Rev Neurosci, 2009. **10**(5): p. 319-32.
211. Yau, K.W., et al., *Dendrites In Vitro and In Vivo Contain Microtubules of Opposite Polarity and Axon Formation Correlates with Uniform Plus-End-Out Microtubule Orientation.* J Neurosci, 2016. **36**(4): p. 1071-85.
212. Resch, G.P., et al., *Visualisation of the actin cytoskeleton by cryo-electron microscopy.* J Cell Sci, 2002. **115**(Pt 9): p. 1877-82.
213. Mudrakola, H.V., K. Zhang, and B. Cui, *Optically resolving individual microtubules in live axons.* Structure, 2009. **17**(11): p. 1433-41.
214. Palay, S.L., et al., *The axon hillock and the initial segment.* J Cell Biol, 1968. **38**(1): p. 193-201.
215. van Coevorden-Hameete, M.H., et al., *Antibodies to TRIM46 are associated with paraneoplastic neurological syndromes.* Ann Clin Transl Neurol, 2017. **4**(9): p. 680-686.
216. Satake, T., et al., *MTCL1 plays an essential role in maintaining Purkinje neuron axon initial segment.* EMBO J, 2017. **36**(9): p. 1227-1242.
217. Wieczorek, M., et al., *Microtubule-associated proteins control the kinetics of microtubule nucleation.* Nat Cell Biol, 2015. **17**(7): p. 907-16.
218. Yu, W., et al., *Microtubule nucleation and release from the neuronal centrosome.* J Cell Biol, 1993. **122**(2): p. 349-59.
219. Ahmad, F.J., et al., *Inhibition of microtubule nucleation at the neuronal centrosome compromises axon growth.* Neuron, 1994. **12**(2): p. 271-80.
220. Petry, S. and R.D. Vale, *Microtubule nucleation at the centrosome and beyond.* Nat Cell Biol, 2015. **17**(9): p. 1089-93.
221. Kollman, J.M., et al., *Microtubule nucleation by gamma-tubulin complexes.* Nat Rev Mol Cell Biol, 2011. **12**(11): p. 709-21.
222. Ori-McKenney, K.M., L.Y. Jan, and Y.N. Jan, *Golgi outposts shape dendrite morphology by functioning as sites of acentrosomal microtubule nucleation in neurons.* Neuron, 2012. **76**(5): p. 921-30.
223. Delandre, C., R. Amikura, and A.W. Moore, *Microtubule nucleation and organization in dendrites.* Cell Cycle, 2016. **15**(13): p. 1685-92.
224. Kapitein, L.C. and C.C. Hoogenraad, *Building the Neuronal Microtubule Cytoskeleton.* Neuron, 2015. **87**(3): p. 492-506.
225. Baas, P.W. and S. Lin, *Hooks and comets: The story of microtubule polarity orientation in the neuron.* Dev Neurobiol, 2011. **71**(6): p. 403-18.
226. Yan, J., et al., *Kinesin-1 regulates dendrite microtubule polarity in Caenorhabditis elegans.* Elife, 2013. **2**: p. e00133.

227. Akhmanova, A. and M.O. Steinmetz, *Microtubule +TIPs at a glance.* J Cell Sci, 2010. **123**(Pt 20): p. 3415-9.
228. Roll-Mecak, A., *Intrinsically disordered tubulin tails: complex tuners of microtubule functions?* Semin Cell Dev Biol, 2015. **37**: p. 11-9.
229. Dehmelt, L., et al., *The role of microtubule-associated protein 2c in the reorganization of microtubules and lamellipodia during neurite initiation.* J Neurosci, 2003. **23**(29): p. 9479-90.
230. Ahmad, F.J., et al., *An essential role for katanin in severing microtubules in the neuron.* J Cell Biol, 1999. **145**(2): p. 305-15.
231. Roll-Mecak, A. and F.J. McNally, *Microtubule-severing enzymes.* Curr Opin Cell Biol, 2010. **22**(1): p. 96-103.
232. Wang, L. and A. Brown, *Rapid movement of microtubules in axons.* Curr Biol, 2002. **12**(17): p. 1496-1501.
233. Yau, K.W., et al., *Microtubule minus-end binding protein CAMSAP2 controls axon specification and dendrite development.* Neuron, 2014. **82**(5): p. 1058-73.
234. Leterrier, C., *The Axon Initial Segment, 50Years Later: A Nexus for Neuronal Organization and Function.* Curr Top Membr, 2016. **77**: p. 185-233.
235. Leterrier, C., et al., *End-binding proteins EB3 and EB1 link microtubules to ankyrin G in the axon initial segment.* Proc Natl Acad Sci U S A, 2011. **108**(21): p. 8826-31.
236. Freal, A., et al., *Cooperative Interactions between 480 kDa Ankyrin-G and EB Proteins Assemble the Axon Initial Segment.* J Neurosci, 2016. **36**(16): p. 4421-33.
237. Leterrier, C., et al., *Nanoscale Architecture of the Axon Initial Segment Reveals an Organized and Robust Scaffold.* Cell Rep, 2015. **13**(12): p. 2781-93.
238. Perlson, E., et al., *Dynein interacts with the neural cell adhesion molecule (NCAM180) to tether dynamic microtubules and maintain synaptic density in cortical neurons.* J Biol Chem, 2013. **288**(39): p. 27812-24.
239. Ahmad, F.J., et al., *Motor proteins regulate force interactions between microtubules and microfilaments in the axon.* Nat Cell Biol, 2000. **2**(5): p. 276-80.
240. Hirokawa, N., M.A. Glicksman, and M.B. Willard, *Organization of mammalian neurofilament polypeptides within the neuronal cytoskeleton.* J Cell Biol, 1984. **98**(4): p. 1523-36.
241. Brown, A., *Axonal transport of membranous and nonmembranous cargoes: a unified perspective.* J Cell Biol, 2003. **160**(6): p. 817-21.
242. Uchida, A., et al., *Severing and end-to-end annealing of neurofilaments in neurons.* Proc Natl Acad Sci U S A, 2013. **110**(29): p. E2696-705.
243. Uchida, A., N.H. Alami, and A. Brown, *Tight functional coupling of kinesin-1A and dynein motors in the bidirectional transport of neurofilaments.* Mol Biol Cell, 2009. **20**(23): p. 4997-5006.
244. Akhmanova, A. and J.A. Hammer, 3rd, *Linking molecular motors to membrane cargo.* Curr Opin Cell Biol, 2010. **22**(4): p. 479-87.
245. Hirokawa, N. and R. Takemura, *Molecular motors and mechanisms of directional transport in neurons.* Nat Rev Neurosci, 2005. **6**(3): p. 201-14.
246. Kardon, J.R. and R.D. Vale, *Regulators of the cytoplasmic dynein motor.* Nat Rev Mol Cell Biol, 2009. **10**(12): p. 854-65.

247. Karcher, R.L., S.W. Deacon, and V.I. Gelfand, *Motor-cargo interactions: the key to transport specificity.* Trends Cell Biol, 2002. **12**(1): p. 21-7.
248. Strom, M., et al., *A family of Rab27-binding proteins. Melanophilin links Rab27a and myosin Va function in melanosome transport.* J Biol Chem, 2002. **277**(28): p. 25423-30.
249. Sahlender, D.A., et al., *Optineurin links myosin VI to the Golgi complex and is involved in Golgi organization and exocytosis.* J Cell Biol, 2005. **169**(2): p. 285-95.
250. Hoogenraad, C.C., et al., *Bicaudal D induces selective dynein-mediated microtubule minus end-directed transport.* EMBO J, 2003. **22**(22): p. 6004-15.
251. Rocha, N., et al., *Cholesterol sensor ORP1L contacts the ER protein VAP to control Rab7-RILP-p150 Glued and late endosome positioning.* J Cell Biol, 2009. **185**(7): p. 1209-25.
252. Glater, E.E., et al., *Axonal transport of mitochondria requires milton to recruit kinesin heavy chain and is light chain independent.* J Cell Biol, 2006. **173**(4): p. 545-57.
253. Yu, C., et al., *Myosin VI undergoes cargo-mediated dimerization.* Cell, 2009. **138**(3): p. 537-48.
254. Spudich, J.A. and S. Sivaramakrishnan, *Myosin VI: an innovative motor that challenged the swinging lever arm hypothesis.* Nat Rev Mol Cell Biol, 2010. **11**(2): p. 128-37.
255. Ally, S., et al., *Opposite-polarity motors activate one another to trigger cargo transport in live cells.* J Cell Biol, 2009. **187**(7): p. 1071-82.
256. Gallo, G., *More than one ring to bind them all: recent insights into the structure of the axon.* Dev Neurobiol, 2013. **73**(11): p. 799-805.
257. Pathak, D., K.J. Sepp, and P.J. Hollenbeck, *Evidence that myosin activity opposes microtubule-based axonal transport of mitochondria.* J Neurosci, 2010. **30**(26): p. 8984-92.
258. Wu, X.S., et al., *Identification of an organelle receptor for myosin-Va.* Nat Cell Biol, 2002. **4**(4): p. 271-8.
259. Semenova, I., et al., *Actin dynamics is essential for myosin-based transport of membrane organelles.* Curr Biol, 2008. **18**(20): p. 1581-6.
260. Nelson, S.R., et al., *Random walk of processive, quantum dot-labeled myosin Va molecules within the actin cortex of COS-7 cells.* Biophys J, 2009. **97**(2): p. 509-18.
261. Macaskill, A.F., et al., *Miro1 is a calcium sensor for glutamate receptor-dependent localization of mitochondria at synapses.* Neuron, 2009. **61**(4): p. 541-55.
262. He, Y., et al., *Role of cytoplasmic dynein in the axonal transport of microtubules and neurofilaments.* J Cell Biol, 2005. **168**(5): p. 697-703.
263. McQuarrie, I.G., S.T. Brady, and R.J. Lasek, *Diversity in the axonal transport of structural proteins: major differences between optic and spinal axons in the rat.* J Neurosci, 1986. **6**(6): p. 1593-605.
264. Henne, W.M., N.J. Buchkovich, and S.D. Emr, *The ESCRT pathway.* Dev Cell, 2011. **21**(1): p. 77-91.
265. Settembre, C., et al., *Signals from the lysosome: a control centre for cellular clearance and energy metabolism.* Nat Rev Mol Cell Biol, 2013. **14**(5): p. 283-96.
266. Ehlers, M.D., *Reinsertion or degradation of AMPA receptors determined by activity-dependent endocytic sorting.* Neuron, 2000. **28**(2): p. 511-25.
267. Schwarz, L.A., B.J. Hall, and G.N. Patrick, *Activity-dependent ubiquitination of GluA1 mediates a distinct AMPA receptor endocytosis and sorting pathway.* J Neurosci, 2010. **30**(49): p. 16718-29.

268. Goo, M.S., et al., *Activity-dependent trafficking of lysosomes in dendrites and dendritic spines.* J Cell Biol, 2017. **216**(8): p. 2499-2513.
269. Farias, G.G., et al., *BORC/kinesin-1 ensemble drives polarized transport of lysosomes into the axon.* Proc Natl Acad Sci U S A, 2017. **114**(14): p. E2955-E2964.
270. Cordonnier, M.N., et al., *Actin filaments and myosin I alpha cooperate with microtubules for the movement of lysosomes.* Mol Biol Cell, 2001. **12**(12): p. 4013-29.
271. Togashi, H., T. Sakisaka, and Y. Takai, *Cell adhesion molecules in the central nervous system.* Cell Adh Migr, 2009. **3**(1): p. 29-35.
272. Lowery, L.A. and D. Van Vactor, *The trip of the tip: understanding the growth cone machinery.* Nat Rev Mol Cell Biol, 2009. **10**(5): p. 332-43.
273. Mitchison, T. and M. Kirschner, *Cytoskeletal dynamics and nerve growth.* Neuron, 1988. **1**(9): p. 761-72.
274. Suter, D.M. and P. Forscher, *Substrate-cytoskeletal coupling as a mechanism for the regulation of growth cone motility and guidance.* J Neurobiol, 2000. **44**(2): p. 97-113.
275. Leshchyns'ka, I. and V. Sytnyk, *Reciprocal Interactions between Cell Adhesion Molecules of the Immunoglobulin Superfamily and the Cytoskeleton in Neurons.* Front Cell Dev Biol, 2016. **4**: p. 9.
276. Li, S., et al., *The neural cell adhesion molecule (NCAM) associates with and signals through p21-activated kinase 1 (Pak1).* J Neurosci, 2013. **33**(2): p. 790-803.
277. Dong, X., et al., *An extracellular adhesion molecule complex patterns dendritic branching and morphogenesis.* Cell, 2013. **155**(2): p. 296-307.
278. Lin, Y.C., M.F. Yeckel, and A.J. Koleske, *Abl2/Arg controls dendritic spine and dendrite arbor stability via distinct cytoskeletal control pathways.* J Neurosci, 2013. **33**(5): p. 1846-57.
279. Leemhuis, J. and H.H. Bock, *Reelin modulates cytoskeletal organization by regulating Rho GTPases.* Commun Integr Biol, 2011. **4**(3): p. 254-7.
280. Meseke, M., G. Rosenberger, and E. Forster, *Reelin and the Cdc42/Rac1 guanine nucleotide exchange factor alphaPIX/Arhgef6 promote dendritic Golgi translocation in hippocampal neurons.* Eur J Neurosci, 2013. **37**(9): p. 1404-12.
281. Kupferman, J.V., et al., *Reelin signaling specifies the molecular identity of the pyramidal neuron distal dendritic compartment.* Cell, 2014. **158**(6): p. 1335-1347.
282. Toriyama, M., et al., *Conversion of a signal into forces for axon outgrowth through Pak1-mediated shootin1 phosphorylation.* Curr Biol, 2013. **23**(6): p. 529-34.
283. Chivet, M., et al., *Exosomes secreted by cortical neurons upon glutamatergic synapse activation specifically interact with neurons.* J Extracell Vesicles, 2014. **3**: p. 24722.
284. Burckhardt, C.J., et al., *Drifting motions of the adenovirus receptor CAR and immobile integrins initiate virus uncoating and membrane lytic protein exposure.* Cell Host Microbe, 2011. **10**(2): p. 105-17.
285. Caspi, A., et al., *A new dimension in retrograde flow: centripetal movement of engulfed particles.* Biophys J, 2001. **81**(4): p. 1990-2000.
286. Ronquist, K.G., et al., *Energy-requiring uptake of prostasomes and PC3 cell-derived exosomes into non-malignant and malignant cells.* J Extracell Vesicles, 2016. **5**: p. 29877.
287. Faure, J., et al., *Exosomes are released by cultured cortical neurones.* Mol Cell Neurosci, 2006. **31**(4): p. 642-8.

288. Svitkina, T.M., A.A. Neyfakh, Jr., and A.D. Bershadsky, *Actin cytoskeleton of spread fibroblasts appears to assemble at the cell edges.* J Cell Sci, 1986. **82**: p. 235-48.
289. Rodriguez, O.C., et al., *Conserved microtubule-actin interactions in cell movement and morphogenesis.* Nat Cell Biol, 2003. **5**(7): p. 599-609.
290. Straight, A.F., et al., *Dissecting temporal and spatial control of cytokinesis with a myosin II Inhibitor.* Science, 2003. **299**(5613): p. 1743-7.
291. Ewers, H., et al., *Single-particle tracking of murine polyoma virus-like particles on live cells and artificial membranes.* Proc Natl Acad Sci U S A, 2005. **102**(42): p. 15110-5.
292. Lehmann, M.J., et al., *Actin- and myosin-driven movement of viruses along filopodia precedes their entry into cells.* J Cell Biol, 2005. **170**(2): p. 317-25.
293. Schelhaas, M., et al., *Human papillomavirus type 16 entry: retrograde cell surface transport along actin-rich protrusions.* PLoS Pathog, 2008. **4**(9): p. e1000148.
294. Drago, F., et al., *ATP Modifies the Proteome of Extracellular Vesicles Released by Microglia and Influences Their Action on Astrocytes.* Front Pharmacol, 2017. **8**: p. 910.
295. Coco, S., et al., *Storage and release of ATP from astrocytes in culture.* J Biol Chem, 2003. **278**(2): p. 1354-62.
296. Fumagalli, M., et al., *Phenotypic changes, signaling pathway, and functional correlates of GPR17-expressing neural precursor cells during oligodendrocyte differentiation.* J Biol Chem, 2011. **286**(12): p. 10593-604.
297. Riganti, L., et al., *Sphingosine-1-Phosphate (S1P) Impacts Presynaptic Functions by Regulating Synapsin I Localization in the Presynaptic Compartment.* J Neurosci, 2016. **36**(16): p. 4624-34.
298. Chiarini, A., et al., *Amyloid beta-Exposed Human Astrocytes Overproduce Phospho-Tau and Overrelease It within Exosomes, Effects Suppressed by Calcilytic NPS 2143-Further Implications for Alzheimer's Therapy.* Front Neurosci, 2017. **11**: p. 217.
299. Eitan, E., et al., *Extracellular Vesicle-Associated Abeta Mediates Trans-Neuronal Bioenergetic and Ca(2+)-Handling Deficits in Alzheimer's Disease Models.* NPJ Aging Mech Dis, 2016. **2**.
300. Braak, H. and E. Braak, *Neuropathological stageing of Alzheimer-related changes.* Acta Neuropathol, 1991. **82**(4): p. 239-59.
301. Sardar Sinha, M., et al., *Alzheimer's disease pathology propagation by exosomes containing toxic amyloid-beta oligomers.* Acta Neuropathol, 2018. **136**(1): p. 41-56.
302. Nieznanski, K., *Interactions of prion protein with intracellular proteins: so many partners and no consequences?* Cell Mol Neurobiol, 2010. **30**(5): p. 653-66.
303. Dickson, T.C., et al., *Functional binding interaction identified between the axonal CAM L1 and members of the ERM family.* J Cell Biol, 2002. **157**(7): p. 1105-12.
304. Nishimura, K., et al., *L1-dependent neuritogenesis involves ankyrinB that mediates L1-CAM coupling with retrograde actin flow.* J Cell Biol, 2003. **163**(5): p. 1077-88.
305. Slapsak, U., et al., *The N Terminus of the Prion Protein Mediates Functional Interactions with the Neuronal Cell Adhesion Molecule (NCAM) Fibronectin Domain.* J Biol Chem, 2016. **291**(42): p. 21857-21868.
306. Raab-Traub, N. and D.P. Dittmer, *Viral effects on the content and function of extracellular vesicles.* Nat Rev Microbiol, 2017. **15**(9): p. 559-572.
307. Sartori-Rupp, A., et al., *Correlative cryo-electron microscopy reveals the structure of TNTs in neuronal cells.* Nat Commun, 2019. **10**(1): p. 342.

308. Lledo, P.M., et al., *Mice deficient for prion protein exhibit normal neuronal excitability and synaptic transmission in the hippocampus.* Proc Natl Acad Sci U S A, 1996. **93**(6): p. 2403-7.
309. Pyronneau, A., et al., *Aberrant Rac1-cofilin signaling mediates defects in dendritic spines, synaptic function, and sensory perception in fragile X syndrome.* Sci Signal, 2017. **10**(504).
310. Rohou, A. and N. Grigorieff, *CTFFIND4: Fast and accurate defocus estimation from electron micrographs.* J Struct Biol, 2015. **192**(2): p. 216-21.
311. Zivanov, J., et al., *New tools for automated high-resolution cryo-EM structure determination in RELION-3.* Elife, 2018. **7**.

8 ACKNOWLEDGMENTS

(In Italian)

Vorrei ringraziare il prof. Giuseppe Legname per avermi dato la possibilità di svolgere il dottorato nel suo laboratorio e per aver seguito il lavoro che ho svolto a Trieste e averlo supportato e monitorato durante il periodo trascorso a Milano.

Ringrazio la dott.ssa Claudia Verderio che mi ha seguito lungo tutto il percorso che ho compiuto nel suo laboratorio a Milano e che ha profondamente lavorato alla mia formazione, insegnandomi non solo a impostare i protocolli sperimentali e a formulare le ipotesi di ricerca, ma anche ad elaborare un'analisi critica e ragionata dei risultati ottenuti.

Un grazie va anche al dott. Dan Cojoc che ha contribuito a tutta la mia formazione sull'utilizzo degli optical tweezers e su quello che oggi so di MATLAB, e che ha reso possibile l'utilizzo della manipolazione ottica sui nostri setup di imaging.

Thank to prof. Maria-Eva Krämer Albers and to prof. Laura Ballerini, to have critically evaluated my thesis and my work. It was a pleasure for me having an important external feedback after a study lasted fourth years. Thanks for your comments and advices.

Ci sono davvero tantissime persone che hanno contribuito alla riuscita di questo lavoro e ai risultati ottenuti durante il mio percorso di dottorato di ricerca: tra queste vorrei ringraziarne alcune in particolare.

Prima di tutto un grazie va a chi ha dato un svolta decisiva in modo indiretto e diretto all'analisi dei miei dati: grazie al prof. Remo Sanges che ha tenuto il corso su R e ha Gabriele Leoni che mi ha aiutato a scrivere le tre righe più difficili del mio primo script su R con cui ho potuto analizzare una grossa fetta dei miei dati premendo un solo pulsante!

Un grazie di cuore va a Martina Gabrielli che ha aperto la strada a questo progetto con i primi esperimenti svolti a Trieste e che mi ha aiutato ad affrontare le difficoltà non solo sperimentali ma anche tecnico-pratiche e che ha criticamente contribuito al settaggio degli esperimenti e delle analisi.

Grazie a Ilaria Prada che è stata per me in tutti questi anni il mio mentore e che oltre agli insegnamenti essenziali, ha saputo darmi innumerevoli suggerimenti e consigli, soprattutto nei momenti di difficoltà. Oltre che un esempio, per me è anche una cara e stimata amica a cui devo gran parte di quello che sono oggi come ricercatore e persona.

Grazie a Federica Scaroni, collega, ma soprattutto amica, con cui ho condiviso tantissimi momenti luminosi e bui di questo percorso, che ha saputo davvero ascoltarmi quando ne ho avuto bisogno, supportandomi e consigliandomi, ma oserei dire anche sopportandomi, nelle mie scelte sperimentali e della vita. Grazie anche per il contributo importante che ha dato ai risultati di questa tesi.

Un grazie va anche a Marta Lombardi con cui ho condiviso oltre al lavoro di tutti i giorni dentro al laboratorio, anche innumerevoli e alle volte purtroppo infiniti viaggi, spesi spesso a speculare sui risultati dei nostri progetti o ad escogitare nuove tecniche sperimentali innovative, discorsi grazie ai quali il tragitto mi è sembrato più breve e piacevole.

Grazie a tutte le amiche e colleghe del lab di Milano che hanno dato solarità anche alle giornate più negative, grazie per essere sempre state collaborative e per tutti i consigli preziosi di cui ho fatto tesoro: grazie in particolare a Elisa, Clara, Lara e Silvia.

Anche discorrendo verso Est ci sono parecchie persone che meritano una menzione.

Primo fra tutti, un grazie di cuore va ad Ilenia Bagnano, oltre che compagna di dottorato, mia carissima amica. Lei c'è sempre stata da vicino, tutte le volte che sono passata o rimasta a Trieste, ma anche quando c'erano quei 400km a separarci, questi non le hanno impedito di essermi vicino nei giorni belli e felici, e nei giorni difficili. In questi anni è stata una delle poche e più importanti consigliere della mia vita, che grazie alla sua saggezza e generosità mi ha dato la forza per credere in me stessa e per affrontare i momenti di difficoltà e incertezza, dimostrandosi sempre leale e sincera.

Grazie a Luigi, che ho incontrato per la prima volta a Trieste, ma che è stato fin da subito un amico d'eccezione e probabilmente anche molto di più. Attraverso la passione condivisa per la fotografia abbiamo condiviso tanti luoghi e momenti assieme. Grazie perché per me Trieste avrebbe un ricordo diverso oggi se non ti avessi conosciuto.

Grazie ai miei colleghi e agli amici più stretti della SISSA: grazie in particolare a Elena D., Martina, Jessica, Wendy, Gabriele, Nicola S., Nicola M., Teresa, Silvia, Giulia S., Kevin, Xuan, Chiara G., Arianna, Marco, Osvaldo, che ci sono stati tutte le volte che ho avuto bisogno di una mano, che anche se non ci conoscevamo e con alcuni di loro non ho condiviso molti momenti assieme, hanno saputo ascoltare le mie richieste e problemi, e grazie ai quali tutte le volte che ero in SISSA e a Trieste mi sono sentita come se non mi fossi mai mossa da casa e sempre circondata da amici.

Un grazie ai miei amici più stretti di Varese: in particolare grazie a Jenny, Roby e Alessandra perché le serate e i viaggi trascorsi assieme sono stati momenti importanti di spensieratezza e ilarità che spesso hanno alleggerito i periodi stressanti e complicati di questo percorso.

Grazie a tutti quelli presenti nel giorno della mia defense, è stato davvero importante avervi qui tutti in uno dei giorni più importanti della mia vita.

Infine, un grazie va alla mia famiglia, che nonostante il mio carattere e la mia personalità, mi ha sempre sostenuta in questo viaggio, che mi è stata vicino tutti i giorni anche quando ero lontano da casa. Anche se il loro contributo per questo lavoro può sembrare piccolo, in realtà è stato quello più importante, corposo e decisivo, senza il quale questo sogno non si sarebbe mai realizzato.

In particolare, grazie a mia mamma e a mio papà che mi hanno sostenuto non solo economicamente, ma che mi hanno ascoltato e dato consigli per ogni passo che ho compiuto in questo percorso. Anche se loro mi vedono ormai arrivata ad un traguardo importante e lontano, io li sento sempre una componente importante della meta che ho raggiunto oggi.

Grazie a mia sorella, la mia star, la mia luce. Il mio percorso è sempre stato illuminato dalla sua solarità, dal suo carisma e da ciò che solo una sorella può dare.

Vi voglio bene, e questa tesi è dedicata a voi, che siete i pilastri della mia vita.

p.s.: non posso dimenticare le mie gatte: Mishka, Milù e Oasis, che con la loro dolcezza e morbidezza hanno portato nella nostra casa un clima di serenità e amore. Grazie.